Accession No. _____

SID 66-46-1

A STUDY OF LONGITUDINAL OSCILLATIONS OF PROPELLANT TANKS AND WAVE PROPAGATIONS IN FEED LINES

Part I—One-Dimensional Wave Propagation in a Feed Line

31 March 1966 NAS8-11490

Prepared by

Henry Wing, Staff Investigator
Clement L. Tai, Principal Investigator

Approved by

F. C. Hung
Assistant Director, Structures and Dynamics

NORTH AMERICAN AVIATION, INC.
SPACE and INFORMATION SYSTEMS DIVISION

Accession No. _____

1

SID 66-46-1

A STUDY OF LONGITUDINAL OSCILLATIONS OF PROPELLANT TANKS AND WAVE PROPAGATIONS IN FEED LINES

Part I—One-Dimensional Wave Propagation in a Feed Line

31 March 1966

NAS8-11490

Prepared by

Henry Wing, Staff Investigator
Clement L. Tai, Principal Investigator

Approved by

F. C. Hung
Assistant Director, Structures and Dynamics

NORTH AMERICAN AVIATION, INC.
SPACE and INFORMATION SYSTEMS DIVISION

TECHNICAL REPORT INDEX/ABSTRACT

ACCESSION NUMBER							DOCUMENT SECURITY CLASSIFICATION	
							Unclassified	

TITLE OF DOCUMENT

"A Study of Longitudinal Oscillations of Propellant Tanks and Wave Propagations in Feed Lines"

LIBRARY USE ONLY

AUTHOR(S)

C. L. Tai, M. M. H. Loh, S. A. Fung, H. Wing, S. Uchiyama

CODE	ORIGINATING AGENCY AND OTHER SOURCES	DOCUMENT NUMBER
	S&ID, NAA	SID 66-46 (Five Volumes)

PUBLICATION DATE	CONTRACT NUMBER
31 March 1966	NAS8-11490

DESCRIPTIVE TERMS

fluid dynamics
pipeline dynamics
wave propagation
longitudinal oscillations
shell dynamics

ABSTRACT

The work done under this contract is being published in five separate parts:

(SID 66-46-1) Part I — One-Dimensional Wave Propagation in a Feed Line (by H. Wing and C. L. Tai)

(SID 66-46-2) Part II — Wave Propagation in an Elastic Pipe Filled with Incompressible Viscous Fluid (by M. M. H. Loh and C. L. Tai)

(SID 66-46-3) Part III — Wave Propagation in an Elastic Pipe Filled with Incompressible Viscous Streaming Fluid (by S. A. Fung and C. L. Tai)

(SID 66-46-4) Part IV — Longitudinal Oscillation of a Propellant-Filled Flexible Hemispherical Tank (by H. Wing and C. L. Tai)

(SID 66-46-5) Part V — Longitudinal Oscillation of a Propellant-Filled Flexible Oblate Spheroidal Tank (by S. Uchiyama and C. L. Tai)

FOREWORD

This report was prepared by the Space and Information Systems Division of North American Aviation, Inc., Downey, California, for the George C. Marshall Space Flight Center, National Aeronautics and Space Administration, Huntsville, Alabama, under Contract No. NAS8-11490, "Study of Longitudinal Oscillations of Propellant Tanks and Wave Propagations in Feed Lines," dated January 6, 1965. Dr. George F. McDonough (Principal) and Mr. Robert S. Ryan (Alternate) of Aero-Astrodynamics Laboratory, MSFC, are Contracting Officer Representatives. The work is published in five separate parts:

Part I - One-Dimensional Wave Propagation in a Feed Line

Part II - Wave Propagation in an Elastic Pipe Filled With Incompressible Viscous Fluid

Part III - Wave Propagation in an Elastic Pipe Filled With Incompressible Viscous Streaming Fluid

Part IV - Longitudinal Oscillation of a Propellant-Filled Flexible Hemispherical Tank

Part V - Longitudinal Oscillation of a Propellant-Filled Flexible Oblate Spheroidal Tank

The project was carried out by the Launch Vehicle Dynamics Group, Structures and Dynamics Department of Research and Engineering Division, S&ID. Dr. F. C. Hung was the Program Manager for North American Aviation, Inc. The study was conducted by Dr. Clement L. Tai (Principal Investigator), Dr. Michael M. H. Loh, Mr. Henry Wing, Dr. Sui-An Fung, and Dr. Shoichi Uchiyama. Dr. James Sheng, who started the investigation of Part IV, left in the middle of the program to teach at the University of Wisconsin. The computer program was developed by Mr. R. A. Pollock, Mr. F. W. Egeling, and Mr. S. Miyashiro.

ABSTRACT

In this report, the dynamics of elastic propellant feed lines with streaming fluid are analyzed using the nonlinear one-dimensional unsteady compressible fluid flow equations. The viscous effect of the fluid is assumed to be expressible in the form of a hydraulic resistance corresponding to turbulent flow. Transfer functions relating the pressures, velocities, and the corresponding phase angles were derived from the linearized equations for the perturbed state. The governing equations were also converted into a system of four first-order ordinary nonlinear differential equations by the method of characteristics. These were then transposed into finite difference form and solved numerically on a digital computer. Impulse, step, and sinusoidal velocity disturbances were considered in the numerical solution for a feed line with and without a control device. The physical parameters of the liquid hydrogen line on the Saturn S-II engine are used for the numerical calculations to illustrate the results.

Author

CONTENTS

Page

NOMENCLATURE

a	Velocity of pressure wave
a_m	Missile acceleration
A	Cross-sectional area of feed line
A_d	Cross-sectional area of tank damper
A_h	Cross-sectional area of feed line wall
A_s	Cross-sectional area of surge tank
A_{pi}	Cross-sectional area of pump inlet
C	Feed line restriction coefficient
D	Feed line diameter
E	Young's modulus of line material
f	Darcy-Weisbach friction coefficient
$f(t)$	Prescribed function for pressure at left end of line
g	Gravitational constant
$g(t)$	Prescribed function for mass flow rate at right end of line
h	Wall thickness
I_1, I_2	Functions defined by Equation (48)
j	Square root of minus one
k_ℓ, k_t	Laminar and turbulent resistance coefficient
K	Modified bulk modulus defined by Equation (13)
K_l	Bulk modulus of fluid
L	Length of feed line

m_1, m_2	Roots of Equation (46)
p	Fluid pressure
$\bar{p}$	Reference pressure
P	Laplace transform of fluid pressure
Q	Mass flow rate
$Q_1(t)$	Mass discharge rate
r	Internal radius of line
R	Reynold's number
s	Laplace transform variable
t	Time
u	Average fluid velocity over line cross section
$\bar{u}$	Reference fluid velocity
$v(t)$	Fluid discharge velocity
V	Volume
x	Spatial coordinate along axis of feed line
z	Axial displacement component
Z	Laplace transform of axial displacement component
α	Density of line material
Δ	Incremental change
ζ	Damping coefficient of bellows
η	Liquid elevation in surge tank from equilibrium level
θ	Angle between axis of feed line and normal to flight path of missile

κ, $\bar{\kappa}$	Constant characterizing pressure regulating device
μ	Viscosity of fluid
ν	Poisson's ratio of line material
ρ	Density of fluid
$\phi(u)$	Function defined by either Equations (3) or (4)
ω	Frequency

Subscripts

A, B, C, R, S	Pertain to points according to Figure 2
0	Designate value at steady-state condition or value at x = 0
ℓ	Designate value at x = L

Superscripts

o	Initial guess value
1	Value of first iteration

INTRODUCTION

Pressure wave propagation in a pipe filled with fluid has been investigated extensively, from the early studies of surging phenomena to the recent work on unsteady flow in blood vessels and hydraulic control systems (References 1 to 17). Various simplifying assumptions were employed in each particular problem to facilitate a mathematical solution. In general, the formulation is not applicable to any problem with conditions other than those appropriate to the particular problem.

The classical theory of surging phenomena or "water hammer," formulated by Joukowsky (Reference 1), is based on the linearized one-dimensional Navier-Stokes equation for an inviscid fluid. It assumes that the pressure is uniform across any section of the pipe and that the deflection of the pipe is equal to the static deflection due to the instantaneous pressure in the fluid. This theory has since been extended to two-dimensional space (References 12 and 13), with some of the simplifications made in the Joukowsky theory relaxed (Reference 14). As far as the relations between fluid velocity, pressure, and hoop stress are concerned, however, the improved theory gave essentially the same results as Joukowsky's theory, which had been confirmed experimentally.

Recently, the method of characteristics was applied successfully to the numerical solutions of one-dimensional "water hammer" analysis (References 16 and 17), including the nonlinear terms for the convective acceleration and fluid friction. Similar nonlinear differential equations describing the unsteady motion of a viscous compressible fluid in tubes in terms of a hydraulic resistance were also applied to the self-induced oscillations of heavy fluids (Reference 18). In this reference, the fluid density term is assumed to be large, and the pressure gradient term is neglected, thus making it possible to reduce the problem to the solution of first-order quasilinear partial differential equations with nonperiodic boundary conditions.

The investigation of the pressure wave in the blood vessel was concerned primarily with the influence of the elasticity of the walls on the propagation of sound through the fluid medium in the vessel. Since the physiologists considered the distensibility of the tube to be of far greater importance than the compressibility of the fluid, the authors assumed an incompressible and viscous fluid (References 6 to 8). The stresses and shear are expressed in terms of the displacements, but the inertia terms

are neglected. The significance of the effect of viscosity and internal damping on the wave propagation is somewhat obscured in the authors' over-simplification of the complicated solution.

The approaches used in the hydraulic and pneumatic control systems are generally straightforward. Since pipe diameters are small, the elasticity of the pipe may be neglected; and, because the flow rate is usually low in the control system, the use of linearized equations with the laminar friction loss (References 9 to 11) is justified. The results of the theoretical frequency-response analysis compare quite well with the experimental data from the test.

In the present investigation, it is assumed that the propellant line connects the propellant tank and propellant pump. The diameter of the line is much larger than that of hydraulic control lines or blood vessels, but much smaller than the diameter of penstock in the lower plant. The source of disturbance may be either the fuel sloshing in the propellant tank or the variation of flow in the propellant pump. Another possibility is that the changes in the natural frequency of the missile structure at different flight times may also create unsteady flow in the fuel line.

The aim of this study is to determine analytically the general dynamic behavior of the unsteady motion and to construct a reasonable model that can be applied directly to the overall system analysis of longitudinal oscillations of large missiles.

SECTION 1. EQUATIONS OF UNSTEADY FLOW IN PIPES

If we consider the motion of the fluid in a pipe as a whole and introduce the average values of velocity u, density ρ, and pressure p over the cross-section A, the basic equations describing the unsteady motion of a viscous compressible fluid in an elastic tube in terms of a hydraulic resistance are the law of conservation of mass

$$\frac{\partial}{\partial x}(\rho u A) = -\frac{\partial}{\partial t}(\rho A) \tag{1}$$

and the law of momentum

$$\frac{\partial}{\partial t}(\rho u A) + \frac{\partial}{\partial x}(\rho u^2 A) = -A\frac{\partial p}{\partial x} - A\phi(u) \tag{2}$$

The function $\phi(u)$ is taken to be linear for laminar flow

$$\phi(u) = \frac{32\mu}{D^2}u, \quad \text{for} \quad R < 2000 \tag{3}$$

and quadratic for turbulent flow

$$\phi(u) = \frac{f}{2D}\rho u^2, \quad \text{for} \quad R > 2000 \tag{4}$$

where μ is the viscosity, D the inside diameter of the pipe, R the Reynolds number, and f the Darcy-Weisbach resistance coefficient.

To the above equations must be added the state equation for compressible flow

$$d\rho = \frac{\rho}{K_1}dp \tag{5}$$

where K_1 is the bulk modulus of the fluid which is defined as the change in pressure per unit change in specific volume.

If the pressure variation is small, Hooke's law can be considered valid for a liquid, i.e.,

$$\rho = \rho_o \left(1 + \frac{p - p_o}{K_1}\right) \tag{6}$$

$$d\rho = \frac{\rho_o}{K_1} dp \tag{7}$$

where the subscript "o" designates the variables at steady state.

1.1 VARIATION OF CROSS-SECTIONAL AREA OF A PIPE AS A FUNCTION OF PRESSURE

It will be assumed that the pipe has a thin elastic wall and is made of a material for which Hooke's law holds true. Let the initial pressure in the pipe be p and the radius be r. Then the tangential and axial forces per unit width are given by

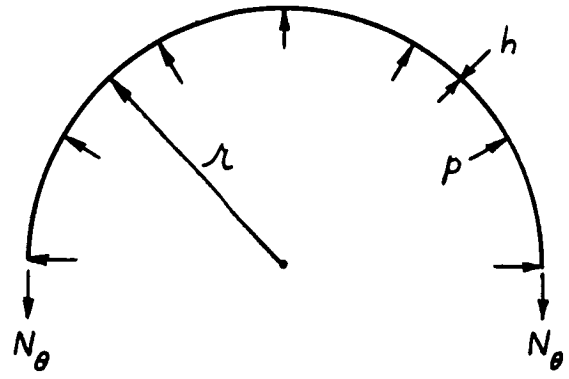

$$N_\theta = \sigma_\theta h = pr$$
$$N_x = \sigma_x h = C_1 pr \tag{8}$$

Figure 1.

and the tangential strain by

$$\epsilon_\theta = \frac{1}{E}(\sigma_\theta - \nu\sigma_x) = \frac{pr}{Eh}(1 - \nu C_1) \tag{9}$$

where $C_1 = 1/2$ for a pipe fixed at one end and free to move throughout the rest of its length, $C_1 = \nu$ for a pipe anchored against longitudinal movement along its length, and $C_1 = 0$ for a pipe having expansion joints between anchors throughout the length of the pipe.

When the internal pressure is varied, the tangential strain varies by

$$\delta\epsilon_\theta = \frac{\delta r}{r} = \frac{1}{Eh}(1 - \nu C_1)(p\delta r + r\delta p)$$

or

$$\delta r = \frac{r^2 \delta p (1 - \nu C_1)}{Eh - rp(1 - \nu C_1)}$$

Multiplying the above equation by $2\pi r$ and denoting $C = 1 - \nu C_1$, it becomes

$$\delta A = \frac{2rAC\delta p}{Eh - Crp} \tag{10}$$

From Equation (9), $Eh = (C/\epsilon_\theta)pr$. Since $\epsilon_\theta \ll 1$, the term Crp is negligible in comparison with the term Eh, and hence

$$dA = \frac{CDA}{Eh} dp \tag{11}$$

1.2 BASIC EQUATIONS OF UNSTEADY MOTION

Combining (1), (5) and (11) yields

$$-\left[\frac{1}{K_1} + \frac{CD}{Eh}\right] u \frac{\partial p}{\partial x} - \frac{\partial u}{\partial x} = \left[\frac{1}{K_1} + \frac{CD}{Eh}\right] \frac{\partial p}{\partial t} \tag{12}$$

Define

$$\frac{1}{a^2} = \rho\left[\frac{1}{K_1} + \frac{CD}{Eh}\right] = \rho \frac{1}{K} \tag{13}$$

where a is the velocity of pressure wave propagation in a fluid medium contained in an elastic pipe. Since the velocity of sound in the fluid is $a^2 = dp/d\rho = K_1/\rho$, the term CD/Eh is a correction of K_1, accounting for the elasticity of the pipe wall. Equation (12) now becomes

$$\frac{\partial p}{\partial t} + u \frac{\partial p}{\partial x} = -\rho a^2 \frac{\partial u}{\partial x} \tag{14}$$

From (1) and (2), we have

$$\frac{\partial u}{\partial t} + u \frac{\partial u}{\partial x} = -\frac{1}{\rho}\frac{\partial p}{\partial x} - \frac{1}{\rho}\phi(u) \tag{15}$$

Equations (14) and (15) are the basic equations of unsteady motion in an elastic pipe. For small pressure variations, the value of ρ in the above equations may be considered to be equal to ρ_o of the steady state.

In the case where the effect of missile acceleration a_m and the angle, θ, which the pipe makes with the horizontal are to be taken into consideration, the term $a_m \sin\theta$ has to be added to Equation (15); i.e.,

$$\frac{\partial u}{\partial t} + u\frac{\partial u}{\partial x} = -\frac{1}{\rho}\frac{\partial p}{\partial x} - \frac{1}{\rho}\phi(u) + a_m \sin\theta \qquad (15a)$$

1.3 INITIAL AND BOUNDARY CONDITIONS

It will be assumed, in this treatment of unsteady fluid motion in pipes, that up to the moment $t = 0$ the fluid is in steady motion; i.e.,

$$\begin{aligned} u(x,o) &= u_o \\ p(x,o) &= p_o \end{aligned} \qquad (16)$$

The boundary conditions depend on the nature of the disturbance of flow at the boundaries. The following boundary conditions are expected to be encountered in the present problem: (1) at one end of the pipe the pressure is given as a function of time (as a particular case, this pressure may be constant); (2) at the other end of the pipe a device is connected which varies the flow rate of the fluid with time according to some known law—this may be a pump, turbine, etc. This device may be connected either directly to the pipe or through a chamber serving to regulate the flow rate or to diminish the pressure oscillations. The boundary conditions in such cases as these can be written functionally as

$$x = o \qquad p(o,t) = p_o + f(t) \qquad (17a)$$

$$x = \ell \qquad \kappa\frac{\partial}{\partial x}Q(\ell,t) + Q(\ell,t) = g(t) \qquad (17b)$$

where $f(t)$ and $g(t)$ are given functions, with

$$f(t) = g(t) = 0 \quad \text{at } t \le 0$$

Q is the mass flow rate and κ is a positive constant characterizing the type of chamber in those cases where a chamber is present.

The boundary conditions of three cases at $x = \ell$ when the pipe is connected to a chamber designed to reduce the pressure oscillations will be discussed in the following paragraphs.

1.3.1 Air Chamber

Let p and V be the pressure and volume of the air in the vessel, and let p_o and V_o be their steady flow values. If the compression of the air in the chamber is considered as isothermal, then

$$pV = p_o V_o \tag{18}$$

During unsteady flow the increase in the quantity of liquid in the vessel will be

$$\rho_o \frac{d(V_o - V)}{dt} = (\rho u A)_{x=\ell} - Q_1(t) \tag{19}$$

where $(\rho u A)_{x=\ell} = Q$ is the mass flow rate of the liquid out of the pipe and into the air vessel, and $Q_1(t)$ is the mass discharge rate of the liquid from the vessel.

For small pressure variations, it is permissible to use the linearized continuity equation. From (18), (14), and (13) it follows:

$$\frac{dV}{dt} = -\frac{p_o V_o}{p^2} \frac{\partial p}{\partial t} \approx \frac{V_o}{p_o} \frac{K}{\rho_o A_o} \frac{\partial Q}{\partial x} \tag{20}$$

The substitution of (20) into (19) gives the following boundary conditions at $x = \ell$:

$$\frac{V_o K}{p_o A_o} \frac{\partial Q}{\partial x} + Q = Q_1(t) \tag{21}$$

1.3.2 Surge Tank

If the same notation is used, then the rate of increase of the liquid volume in the surge tank is

$$\rho_o \frac{dV}{dt} = Q_{x=\ell} - Q_1(t) \tag{22}$$

where

$V = \eta A_s$

η = the increase of liquid level in the surge tank

A_s = cross-sectional area of the tank

The increase in pressure of the liquid in the tank will be

$$p - p_o = \rho_o g \eta = \rho_o g \frac{V}{A_s}$$

$$\frac{dV}{dt} = \frac{A_s}{\rho_o g} \frac{\partial p}{\partial t} = \frac{A_s}{\rho_o g} \left(\frac{-K}{\rho_o A_o} \frac{\partial Q}{\partial x} \right)$$

Hence the boundary condition at $x = \ell$ will have the form

$$\frac{A_s}{A_o} \frac{K}{\rho_o g} \frac{\partial Q}{\partial x} + Q = Q_1(t) \tag{23}$$

1.3.3 Tank-Type Damper

The variation of the mass rate of the liquid contained in the damping tank is

$$\frac{d\rho V}{dt} = (\rho A u)_{x=\ell} - Q_1(t) \tag{24}$$

where V is the volume of the tank, $Q_{x=\ell} = (\rho A u)_{x=\ell}$ is the mass of liquid passing from the pipe into the tank, and $Q_1(t)$ is the mass discharge rate.

If the tank volume is $V = A_d L$ with the variation of tank length being assumed small, then

$$\frac{d\rho V}{dt} = V \frac{d\rho}{dt} + \rho L \frac{dA_d}{dt} \tag{25}$$

From (20), (7), and (11)

$$\frac{\partial p}{\partial t} = -\frac{K}{\rho_o A_o}\frac{\partial Q}{\partial x}, \quad \frac{\partial \rho}{\partial t} = \frac{\rho_o}{K_1}\frac{\partial p}{\partial t}, \quad \frac{\partial A_d}{\partial t} = \frac{C_d D_d A_d}{Eh}\frac{\partial p}{\partial t}$$

then

$$\frac{d\rho V}{dt} = -KL\frac{A_d}{A_o}\left(\frac{1}{K_1} + \frac{C_d D_d}{Eh_d}\right)\frac{\partial Q}{dx} \tag{26}$$

where A_d, D_d and C_d are the cross-sectional area, diameter, and the end restraint constant of the damper, respectively.

The boundary condition for $x = \ell$ will be

$$KL\frac{A_d}{A_o}\left(\frac{1}{K_1} + \frac{C_d D_d}{Eh_d}\right)\frac{\partial Q}{\partial x} + Q = Q_1(t) \tag{27}$$

SECTION 2. SOLUTION OF EQUATIONS OF UNSTEADY MOTION BY LINEARIZATION

For small pressure variations, the equations of unsteady motion in an elastic pipe with turbulent friction losses from (14) and (15) are

$$\frac{\partial p}{\partial t} + u \frac{\partial p}{\partial x} = -\rho_o a^2 \frac{\partial u}{\partial x} \tag{28}$$

$$\frac{\partial u}{\partial t} + u \frac{\partial u}{\partial x} = -\frac{1}{\rho_o} \frac{\partial p}{\partial x} - \frac{f}{2D} u^2 \tag{29}$$

Let

$$\left.\begin{aligned} p = p_o + \Delta p \quad &\text{or written simply as} \quad p = p_o + p \\ u = u_o + \Delta u \quad &\text{or written simply as} \quad u = u_o + u \end{aligned}\right\} \tag{30}$$

Equations (28) and (29) yield the following sets of equations for the steady and the perturbed motions.

$$u_o \frac{\partial p_o}{\partial x} = -\rho_o a^2 \frac{\partial u_o}{\partial x} \tag{31}$$

$$u_o \frac{\partial u_o}{\partial x} = -\frac{1}{\rho_o} \frac{\partial p_o}{\partial x} - \frac{f}{2D} u_o^2 \tag{32}$$

$$\frac{\partial p}{\partial t} + (u_o + u)\left(\frac{\partial p_o}{\partial x} + \frac{\partial p}{\partial x}\right) = -\rho_o a^2 \left(\frac{\partial u_o}{\partial x} + \frac{\partial u}{\partial x}\right) \tag{33}$$

$$\frac{\partial u}{\partial t} + (u_o + u)\left(\frac{\partial u_o}{\partial x} + \frac{\partial u}{\partial x}\right) = -\frac{1}{\rho_o}\left(\frac{\partial p_o}{\partial x} + \frac{\partial p}{\partial x}\right) - \frac{f}{2D}(u_o + u)^2 \tag{34}$$

Considering the steady-state values of p_o and u_o to be known and their variations along the x-axis small, then the perturbed equations after neglecting terms of higher order will be

$$\frac{\partial p}{\partial t} + u_o \frac{\partial p}{\partial x} = -\rho_o a^2 \frac{\partial u}{\partial x} \tag{35}$$

$$\frac{\partial u}{\partial t} + u_o \frac{\partial u}{\partial x} = -\frac{1}{\rho_o} \frac{\partial p}{\partial x} - ku \tag{36}$$

where

$$k = \frac{fu_o}{D_o} = k_t \qquad \text{for turbulent friction loss and}$$

$$k = \frac{32\mu}{\rho_o D_o^2} = k_\ell \quad \text{for laminar friction loss}$$

Using Laplace transform and the assumption of zero initial conditions

$$p(x, 0) = 0, \qquad u(x, 0) = 0 \tag{37}$$

Equations (35) and (36) become

$$sP + u_o \frac{\partial P}{\partial x} = -\rho_o a^2 \frac{\partial U}{\partial x} \tag{38}$$

$$(s + k)U + u_o \frac{\partial U}{\partial x} = -\frac{1}{\rho_o} \frac{\partial P}{\partial x} \tag{39}$$

or upon differentiation,

$$u_o \frac{\partial^2 P}{\partial x^2} + s \frac{\partial P}{\partial x} = -\rho_o a^2 \frac{\partial^2 U}{\partial x^2} \tag{40}$$

$$u_o \frac{\partial^2 U}{\partial x^2} + (s + k) \frac{\partial U}{\partial x} = -\frac{1}{\rho_o} \frac{\partial^2 P}{\partial x^2} \tag{41}$$

After some algebraic manipulation between Equations (38) through (41), we have two decoupled differential equations, one for U(x, s) and one for P(x, s).

$$(a^2 - u_o^2)\frac{\partial^2 U}{\partial x^2} - u_o(2s + k)\frac{\partial U}{\partial x} - s(s + k)\,U = 0 \tag{42}$$

$$(a^2 - U_o^2)\frac{\partial^2 P}{\partial x^2} - u_o(2s + k)\frac{\partial P}{\partial x} - s(s + k)\,P = 0 \tag{43}$$

Let

$$\left.\begin{aligned} U(x, s) &= A(s)\, e^{mx} \\ P(x, s) &= B(s)\, e^{mx} \end{aligned}\right\} \tag{44}$$

where m is determined by the characteristic equation

$$(a^2 - u_o^2)m^2 - u_o(2s + k)m - s(s + k) = 0 \tag{45}$$

$$m = \frac{u_o(2s + k) \pm \sqrt{u_o^2 k^2 + 4a^2 s(s + k)}}{2(a^2 - u_o^2)} \tag{46}$$

Hence

$$\left.\begin{aligned} U &= A_1\, e^{m_1 x} + A_2\, e^{m_2 x} \\ P &= B_1\, e^{m_1 x} + B_2\, e^{m_2 x} \end{aligned}\right\} \tag{47}$$

The relations between A and B can be determined by putting (47) into (38) and (39)

$$\left[A_1\rho_o a^2 m_1 + B_1 u_o m_1 + B_1 s\right]e^{m_1 x} + \left[A_2\rho_o a^2 m_2 + B_2 u_o m_2 + B_2 s\right]e^{m_2 x} = 0$$

$$\left[A_1 u_o m_1 + \frac{B_1}{\rho_o} m_1 + A_1(s + k)\right]e^{m_1 x} + \left[A_2 u_o m_2 + \frac{B_2}{\rho_o} m_2 + A_2(s + k)\right]e^{m_2 x} = 0$$

Since

$$e^{m_1 x} \neq 0, \qquad e^{m_2 x} \neq 0$$

we have

$$B_1 = -A_1 \left[\frac{\rho_o a^2 m_1}{u_o m_1 + s}\right] \qquad B_2 = -A_2 \left[\frac{\rho_o a^2 m_2}{u_o m_2 + s}\right]$$

$$B_1 = -A_1 \left[\frac{\rho_o (u_o m_1 + s + k)}{m_1}\right] \qquad B_2 = -A_2 \left[\frac{\rho_o (u_o m_2 + s + k)}{m_2}\right]$$

Hence

$$\frac{\rho_o a^2 m}{u_o m + s} = \rho_o u_o + \rho_o \frac{s + k}{m} = \begin{cases} I_1, & \text{for } m = m_1 \\ I_2, & \text{for } m = m_2 \end{cases} \tag{48}$$

and

$$\left.\begin{aligned} U(x, s) &= A_1 e^{m_1 x} + A_2 e^{m_2 x} \\ P(x, s) &= -A_1 I_1 e^{m_1 x} - A_2 I_2 e^{m_2 x} \end{aligned}\right\} \tag{49}$$

Let the boundary condition at x = 0 be

$$U(o, s) = U_o(s) \qquad P(o, s) = P_o(s)$$

When applied to (49), it yields

$$\left.\begin{aligned} U_o &= A_1 + A_2 \\ P_o &= -A_1 I_1 - A_2 I_2 \end{aligned}\right\} \Longrightarrow \begin{cases} A_1 = \dfrac{P_o + U_o I_2}{I_2 - I_1} \\ A_2 = \dfrac{P_o + U_o I_1}{I_1 - I_2} \end{cases}$$

Hence

$$\left.\begin{aligned} U(x,s) &= \frac{P_o + U_o I_2}{I_2 - I_1} e^{m_1 x} - \frac{P_o + U_o I_1}{I_2 - I_1} e^{m_2 x} \\ P(x,s) &= \frac{I_1(P_o + U_o I_2)}{I_2 - I_1} e^{m_1 x} + \frac{I_2(P_o + U_o I_1)}{I_2 - I_1} e^{m_2 x} \end{aligned}\right\} \tag{50}$$

At $x = \ell$

$$U_\ell = U_o\left[\frac{I_2}{I_2 - I_1} e^{m_1 \ell} - \frac{I_1}{I_2 - I_1} e^{m_2 \ell}\right] + P_o\left[\frac{1}{I_2 - I_1}(e^{m_1 \ell} - e^{m_2 \ell})\right] \tag{51}$$

$$P_\ell = U_o\left[\frac{I_1 I_2}{I_2 - I_1}(e^{m_2 \ell} - e^{m_1 \ell})\right] + P_o\left[\frac{I_2}{I_2 - I_1} e^{m_2 \ell} - \frac{I_1}{I_2 - I_1} e^{m_1 \ell}\right]$$

Let G(s) be the transfer matrix defined by

$$G(s) = \begin{pmatrix} \frac{I_2}{I_2 - I_1} e^{m_1 \ell} - \frac{I_1}{I_2 - I_1} e^{m_2 \ell} & \frac{1}{I_2 - I_1}(e^{m_1 \ell} - e^{m_2 \ell}) \\ \frac{I_1 I_2}{I_2 - I_1}(e^{m_2 \ell} - e^{m_1 \ell}) & \frac{I_2}{I_2 - I_1} e^{m_2 \ell} - \frac{I_1}{I_2 - I_1} e^{m_1 \ell} \end{pmatrix} \tag{52}$$

then (50) can be written as

$$\begin{Bmatrix} U_\ell \\ P_\ell \end{Bmatrix} = G(s) \begin{Bmatrix} U_o \\ P_o \end{Bmatrix} \tag{53}$$

which represents the dynamic characteristics of the unsteady friction flow in an elastic line.

From (53), we have the following relations:

$$\frac{U_o(s)}{P_o(s)} = \frac{\left(\frac{U_\ell}{P_\ell} I_2 + 1\right) e^{m_2 \ell} - \left(\frac{U_\ell}{P_\ell} I_1 + 1\right) e^{m_1 \ell}}{\left(\frac{U_\ell}{P_\ell} I_1 + 1\right) I_2 e^{m_1 \ell} - \left(\frac{U_\ell}{P_\ell} I_2 + 1\right) I_1 e^{m_2 \ell}}, \tag{54}$$

$$\frac{P_\ell(s)}{P_o(s)} = \frac{(I_2 - I_1) e^{(m_1+m_2)\ell}}{\left(\frac{U_\ell}{P_\ell} I_1 + 1\right) I_2 e^{m_1 \ell} - \left(\frac{U_\ell}{P_\ell} I_2 + 1\right) I_1 e^{m_2 \ell}} \tag{55}$$

$$\frac{U_\ell(s)}{U_o(s)} = \frac{\frac{U_\ell}{P_\ell} (I_2 - I_1) e^{(m_1+m_2)\ell}}{\left(\frac{U_\ell}{P_\ell} I_2 + 1\right) e^{m_2 \ell} - \left(\frac{U_\ell}{P_\ell} I_1 + 1\right) e^{m_1 \ell}} \tag{56}$$

where m_1, m_2, I_1 and I_2 are functions of s as defined in Equations (46) and (48).

Substituting $s = j\omega$ in (54) to (56), we can compute the magnitude and phase angle of

(a) the ratio of velocity to pressure deviations, $\frac{U_o(j\omega)}{P_o(j\omega)}$, at $x = 0$, versus frequency

(b) the ratio of pressure deviation at $x = \ell$ to pressure deviation at $x = 0$ $\frac{P_\ell(j\omega)}{P_o(j\omega)}$, versus frequency.

(c) the ratio of velocity deviation at $x = \ell$ to velocity deviation at $x = 0$, $\frac{U_\ell(j\omega)}{U_o(j\omega)}$, versus frequency.

The boundary condition at $x = \ell$ is

$$A_1 E \frac{\partial}{\partial x} z(\ell, t) + \zeta \frac{\partial}{\partial t} z(\ell, t) = p_\ell (A - A_{pi}) \tag{62}$$

where A is the cross-sectional area of pipe, A_1, the cross-sectional area of pipe wall, A_{pi} the cross-sectional area of pump inlet and ζ the coefficient of damping of the bellow. The Laplace transform of (62) is

$$A_1 E \frac{\partial}{\partial x} Z(x, s) \Big|_{x=\ell} + \zeta s Z(x, s) \Big|_{x=\ell} = p_\ell(s)[A - A_{pi}] \tag{63}$$

Substituting

$$Z(x, s) \Big|_{x=\ell} = B(s) \sinh \sqrt{\frac{a}{E}} s x \Big|_{x=\ell} \tag{64}$$

into the above equation and solving for B(s), we have

$$B(s) = \frac{P_\ell(s) [A - A_{pi}]}{A_1 E \, s \sqrt{\frac{a}{E}} \cosh \sqrt{\frac{a}{E}} s\ell + \zeta \, s \sinh \sqrt{\frac{a}{E}} s\ell} \tag{65}$$

Hence, (64) becomes

$$Z(\ell, s) = \frac{P_\ell(s) [A - A_{pi}]}{S \left[A_1 E \sqrt{\frac{a}{E}} \coth \sqrt{\frac{a}{E}} s\ell + \zeta\right]} \tag{66}$$

The transfer function relating the velocity at $x = \ell$ to the pressure at $x = \ell$ is

$$\frac{s \, Z(\ell, s)}{P_\ell(s)} = \frac{A - A_{pi}}{A_1 E \sqrt{\frac{a}{E}} \coth \sqrt{\frac{a}{E}} s\ell + \zeta} \tag{67}$$

This factor is to be added to the term U_ℓ / P_ℓ in Equations (54), (55), and (56). The deviations in magnitude and phase which occur near the natural frequency of the longitudinal vibrations of the pipe can be seen from the computational results shown in Appendix A.

2.2 PHYSICAL CONSTANTS AND RESULTS OF LINEARIZED ANALYSIS

The following physical constants are based mostly on information applicable to Saturn S-II Stage.

Table I

	Constant	Values for LH_2 Line
r	internal radius of pipe (D = 2r)	0.333 ft.
ℓ	length of pipe between tank and pump	20.83 ft. (outboard) 31.92 ft. (center
a	velocity of pressure wave $a = \frac{1}{\sqrt{\rho \frac{1}{K_1} + \frac{CD}{Eh}}}$	3700 ft/sec
ρ	density of fluid at steady state	0.136 lb-sec^2/ft^2
K_1	bulk modulus of fluid	2.15×10^6 lb/ft^2
h	thickness of pipe wall	1.83×10^{-3} ft
E	Young's modulus of pipe wall	4.32×10^9 lb/ft^2
α	density of pipe wall	14.8 lb-sec^2/ft^4
A	cross-sectional area of pipe	0.348 ft^2
A_h	cross-sectional area of pipe wall	0.00383 ft^2
A_{pi}	cross-sectional area of pump inlet	0.256 ft^2
C	restriction factor of pipe	0.85
ν	Poisson's ratio of pipe wall	0.30
ζ	damping coefficient of bellow	0 (assumed)
μ	viscosity of fluid	0.029×10^{-5} lb-sec/ft^2
u_o	steady-state fluid velocity	51.5 ft/sec

Table I (Cont)

Constant		Values for LH_2 Line
$\frac{U_\ell}{P_\ell}$	steady-state velocity-pressure ratio (determined from the steady-state pressure versus flow curve)	1.55×10^{-4} per sec
k_ℓ	laminar resistance coefficient $k_\ell = 32\mu/\rho_o D^2$	1.55×10^{-4} per sec
f	Darcy-Weisback resistance coeff.	0.0775 (outboard) 0.059 (center)
k_t	turbulent resistance coefficient $k_t = \frac{fu_o}{D}$	5.98 per sec (outboard) 4.54 per sec (center)

With the above information the frequency response equations (54), (55), and (56) were programmed on the IBM 7094 for both LOX and LH_2 lines. The numerical results for the outboard LH_2 line of S-II stage are illustrated in Appendix A, Figures A-1 through A-12. The magnitude and phase angle of $U_o(j\omega)/P_o(j\omega)$ versus ω are shown in Figures A-1 through A-4 according to the type of hydraulic resistances and with or without the effect of line vibrations. Similarly, the magnitude and phase angle of $P_\ell(j\omega)/P_o(j\omega)$ versus ω are shown in Figures A-5 through A-8. The magnitude and phase angle of $U_\ell(j\omega)/U_o(j\omega)$ versus ω are shown in Figures A-9 through A-12.

SECTION 3. SOLUTION OF NONLINEAR EQUATIONS OF UNSTEADY MOTION BY THE METHOD OF CHARACTERISTICS

The transient pressure of unsteady flow with a turbulent resistance in an elastic pipe undergoing an acceleration a_m requires the solution of the two nonlinear partial differential Equations (14) and (15a).

$$\frac{\partial p}{\partial t} + u\frac{\partial p}{\partial x} = -\rho a^2 \frac{\partial u}{\partial x} \tag{68}$$

$$\frac{\partial u}{\partial t} + u\frac{\partial u}{\partial x} = \frac{1}{\rho}\frac{\partial p}{\partial x} - \frac{f}{2D}u^2 + a_m \sin\theta \tag{69}$$

The governing equations cannot be solved analytically. However, these two equations can be transformed into a set of ordinary differential equations by the method of characteristics and then solved numerically.

Define a characteristic curve of Equations (68) and (69) to be a curve along which a solution of Equations (68) and (69) may have discontinuities in the derivatives of the velocity and pressure. Suppose that such a curve is given by

$$x = x(s), \qquad t = t(s) \tag{70}$$

and that u and p are prescribed at each point of this curve. Then u and p become functions of s and we have a system of four equations in four unknown partial derivatives u_x, u_t, p_x and p_t. These four equations are

$$\frac{\partial u}{\partial t} + u\frac{\partial u}{\partial x} + \frac{1}{\rho}\frac{\partial p}{\partial x} = -\frac{f}{2D}u^2 + a_m \sin\theta$$

$$\rho a^2 \frac{\partial u}{\partial x} + \frac{\partial p}{\partial t} + u\frac{\partial p}{\partial x} = 0$$

(continued on next page)

$$\frac{\partial u}{\partial t} dt + \frac{\partial u}{\partial x} dx = du$$

$$\frac{\partial p}{\partial t} dt + \frac{\partial p}{\partial x} dx = dp \qquad (71)$$

The discontinuity relation requires that there be at least two distinct sets of values of these derivatives which satisfy Equations (71). The conditions under which Equations (71) will admit of more than one solution require that

$$\begin{vmatrix} 1 & u & 0 & \frac{1}{\rho} \\ 0 & \rho a^2 & 1 & u \\ dt & dx & 0 & 0 \\ 0 & 0 & dt & dx \end{vmatrix} = 0 \qquad (72)$$

and

$$\begin{vmatrix} 1 & u & 0 & -\frac{fu^2}{2D} + a_m \sin\theta \\ 0 & \rho a^2 & 1 & 0 \\ dt & dx & 0 & du \\ 0 & 0 & dt & dp \end{vmatrix} = 0 \qquad (73)$$

Expanding these determinants (72) gives

$$\frac{dx}{dt} - u = \pm a \qquad (74)$$

and (73) gives

$$\frac{du}{dt} + \frac{f}{2D} u^2 - a_m \sin\theta + \frac{1}{\rho a^2} \left(\frac{dx}{dt} - u \frac{dp}{dt} \right) = 0 \qquad (75)$$

Putting the relation (74) into (75), it becomes

$$\frac{du}{dt} + \frac{f}{2D}u^2 - a_m \sin\theta \pm \frac{1}{\rho a}\frac{dp}{dt} = 0 \qquad (76)$$

In these equations where the ± sign appears, the plus sign is associated with the characteristic C^+ and the minus sign with the characteristic C^-.

Equations (74) define the slope of the characteristics C^+ and C^- as a function of velocity of flow, u, and the velocity of pressure wave, a. Equations (76) are the compatibility equation relating the velocity u and pressure p along the characteristic lines C^+ and C^-.

Equations (76) are two separate, total differential equations with t as independent variable and u and p as dependent variables. If $u = u(x, t)$ and $p = p(x, t)$ satisfies Equations (68) and (69) then Equations (74) determine two families of characteristic curves C^+ and C^- in the x, t plane belonging to the solution $u(x, t)$ and $p(x, t)$. These four Equations (74) and (76) can be solved by finite difference approximations with appropriate initial and boundary conditions.

3.1 SPECIFIED TIME INTERVALS

There are two ways in which the characteristic curves C^+ and C^- may be used to obtain an approximate numerical solution to the original partial differential equations. One method involves the use of a grid of characteristics and the other makes use of specified time intervals. In using the former method, it would be difficult to arrange the computations so that the points of intersection of the characteristics occurred at values of x and t on a rectangular grid. The use of specified time intervals has one main advantage over the use of a grid of characteristics in that it provides results of the flow field at different times. Hence, from a programming viewpoint, the ordering of the computations would appear to be easier by this method than by the use of a characteristic grid, since the values of the dependent variables are known at predetermined points and the additional information of the corresponding x and t coordinates does not have to be recorded. For this reason, this is the approach which will be used in the present analysis.

3.2 SELECTING MESH RATIO

The first step in using the method of specified time intervals requires selecting a mesh ratio $\Delta t/\Delta x$ for the finite difference approximation. The

selection of an "admissible" mesh ratio plays a vital part in the success of the numerical process. It insures that the difference equations actually do approximate the differential equations so that a numerical solution of the former should be a good approximation to the exact solution.

The region bounded by the two characteristics C^+ and C^-, and a third non-characteristic curve such as PRCS shown in Figure 2 is a region in which a unique solution to the original partial differential equations would exist provided conditions along RCS are prescribed. Thus, it is only logical to select a mesh ratio such that the solution will lie within this "zone of influence." This condition will be satisfied if the mesh ratio is less than the slope of the characteristic curves as given by Equation (74), since geometrically the mesh ratio plays the role of "finite difference characteristics." Under this conditon, the finite difference scheme should be a valid representation of the differential Equations (14) and (15a).

If the variation in the velocity of wave propagation is assumed small so that it may be taken equal to its steady-state value a_o, then for

$$\frac{\Delta t}{\Delta x} \leq \frac{1}{u \pm a_o} \tag{77}$$

we would expect the solution of the difference equations to tend to that of the differential equations as $\Delta t \rightarrow 0$. Geometrically, this means that R must lie within AC and S within BC in Figure 2. The condition given by Equation (77) also insures the stability of the numerical process. Since the

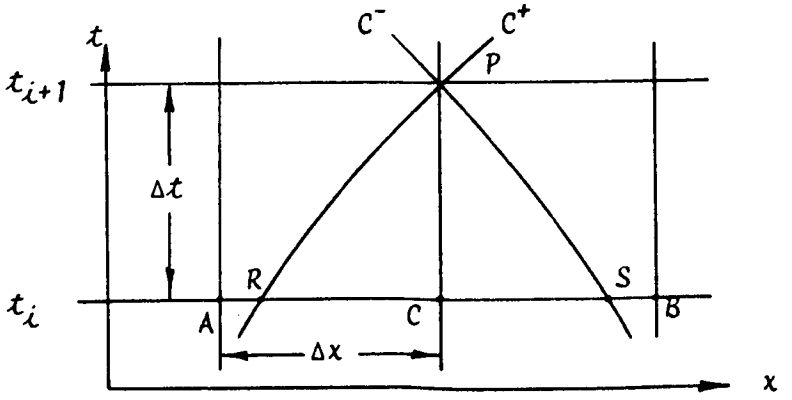

Figure 2.

velocity $u << a_o$, the criteria used in the present study for selecting the mesh ratio was

$$\frac{\Delta t}{\Delta x} < \frac{1}{a_o}$$

The accuracy of the finite approximations deteriorates if the mesh ratio is much less than $1/a_o$ although their solution will be stable. Optimum accuracy is obtained when the finite difference characteristics coincide with the continuous characteristics of the governing differential equations. For a system whose true characteristics are curved such as in the present case, the optimum accuracy cannot be obtained using a fixed rectangular grid since the finite difference characteristics must necessarily have smaller slopes than the true characteristics to ensure stability of the numerical process.

3.3 COMPUTATIONAL PROBLEM

The computational problem which must be dealt with is illustrated in Figure 2. On the rectangular grid in the x, t plane as shown here, the velocity and pressure are known at each mesh point, such as A, B, and C for time t_1, either as given initial conditions or as a result of a previous stage of the calculations. The problem is to determine the conditions (velocity and pressure) at a typical point P corresponding to time $t_i + 1$. The coordinates of point P in the x, t plane are therefore known. Through this known point, we pass the two characteristic curves C^+ and C^-, intersecting the line $t = t_i$ at points R and S respectively. Both the velocity and pressure are unknown at the three points P, R, and S, and the space variable is unknown at the latter two points, giving a total of eight unknowns.

3.4 INTERPOLATION FORMULAS

In the analysis to follow, the various variables associated with a given point will have that point's designation used as a subscript, such as u_A, P_A, x_A, . . . , etc.

Since the characteristics C^+ and C^- pass through points R and S respectively, expressions are needed for the velocity and pressure at these two points in order to compute the condition at P using these two curves. This is done by fitting a parabola through the known values at A, C, and B, and then interpolating. For example, let us consider the case of calculating the velocity u_R at point R. (See Figure 3.)

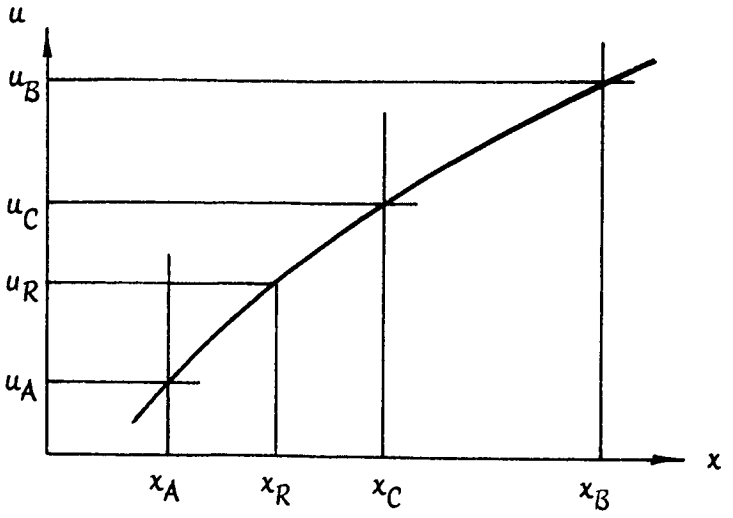

Figure 3.

Using the second order equation

$$u(x) = a + b(x - x_C) + c(x - x_C)^2 \tag{78}$$

and applying it to the three points x_A, x_B, and x_C where the velocities are known, we obtain three algebraic equations for determining the coefficients a, b, and c. Applying Equation (78) to $x = x_C$ shows immediately that

$$a = u_C \tag{79}$$

Application to the remaining two points yields

$$u_A = a + b(x_A - x_C) + c(x_A - x_C)^2 \tag{80}$$

$$u_B = a + b(x_B - x_C) + c(x_B - x_C)^2 \tag{81}$$

Since successive mesh points along the x axis are Δx units apart, we can express x_A and x_B in terms of x_C as

$$x_A = x_C - \Delta x$$

$$x_B = x_C + \Delta x$$

On substituting these two relations into Equations (80) and (81), they become

$$u_A = a - b \cdot \Delta x + c(\Delta x)^2 \tag{82}$$

$$u_B = a + b \cdot \Delta x + c(\Delta x)^2 \tag{83}$$

Making use of the result given by Equation (79) and solving Equations (82) and (83) simultaneously, we find that

$$b = \frac{1}{2\Delta x}(u_B - u_A) \tag{84}$$

$$c = \frac{1}{2(\Delta x)^2}(u_A + u_B - 2u_C) \tag{85}$$

With the three coefficients a, b, and c determined, we apply Equation (78) to $x = x_R$ and obtain

$$u_R = u_C + \frac{1}{2\Delta x}(u_B - u_A)(x_R - x_C) + \frac{1}{2(\Delta x)^2}(u_A + u_B - 2u_C)(x_R - x_C)^2 \tag{86}$$

The same functional form given by Equation (78) is also assumed for the pressure variation between the three adjacent points x_A, x_B, and x_C. Under this assumption, the coefficients given by Equations (79), (84), and (85) are valid provided that the velocities u_A, u_B, and u_C are replaced

respectively by the corresponding pressures p_A, p_B, and p_C. Thus, the following quadratic interpolation relationships can be written down immediately:

$$p_R = p_C + \frac{1}{2\Delta x}(p_B - p_A)(x_R - x_C) + \frac{1}{2(\Delta x)^2}(p_A + p_B - 2p_C)(x_R - x_C)^2 \quad (87)$$

$$u_S = u_C + \frac{1}{2\Delta x}(u_B - u_A)(x_S - x_C) + \frac{1}{2(\Delta x)^2}(u_A + u_B - 2u_C)(x_S - x_C)^2 \quad (88)$$

$$p_S = p_C + \frac{1}{2\Delta x}(p_B - p_A)(x_S - x_C) + \frac{1}{2(\Delta x)^2}(p_A + p_B - 2p_C)(x_S - x_C)^2 \quad (89)$$

These four equations form a necessary part in the computational scheme. The other four equations needed to obtain a solution are given by the characteristic Equations (74) and (76).

3.5 FINITE DIFFERENCE APPROXIMATION

Let us confine our immediate attention to the two characteristic equations associated with the characteristic C^+; i.e., we consider the plus sign in Equations (74) and (76). These two equations are transposed into finite difference form by replacing the differential coefficient by a divided difference over an interval and replacing the other variables by the arithmetic mean over the interval. This finite difference approximation is one of second order, and hence it is compatible with the interpolation formulas given in Equations (86) through (89).

On applying the foregoing procedure to Equations (74) and (76), and transposing, we obtain

$$x_R = x_C - \left(\frac{u_R + u_P}{2} + a_o\right)\Delta t \quad (90)$$

$$u_P - u_R + \frac{f}{8D}(u_R + u_P)^2\Delta t - a_m \sin\theta \cdot \Delta t + \frac{p_P - p_R}{\rho_o a_o} = 0 \quad (91)$$

It is assumed that the friction coefficient is a constant, and furthermore, that the variations in density and velocity of wave propagation are sufficiently small so that they may be taken equal to their respective value at steady-state conditions. The subscript "o" refers to steady-state values.

Similarly, the corresponding equations associated with the characteristic C^- are

$$x_S = x_C - \left(\frac{u_S + u_P}{2} - a_o\right)\Delta t \tag{92}$$

$$u_P - u_S + \frac{f}{8D}(u_S + u_P)^2 \Delta t - a_m \sin\theta \cdot \Delta t - \frac{p_P - p_S}{\rho_o a_o} = O \tag{93}$$

The above four equations, together with the four interpolation formulas, Equations (86) through (89), form a set of eight nonlinear simultaneous algebraic equations for the determination of the eight unknowns x_R, u_R, p_R, x_S, u_S, p_S, u_P and p_P. The problem now is to organize a computational tional procedure suitable for solving these eight equations on a digital computer. Without resorting to a simultaneous solution of these eight equations, the most practical way would be by iteration.

SECTION 4. COMPUTATIONAL PROCEDURE

One method of obtaining the conditions at point P by iteration using the nonlinear algebraic equations (86) through (93) is the following:

1. Make an estimate of the conditions at R, S, and P by assuming that they are the same as those existing at C. In other words,

$$u_R^o = u_S^o = u_P^o = u_C$$

$$p_R^o = p_S^o = p_P^o = p_C$$

The superscript "o" refers to the initial guess, or zeroth approximation.

2. Using these estimates, calculate x_R^o and x_S^o from Equations (90) and (92), respectively.

3. Making use of the results in step 2, calculate u_R^1, p_R^1, u_S^1, and p_S^1 from Equations (86) through (89) inclusive, respectively.

4. With the values obtained thus far for the first iteration, solve Equations (91) and (93) simultaneously for u_P^1 and p_P^1.

The foregoing process is continued until successive values for both velocity and pressure at point P are within the prescribed tolerance.

4.1 INITIAL CONDITIONS

In order to start the computational procedure, as outlined above, we must have the initial conditions corresponding to time t = 0. The initial conditions in the propellant line are taken as those corresponding to the steady-state condition. Due to friction losses along the length of the propellant line, the pressure at each mesh point on the x-axis must necessarily be different from one mesh point to another. The friction coefficient can be calculated from the experimental data that gives pipe resistance versus flow rate. It is tacitly assumed that this friction coefficient obtained under steady-state conditions is applicable to transient phenomena and also remains a constant throughout the line.

Within the framework of one-dimensional flow, the velocity u in the line must be a constant in the case of steady flow. This is immediately apparent from the continuity Equation (1) when one invokes the condition of steady flow whereby the flow field is independent of time, and hence, reducing it to

$$\frac{\partial}{\partial x}(\rho\, u\, a) = 0$$

Since we are considering propellant lines of constant cross-sections and ignoring any variation in ρ, it is readily seen that u must be a constant. Under this condition, the equation of motion given by Equation (15a) reduces to

$$\frac{1}{\rho_o}\frac{dp}{dx} + \frac{f}{D}\cdot\frac{u_o^2}{2} - a_m \sin\theta = 0$$

On integrating this equation and applying the result to two consecutive mesh points, we have

$$p_1 - p_2 = \rho_o \ell\left(\frac{f}{D}\frac{u_o^2}{2} - a_m \sin\theta\right) \tag{94}$$

where the subscript "1" designates the upstream mesh point and the subscript "2" the downstream mesh point. In the absence of the acceleration term $a_m \sin\theta$, Equation (94) is equivalent to the well-known formula used in hydraulics to calculate the head loss in a pipe.

4.2 BOUNDARY CONDITION AT LEFT END OF LINE

For the boundary condition at the left end of the line, we assume that the pressure in the tank remains a constant. This condition is very nearly fulfilled since the behavior of the system is of interest only during the first few seconds following the initiation of the disturbance. The value of this constant pressure is taken equal to the steady-state value just prior to the introduction of the disturbance in the line.

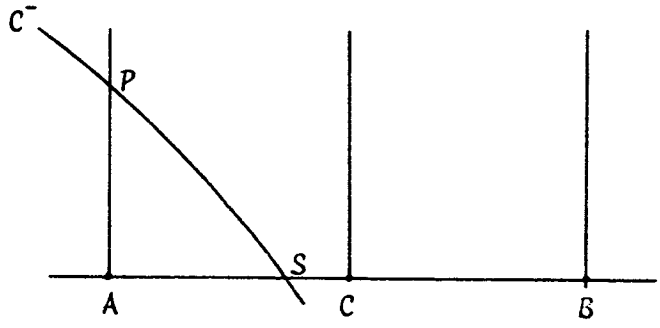

Figure 4.

To calculate the velocity corresponding to this given pressure, we may proceed in the following manner (refer to Figure 4):

1. Assume initially that the velocities u_P and u_S are equal to u_A, i.e., $u_P^o = u_S^o = u_A$.

2. Using these assumed values, calculate x_S^o from Equation (92) with x_C replaced by $x_A = 0$.

3. For this value of x_S, compute u_S^1 and p_S^1 from Equations (88) and (89), respectively.

4. Solve for u_P^1 from Equation (93) using the results of Step 3.

This process is repeated until two consecutive values of u_P agree within the specified accuracy.

4.3 BOUNDARY CONDITION AT RIGHT END OF LINE

It is assumed that the disturbance in the system originates at the right end of the line where the pump is located. Some of the various boundary conditions which may be considered have been already discussed in Section 1.3. Before considering these boundary conditions where some sort of regulating device is present in this preliminary investigation, we will merely specify a particular disturbance. Since any sort of disturbance will affect the flow rate and hence the fluid velocity, we will consider the disturbance as a change in velocity. The disturbance is taken in such a manner that it causes a decrease in velocity at the point of origin, and hence in turn produces an increase in pressure.

4.3.1 Velocity Impulse Disturbance

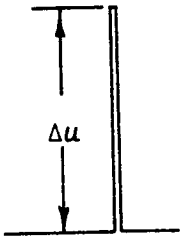

Figure 5.

If the righthand end of the feed line is provided with a valve and this valve is suddenly closed a certain amount and then reopened instantaneously, we would have an impulse disturbance. The magnitude of this disturbance will depend upon the amount of closure before reopening takes place. The maximum impulse will occur, of course, when the valve is closed completely before it is reopened. (See Figure 5.)

For a velocity change that takes the form of an impulse, the conditions at the right end must be recalculated before proceeding with the solution in the x, t plane. The corresponding pressure change Δp due to a Δu change in velocity can be found from momentum considerations. The result is

$$\Delta p = \rho_o a_o \Delta u \tag{95}$$

Therefore, the conditions which we have at the right end at time $t = 0$ due to the impulse are

$$\begin{aligned} u &= u_o - \Delta u \\ p &= p_o + \Delta p \end{aligned} \tag{96}$$

where u_o and p_o are the steady-state velocity and pressure, respectively, prior to the introduction of the impulse.

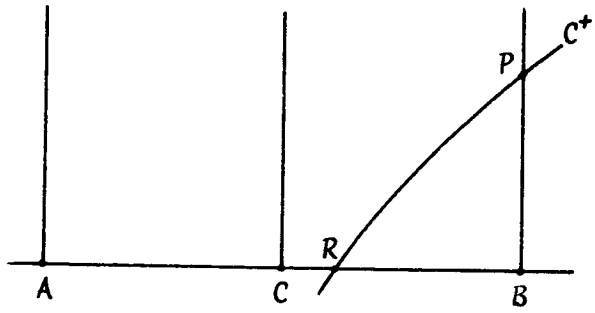

Figure 6.

In calculating the two unknowns at point P when $t > 0$, another relationship is required besides the equation for the characteristic curve C^+. This additional relation is obtained from the condition that the discharge at any time must obey the orifice law. Hence,

$$u_P = \bar{u}\left(\frac{p_P}{\bar{p}}\right)^{1/2} \tag{97}$$

where the quantities with a bar over them represent reference values. They may be thought of as the "equilibrium conditions" about which the transients caused by the disturbance oscillate. In the case of an impulse, the steady-state values are used as reference.

The calculation of u_P and p_P may proceed as follows:

1. Assume that initially the velocities at R and P are equal to that at B (refer to Figure 6); i.e.,

$$u_R^o = u_P^o = u_B$$

2. Calculate x_R^o from Equation (90) with x_C replaced by $x_B = \ell$.

3. Compute u_R^1 and p_R^1 from Equations (86) and (87), respectively.

4. Solve Equations (91) and (97) simultaneously for u_P^1 and p_P^1.

As before, this procedure is repeated until two successive values of both u_P and p_P are within the specified tolerance.

4.3.2 Velocity Step Disturbance

We define a step disturbance as that caused by an instantaneous partial closure of the valve with the valve held at this new position. Thus, the step disturbance in this sense does not mean that the velocity is maintained at this new value for all time, but the position of the valve itself represents a step function. The position of the valve creates a new "equilibrium position" which the flow will eventually attain after the transients due to the disturbance have subsided.

As in the case of a velocity impulse, we must first calculate the new conditions at the right end due to the step disturbance before proceeding with the solution. These new conditions are computed in exactly the same manner as was done in the case of the impulse. The pressure change is given by Equation (95), and the new conditions by Equation (96). The only difference between the two cases is that for the step disturbance we use the new conditions given by Equation (96) for reference values in Equation (97) instead of the steady-state values. With this one change, the computational procedure for calculating the velocity and pressure at point B on the boundary for $t > 0$ is identical to that outlined for the case of an impulse.

4.3.3 Sinusoidal Velocity Disturbance

The procedure given in Section 4.3.2 for handling a step disturbance may be extended to handle any other type of disturbance or pulse shapes simply by replacing the given disturbance by an equivalent series of step functions. By equivalent, it is meant that both the composite step function representation of the given disturbance and the disturbance itself have the same area under the curve.

Suppose that in the absence of propagation effects, the disturbance under consideration took the form of a sine function OAB as shown in Figure 7. We first divide the half-time period t_A into suitable time increments Δ_T. From the computational standpoint, it is convenient to choose Δ_T equal to either Δt, the time interval used in the difference equations, or a multiple thereof. Within each interval, the ordinate for the "step" is selected by either visual inspection or other means such that the area under the "step" is equal to that under the actual curve. In this way we replace

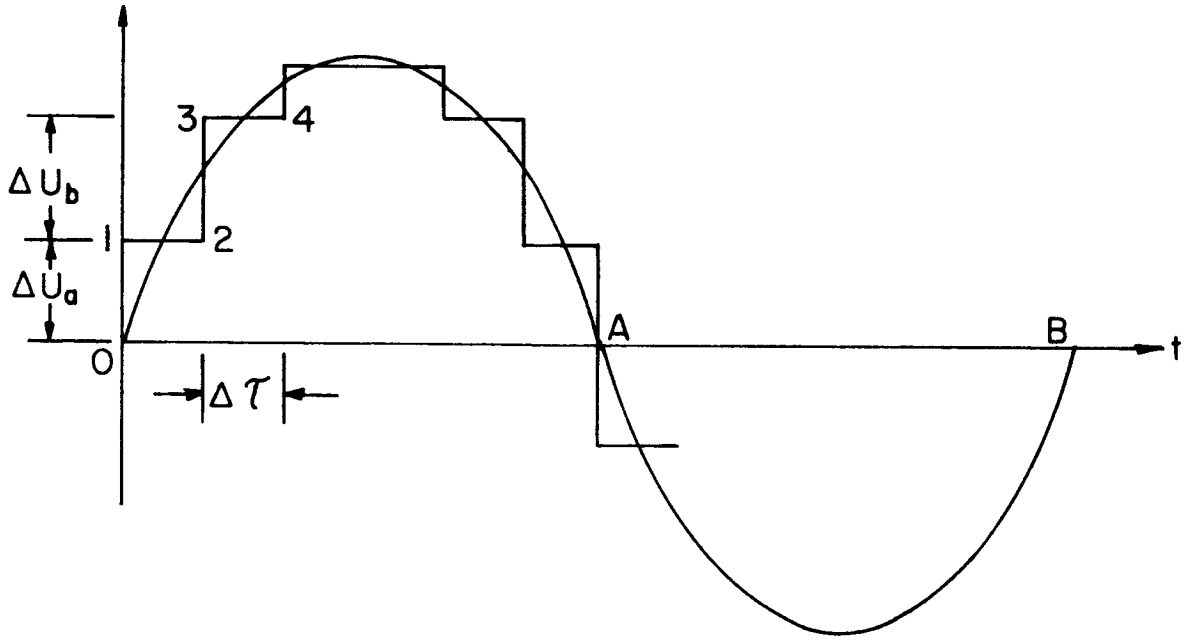

Figure 7.

the sine curve by the "staircase" approximation 01234 A... B, and this function is the one which will be dealt with in our subsequent discussion.

Corresponding to the instantaneous velocity change ΔU_a for the first step "012" of the staircase approximation, the pressure change is obtained from Equation (95) as before. Since it is assumed that the disturbance takes place only after steady-state conditions have prevailed in the line, the new conditions at the righthand end after the disturbance has taken place is given by Equation (96). The calculation for the pressure and velocity at the right end for $0 \leq t \leq \Delta\tau$ now proceed in the manner given in Section 4.3.1 where the new conditions existing there are used as reference values. This iteration process is continued for as many steps as necessary until the specified tolerance on the dependent variables have been met. We now arrive at point "2" on our staircase approximation so that step "234" comes under consideration. The response of the system due to this step input during the time $\Delta\tau \leq t \leq 2\,\Delta\tau$ is handled in the identical fashion as for the previous step in which the reference values to be used now in Equation (97) are furnished by the

conditions existing at time $t = \Delta\tau$ with the effects of ΔU_b included. This same computational procedure is continued for each succeeding "step."

4.3.4 Feed Line With Pressure Regulating Device

In Section 1.3, the boundary condition at the right end was derived for the case of a pressure regulating device, such as a surge tank, air chamber, or tank damper, being present in the line. In each of these three cases, it was shown that the boundary condition can be expressed as a first order partial differential equation in the form

$$\kappa \frac{\partial Q}{\partial X} + Q = g(t) \quad \text{at} \quad x = L \tag{98}$$

where Q is the mass flow rate entering the regulating device, and g(t), a prescribed function, is the mass flow rate discharging from the device. The constant κ is dependent upon the type of regulating device under consideration, and the value it assumes for the various devices is given in Section 1.3.

It would appear that one approach of incorporating Equation (98) as a boundary condition into the righthand end of the feed line would be to integrate it and obtain a relation between Q(t) and g(t). For any prescribed disturbance function g(t) then, Q(t) will be known and hence also the velocity U(L, t) and the discharge velocity are known. Therefore the computational procedure given in Sections 4.3.1, 4.3.2, or 4.3.3 may be employed, depending on the type of disturbance under consideration. Since Equation (98) is a boundary condition, what we are seeking is a particular solution. For any given disturbance, there are a number of particular solutions which would satisfy Equation (98). Without knowing the general form of the closed form solution for the pressure and velocity along the feed line itself, it is impossible to tell which one of the particular solutions is the correct one. Therefore the only other alternative is to express this equation in finite difference form and solve it simultaneously with the other appropriate equations at the right end, numerically.

The derivative $\partial Q/\partial x$ appearing in Equation (98) can be expressed by a divided difference over an interval Δx. However this "average" slope of Q over the interval may be quite different from the slope $\partial Q/\partial x$ at $x = L$. Although this difficulty may be alleviated somewhat by dividing the last interval into smaller intervals, the numerical procedure would be complicated.

The reason for our difficulty in obtaining a representative finite approximation for Equation (98) is that although it dictates the condition which must prevail for all values of time t, it involves the derivative $\partial Q/\partial x$

which in the x,t plane is in a direction normal to the t axis. Thus if the boundary condition can be rewritten so that any derivatives present are with respect to time instead of the spatial variable x , then it can be put in finite difference form solely in terms of the variables at x = L. Having the equation in this form should permit a more accurate numerical treatment of the boundary condition at the right end of the feed line than would be possible otherwise.

4.3.4.1 Modified Form of Boundary Condition

The boundary condition given by Equation (17b) stems from the continuity in mass flow which must exist at the junction of the device and the feed line. For each of the three pressure regulating devices considered, this boundary condition can be rewritten in the form

$$A_o \bar{\kappa} \frac{\partial p}{\partial t} + Q = g(t) \tag{99}$$

by utilizing the relation between $\partial Q/\partial x$ and $\partial p/\partial t$ given in Section 1.3. The constant $\bar{\kappa}$ characterizes the damping device and is equal to κ divided by the modified bulk modulus K defined in Equation (13), and A_o is the cross-sectional area of the feed line.

If our attention is focussed on feed lines of constant cross sections such as in the present case, and the variation in the fluid density is assumed sufficiently small so that it is essentially equal to its steady-state value, it is advantageous from a computational point of view to rewrite the quantity Q in Equation (99) in terms of the fluid velocity u. Since $Q = \rho_o A_o u$, Equation (99) takes the form

$$\bar{\kappa} \frac{\partial p}{\partial t} + u = v(t) \tag{100}$$

The quantity v(t) will be equal to the discharge velocity, provided the discharge cross-sectional area is the same as that of the feed line; otherwise it will be simply proportional to it. The proportionality constant in this case is equal to the ratio of the discharge cross-sectional area to the feed line cross-sectional area.

4.3.5 Numerical Procedure

Equation (100) may be transposed into a finite difference equation using the technique given in Section 3.5. Employing the same notation

as shown in Figure 6, the resulting equation takes the form

$$\bar{\kappa} \frac{p_P - p_B}{\Delta t} + \frac{1}{2}(u_P + u_B) = \frac{1}{2}(v_P + v_B) \qquad (101)$$

The three quantities with the subscript B are known from the calculation for the previous time interval, and since v is a prescribed function, v_P is also known. Thus p_P and u_P are the two unknowns in Equation (101). The computational procedure to determine these two unknowns may proceed in the following manner.

1. Assume initially that $u_R^o = u_P^o = u_B$
2. Calculate x_R^o from Equation (90) with x_C replaced by L .
3. Compute u_R' and p_R' from Equations (86) and (87) respectively.
4. Solve Equations (91) and (101) simultaneously for u_P' and p_P' .

This process is continued until successive values for both u_P and p_P are in agreement within the specified limits.

SECTION 5. COMPUTATIONAL APPROACH TO SPECIFIC PROBLEM

We are now in a position to handle a specific problem under the boundary conditions described previously. Referring to Figure 8, suppose that we have decided to divide the propellant line into five equal incremental lengths so that the left and right boundaries coincide with A_0 and A_5 respectively. One way in which the computation can be carried out would be the following. From the given steady-state condition at A_5, the velocity at A_0 through A_5 is known and the corresponding pressure at these mesh points can be calculated from Equation (94). If the disturbance under consideration involves an instantaneous velocity change, such as a step function, the conditions at mesh point point A_5 must include the effect of the velocity change before we proceed with the calculations. The incremental pressure change corresponding to this incremental velocity change is computed from Equation (95). Superimposing these incremental changes in velocity and pressure according to Equation (96) onto the steady-state values at A_5, we obtain the new conditions which must prevail there because of the disturbance.

In the case where the feed line contains a regulating device and the disturbance is a sinusoidal function, the foregoing calculation is not necessary since the disturbance was not approximated by a series of step functions and hence did not involve any instantaneous velocity changes.

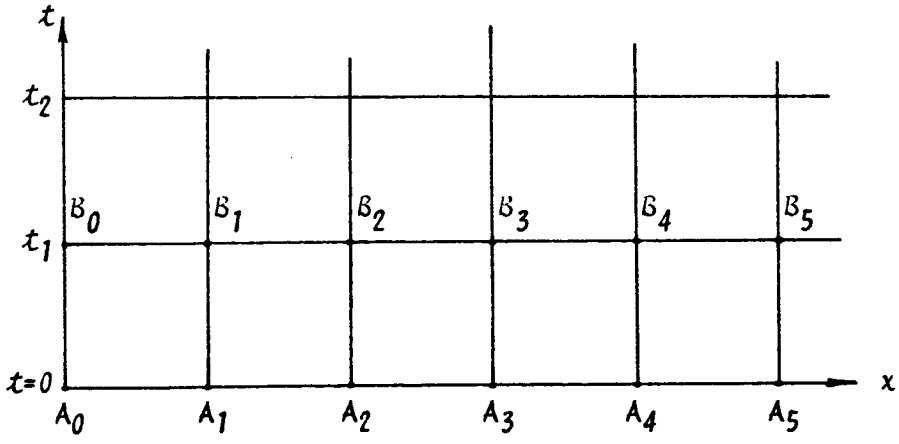

Figure 8

Having the conditions for all mesh points at t=0, we now "march out" to time t_1, and proceed to calculate the conditions at these mesh points. For the prescribed boundary condition of constant pressure at B_0, the velocity may be determined by the procedure outlined in Section 4. 2. The conditions at mesh points B_1 through B_4 are found by the procedure given in Section 4. 0. At mesh point B_5 where both the velocity u and pressure p are unknown, we proceed in the manner described in Section 4. 3. 1, 4. 3. 2, 4. 3. 3, or 4. 3. 4, depending on the type of velocity disturbance and whether a regulating device is present or not. As long as suitable boundary conditions are prescribed at both ends of the feed line, the solution can be "marched out" as far as desired.

SECTION 6. NUMERICAL RESULTS

Some numerical results obtained from the application of the foregoing numerical procedure to the center liquid hydrogen feed line on the Saturn S-II engine are shown in Appendix B, Figures B-1 through B-48. The numerical values used for the various parameters in the analysis are given in Table I (Section 2. 2). Calculations were carried out for the feed line with and without an air chamber when subjected to all three types of velocity disturbances discussed previously. The air chamber was selected over the other two damping devices discussed since it combines the space economy provided by the tank damper and, to a lesser degree, the effectiveness with which the surge tank alleviates pressure changes. Thus it represents a device which might well be incorporated into a propellant feed line.

Two amplitudes were considered for each disturbance expressed as a percent of the steady-state velocity. The amplitudes chosen were 2 and 5 percent since they correspond approximately to the minimum and maximum variation expected in the pump flow of the S-II respectively. Four frequencies were selected for consideration in connection with the sinusoidal disturbance. They were 7. 20, 9. 70, 11. 70, and 21. 11 cps, corresponding respectively to the first four structural modes of the spring mass "POGO" model of the Saturn S-II engine at 95 percent burntime.

6. 1 DISCUSSION OF RESULTS

Pressure and velocity time histories were obtained both at the right end and at the middle of the line for the case when the feed line does not contain a regulating device. The results corresponding to the impulse disturbance and the step disturbance for amplitudes of 2 and 5 percent of steady-state velocity are shown in Figure B-1 through B-8. In all cases, since only partial reflections take place at the right end, both the pressure and velocity in the line regain steady-state conditions in a very short time, approximately 0. 10 second, as shown by a decrease in amplitude of each succeeding "spike" or "step" following the initial disturbance. This is to be expected due to the stabilizing influence of the unidirectional flow. With the exception of the numerical values obtained, the general behavior of the feed line subjected to either a 2 or 5 percent impulse disturbance is the same. This also applies to the step disturbance.

The results for the sine disturbance are given in Figure B-9 to B-24 inclusive. The sine disturbance introduces an additional parameter, input

frequency, which does not appear in either the impulse or sine disturbance. For the liquid hydrogen line under consideration, it takes the pressure wave caused by a disturbance at the right end 0.03455 second to complete one cycle, corresponding to a frequency of 28.96 cps. The initial reflected pressure wave of a sine disturbance with this input frequency will arrive at the right end just when the disturbance is zero. Under this condition, the maximum fluid velocity is equal to the initial steady-state velocity and the trend of velocity variation is toward this value. In the present four cases, the input frequencies were all below 28.98 cps so that the disturbance and the reflected waves are out of phase with one another, causing the general velocity trend to increase with time. This was true both at the right end and at the midpoint of the feed line. The pressure tends to decrease with time but at a much lower rate than does the velocity. If the plots were carried out for a sufficient length of time, the velocity in all four cases tends to oscillate about some equilibrium value, as does the pressure. After the initial transients have subsided in the first cycle, the peak-to-peak variation of each consecutive cycle for both the velocity and pressure is essentially zero. Hence the effect of pipe friction is very small.

Figure B-25 through B-48 contain the results for all three disturbances when an air chamber is located at the right end of the feed line. It was assumed that the air chamber had a cross-sectional area of 3 sq ft (diameter of approximately 2 ft) with the air occupying a 2-foot length of the chamber initially, giving a volume V_o of 6 ft^3 under steady state flow. Since p_o is 4,320 psf, this yield a V value of 4×10^{-3} ft^3/lb. This value of $\bar{\kappa}$ was used throughout the study whenever an air chamber was considered as present in the feed line.

The results obtained for the feed line with and without an air chamber cannot be compared directly to ascertain exactly how effective the air chamber is in alleviating pressure surges, since in the former case the discharge velocity is prescribed for all time while in the latter it obeys the orifice law. This is obvious since the time history in the two cases will differ considerably from one another whether the air chamber is present or not. However, they can be compared with each other from a qualitative point of view. This is particularly true for the pressure variation since, broadly speaking, the general trend and maximum peak amplitudes are approximately the same whether the discharge velocity is "fixed" or "free" as in the case where the orifice law applies.

The effect of the air chamber on velocity and pressure at the right end is illustrated in Figure B-29 and B-31 for a 2 and 5 percent step disturbance respectively. It is seen that the pressure fluctuations which occur in the feed line without a pressure regulating device are completely eliminated by the air chamber and the overpressure decreases very gradually from its

initial value caused by the disturbance. The pressure fluctuations actually are much larger than for a "free" boundary since the damping influence of the streaming fluid is much less in the fixed case. This is shown quite clearly in Figure B-30 and B-32 by the larger pressure fluctuations in the middle of the line. From this observation then, we see that the air chamber is quite an effective damping device.

The results for a prescribed impulse disturbance with an air chamber in the feed line are shown in Figure B-25 through B-28. One feature of these results is that they are very similar to those for the step disturbance and differ only from a quantitative point of view. This is not too surprising when it is seen that the only difference between the two cases is that v(t); the prescribed discharge velocity, assumes a slightly different fixed value after the initiation of the disturbance. Since both cases have the same boundary condition at the right end which differ only by a constant, the two results must necessarily be similar.

Just how effective the particular air chamber is in alleviating pressure surges is illustrated in Figures B-33 to B-48, which are the results for the fixed sine disturbance. Considering the 5 percent sine disturbance, we noticed that in no case does the maximum peak-to-peak pressure variation exceed 15 psf, which is about 1.5 percent of the overpressure for the corresponding "undamped" case. Naturally for the 2 percent case, the peak-to-peak pressure variation is proportionately less. The air chamber also suppresses the velocity so that in all cases it did not vary more than 1/2 fps from the steady-state velocity of 51.5 fps. The high frequency oscillations, which appear in the velocity variation such as in Figure B-33 and in the pressure variation as shown in Figure B-34, have no physical significance but are mathematical in nature. As was mentioned earlier in Section 3.2, if the time interval selected is such that the solution obtained coincides with the true characteristics, then these oscillations will be eliminated.

CONCLUSIONS

The principal objective of the present investigation was to develop some mathematical models for the unsteady fluid motion in a propellant feed line which may be incorporated in a closed loop dynamic system for the analysis of longitudinal oscillations of a large liquid rocket booster. With this in mind, the dynamic behavior of the feed line was looked at both from a linear and a nonlinear viewpoint. The analysis of the linear mathematical model resulted in the transfer functions given in Appendix A. The similarity of results for both the frictionless line and one with friction taken into account indicate that friction loss for this particular line is very small. Since the cross-sectional area of the line is relatively large, this result is to be expected. The inclusion of the longitudinal natural frequency of the line resulted in a modification of the frequency response curve which is similar to those given in Reference 10 and 11.

Some results based on the nonlinear differential equations governing unsteady compressible fluid flow are shown in Appendix B. Although these results cannot be compared directly with any known published data, they do correspond to a modification of the water hammer problem encountered in hydraulics in which the valve is only partially closed and is a function of time. By neglecting the friction term and setting the velocity to zero at the right end, the solution obtained agrees with the classical waterhammer solution. Hence the method provides a useful tool for inclusion in a system dynamic study. Various disturbances were considered under two different boundary conditions to illustrate the flexibility of the method.

AREAS FOR FURTHER STUDY

The propellant feed line considered in the present analysis was straight and of constant cross-section, which is a very special case. In actual practice, feed lines may involve a step change in cross-sectional area, branch lines, bends, or any combination of these. Therefore, in order to obtain a more realistic mathematical model of a propellant feed line, further study should be undertaken to incorporate these additional parameters. The method developed for the nonlinear model can be extended to handle the step change in cross-sectional area or a feed line with branch lines quite readily by using it as a "building block." What these two cases require is a modification of the boundary conditions at either end of the line so that it can accommodate the continuity condition for both mass flow and pressure at the point of discontinuity in cross-section or junction of the branch lines.

Another area for further investigation in connection with the present problem is a parametric study of the various pressure regulating devices to determine how each parameter influences the dynamic response. For example, the volume of air at steady-state flow may be varied by the constant $\bar{\kappa}$ that characterizes the air chamber. In the case where two or more parameters are involved, such as for the tank damper, such a study would indicate which parameter has the greatest influence on the effectiveness of any given device to dampen pressure surges. Going a step further, this data can then be used to make a trade-off study, say between weight and allowable space (total volume) versus damping effectiveness of a particular device. This will provide information which can be used directly to "tailor" a damping device for a particular feed line system and a particular missile.

Besides relieving the overpressure by mechanical devices, there are other means based on the high compressibility of a gas which merit consideration. One such method is injecting a gas, say helium, into the feed line. The gas bubbles "soften" the fluid column and also act as an absorption device whenever a disturbance causes a propagating pressure wave in the line. The other idea is to insert a gas-filled plastic bag in the annulus between two concentric lines. The inner line, which carries the propellant, contains a series of holes, allowing contact between the propellant and the plastic bag. This arrangement has the effect of making the feed line highly compliant to any pressure surges.

REFERENCES

1. Joukowski, N. Water Hammer. Proc. of Am. Water Works Asso. (1904)

2. Allievi, L. Allgemeine Theorie über die veranderliche Bewegung des Wassers in Leitungen. Julius Springer, Berlin, Germany (1909)

3. Symposium on Water Hammer, The A. S. M. E. (1933)

4. Parmakian, J. Waterhammer Analysis. Dover (1963)

5. Rich, G. R. Hydraulic Transients. McGraw-Hill (1951)

6. Morgan, G. W. "On The Steady Laminar Flow of a Viscous Uncompressible Fluid in an Elastic Tube," Bul. Math. Bioph., Vol. 14 (1952)

7. Karreman, G. "Some Contributions to the Mathematical Biology of Blood Circulation Reflection of Pressure Waves in the Arterial System," Bul. Math. Bioph., Vol. 14 (1952)

8. Morgan, G. W. and W. R. Ferrante. "Wave Propagation in Elastic Tubes Filled with Streaming Liquid," J. Acou. So. of Am. (July 1955)

9. Blackburn, Reethof, and Shearer. Fluid Power Control. John Wiley (1960)

10. D'Sonza, A. F. and R. Oldenburger. "Dynamic Response of Fluid Lines," J. Basic Eng. (Sept. 1964)

11. Regetz, Jr., J. D. An Experimental Determination of the Dynamic Response of a Long Hydraulic Line. NASA TND-576 (Dec. 1961)

12. Jacobi, W. J. "Propagation of Sound Waves Along Liquid Cylinders," J. Acou. So. of Am., Vol. 21 (1949), pp. 120-127

13. Thomson, W. T. "Transmission of Pressure Waves in Liquid Filled Tubes," Proc. of 1st U. S. Nat. Congress of App. Mech A. S. M. S. (1951)

14. Skalak, R. "An Extension of the Theory of Water Hammer," Trans. A. S. M. E. (Jan. 1956), pp. 105-116

15. Sabersky, R. H. Effect of Wave Propagation in Feed Lines on Low-Frequency Rocket Instability. Jet Propulsion (May - June 1951)

16. Streeter, V. L. and C. Lai. "Waterhammer Analysis Including Fluid Friction," ASCE Trans., Vol. 128 (1963)

17. Contractor, D. N. The Reflection of Waterhammer Pressure Waves from Minor Losses. A. S. M. E. Paper No. 64-WA/FE-16

18. Kochina, N. N. "On Self-Induced Oscillations of Heavy Fluids in Tubes," PMM, Vol 27, No. 4 (1963), pp. 609-617

19. Lister, M. "The Numerical Solution of Hyperbolic Partial Differential Equations by Characteristics," Mathematical Methods for Digital Computers, Edited by A. Ralston and H. S. Wilf. New York: John Wiley & Sons, Inc. (1960)

20. Hartree, D. R. Some Practical Methods of Using Characteristics in the Calculation of Non-Steady Compressible Flow. Atomic Energy Commission Rept. AECU 2713 (1952)

21. Crandall, S. H. Engineering Analysis. New York: McGraw-Hill (1956), pp. 355-368

APPENDIX A. TRANSFER FUNCTIONS

Transfer functions for the outboard liquid hydrogen line on the Saturn S-II engine

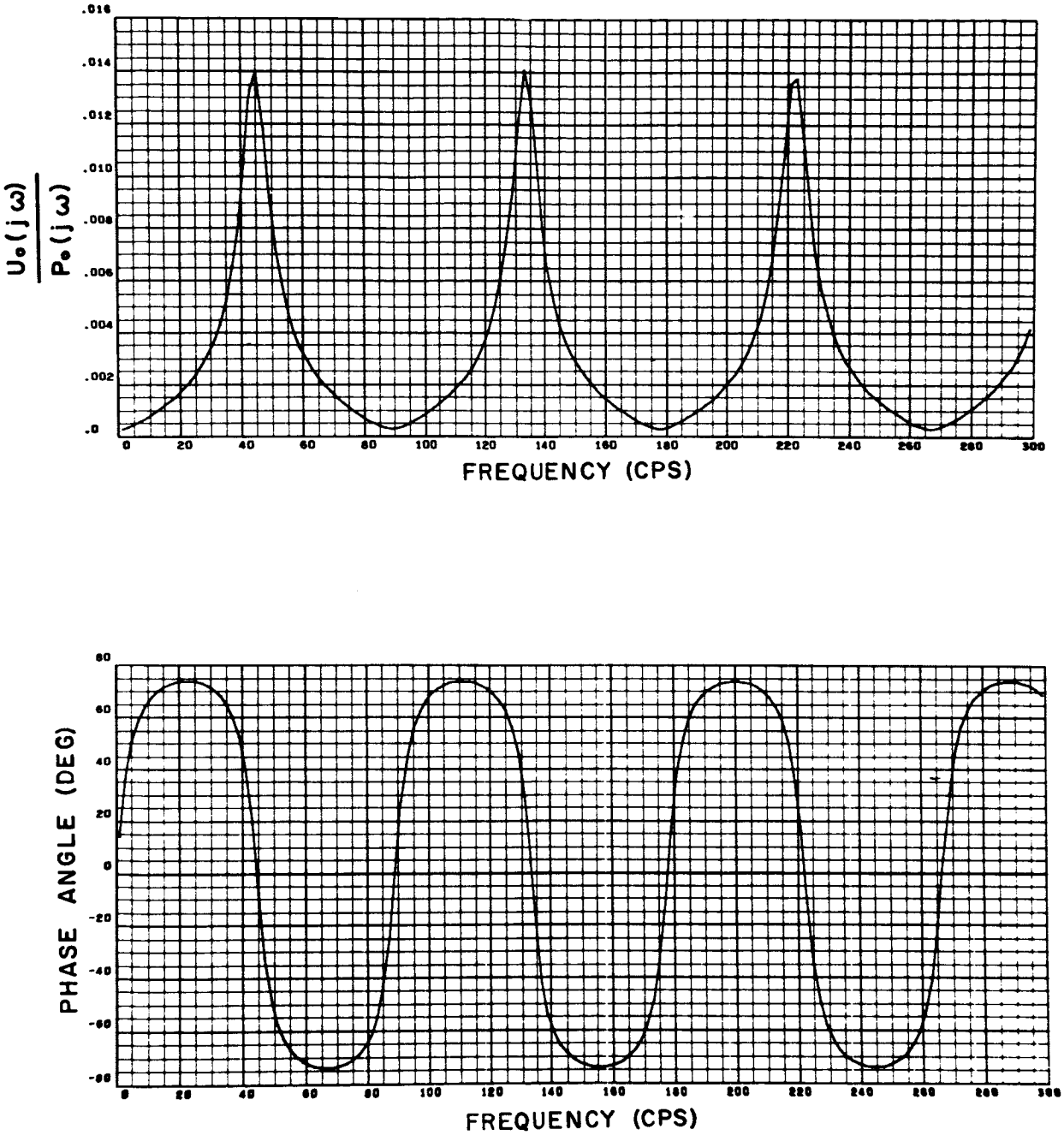

Figure A-1. The Ratio of Velocity to Pressure Deviation at x = 0 Versus Frequency for Outboard LH_2 Line, Frictionless and Without Pipe Vibration

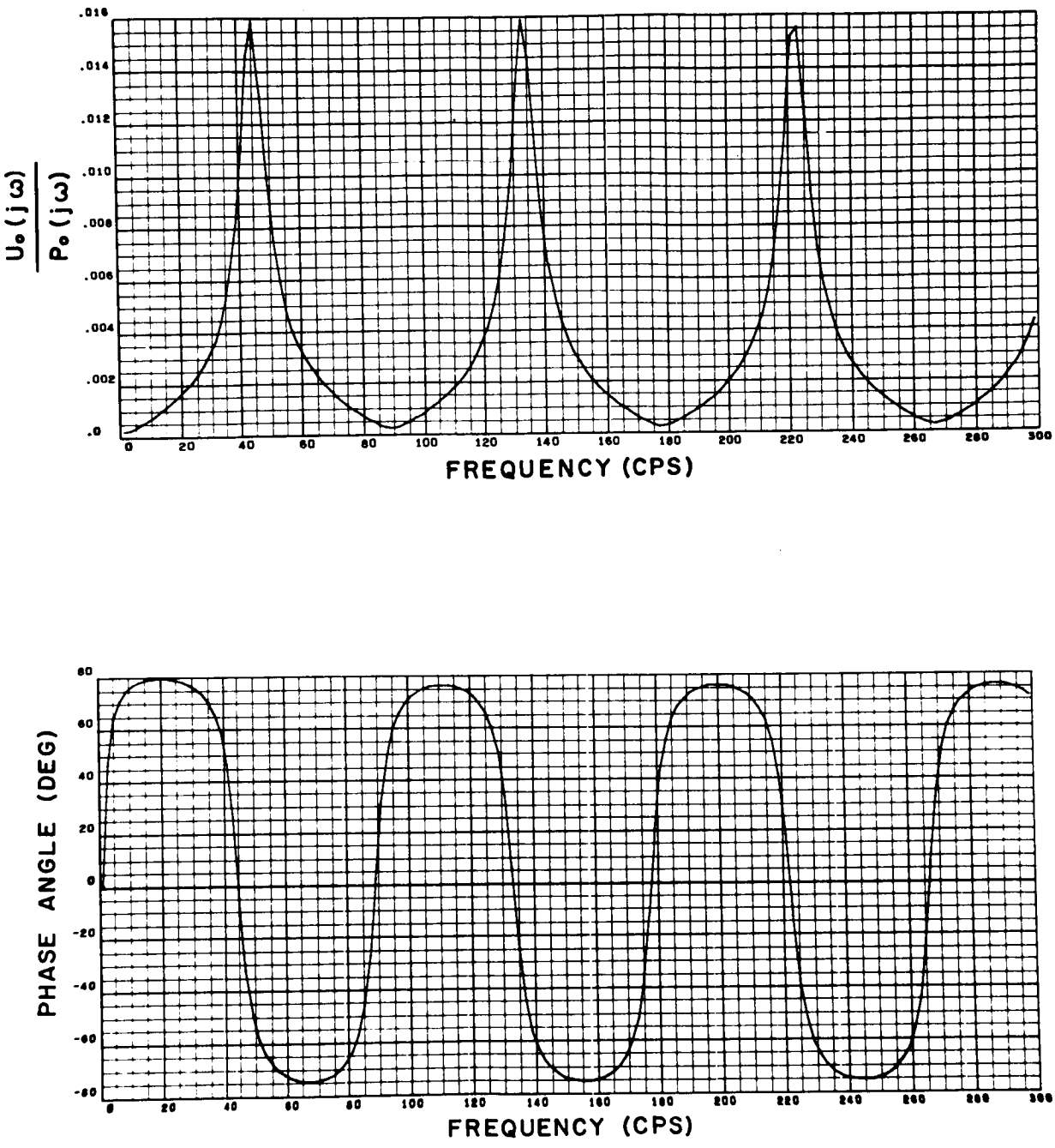

Figure A-2. The Ratio of Velocity to Pressure Deviation at x = 0 Versus Frequency for Outboard LH_2 Line, With Turbulent Resistance and Without Pipe Vibration

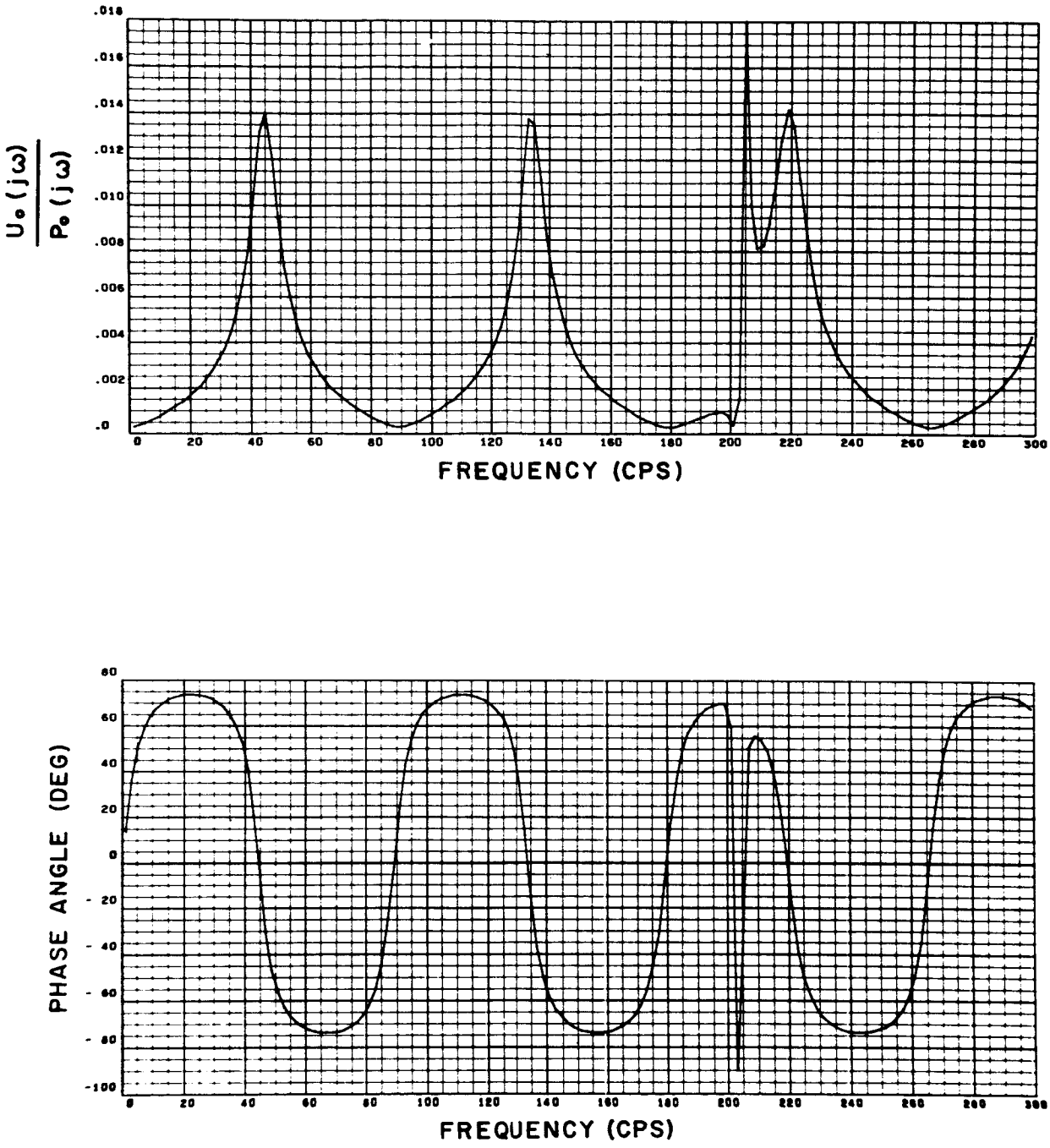

Figure A-3. The Ratio of Velocity to Pressure Deivation at x = 0 Versus Frequency for Outboard LH_2 Line, Frictionless and Including Pipe Vibration

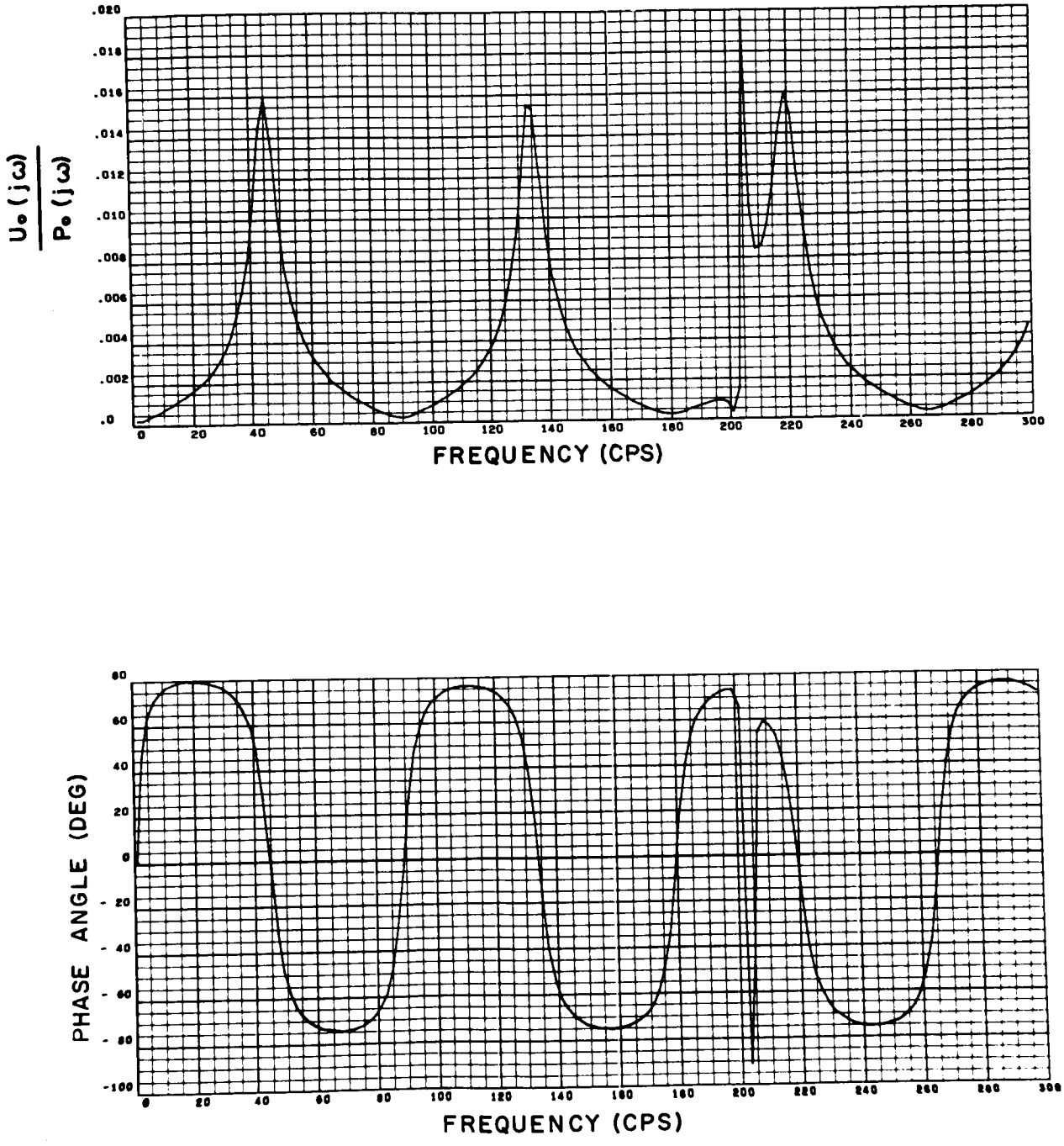

Figure A-4. The Ratio of Velocity to Pressure Deviation at x = 0 Versus Frequency for Outboard LH_2 Line, With Turbulent Resistance and Including Pipe Vibration

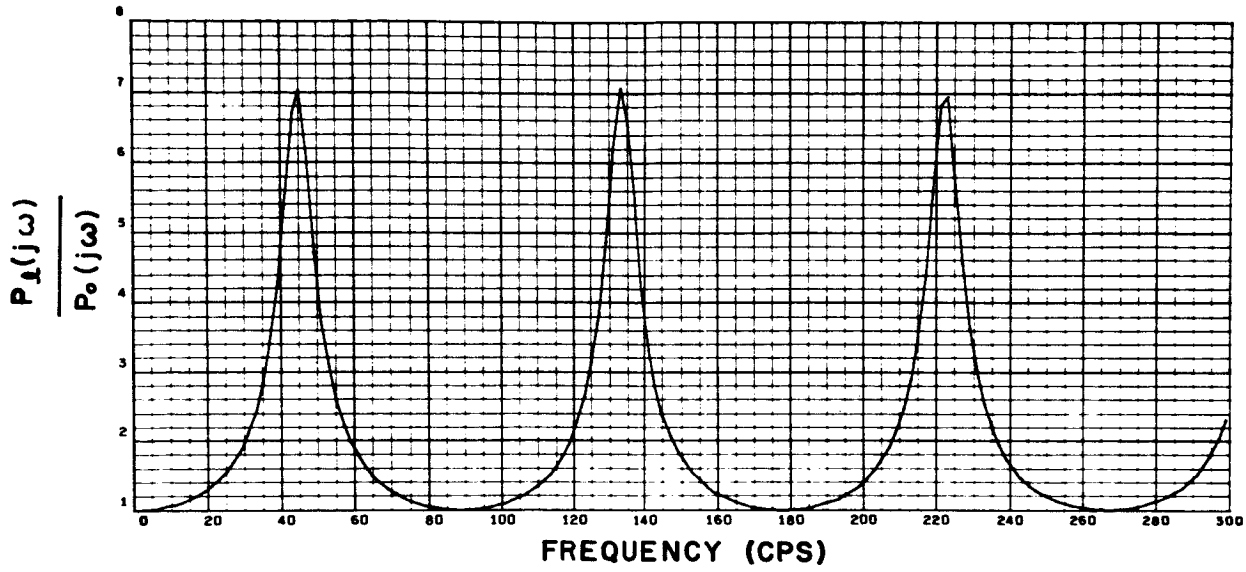

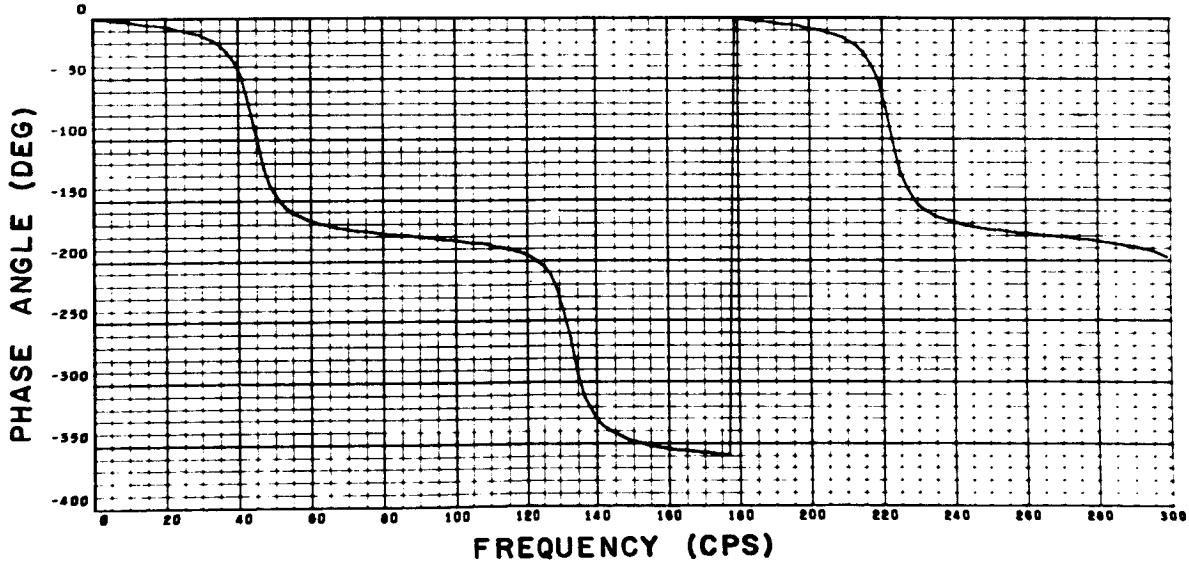

Figure A-5. The Ratio of Pressure Deviation at x = ℓ to Pressure Deviation at x = 0 for Outboard LH_2 Line, Frictionless and Without Pipe Vibration

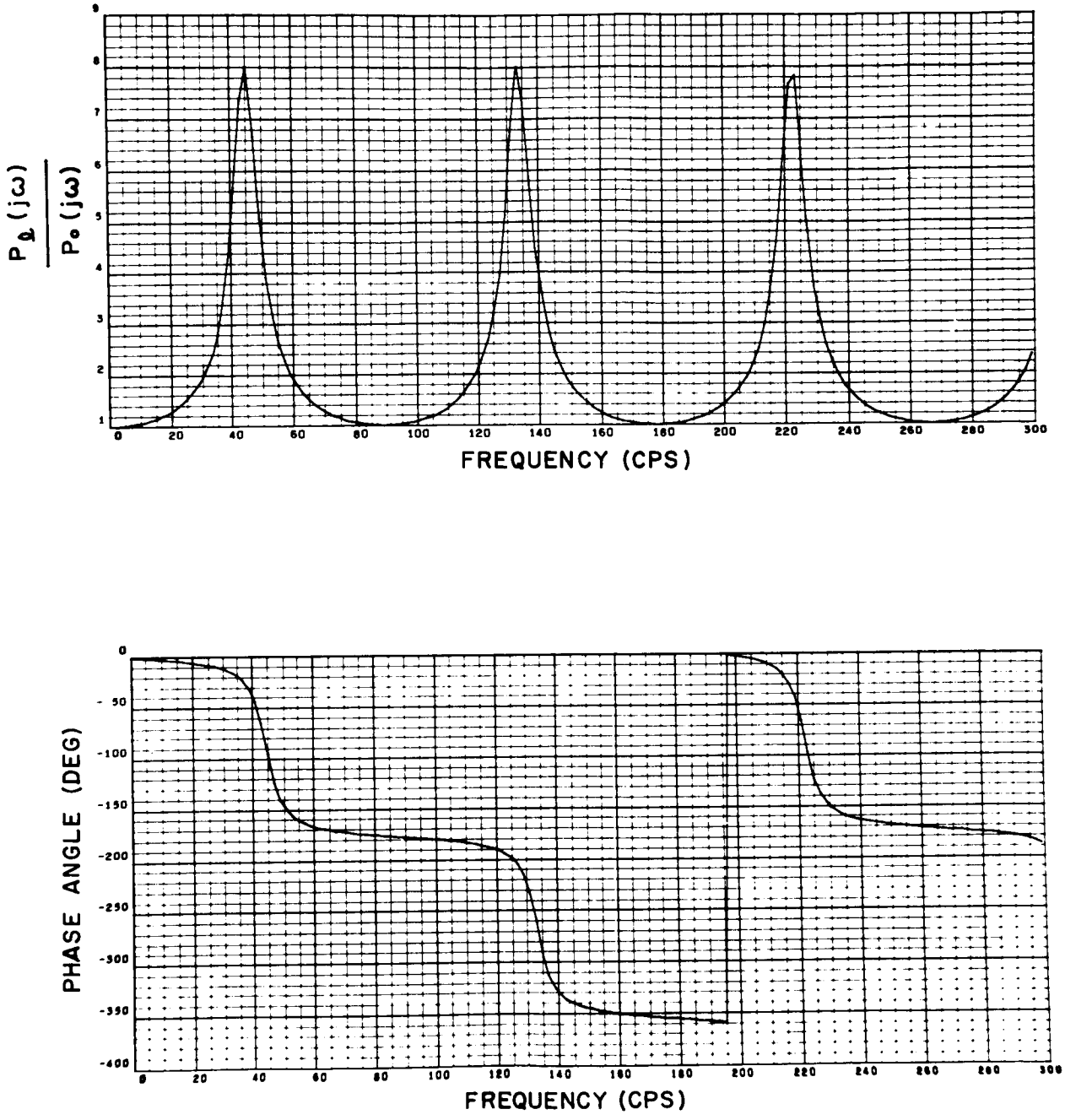

Figure A-6. The Ratio of Pressure Deviation at $x = \ell$ to Pressure Deviation at $x = 0$ for Outboard LH_2 Line, With Turbulent Resistance and Without Pipe Vibrations

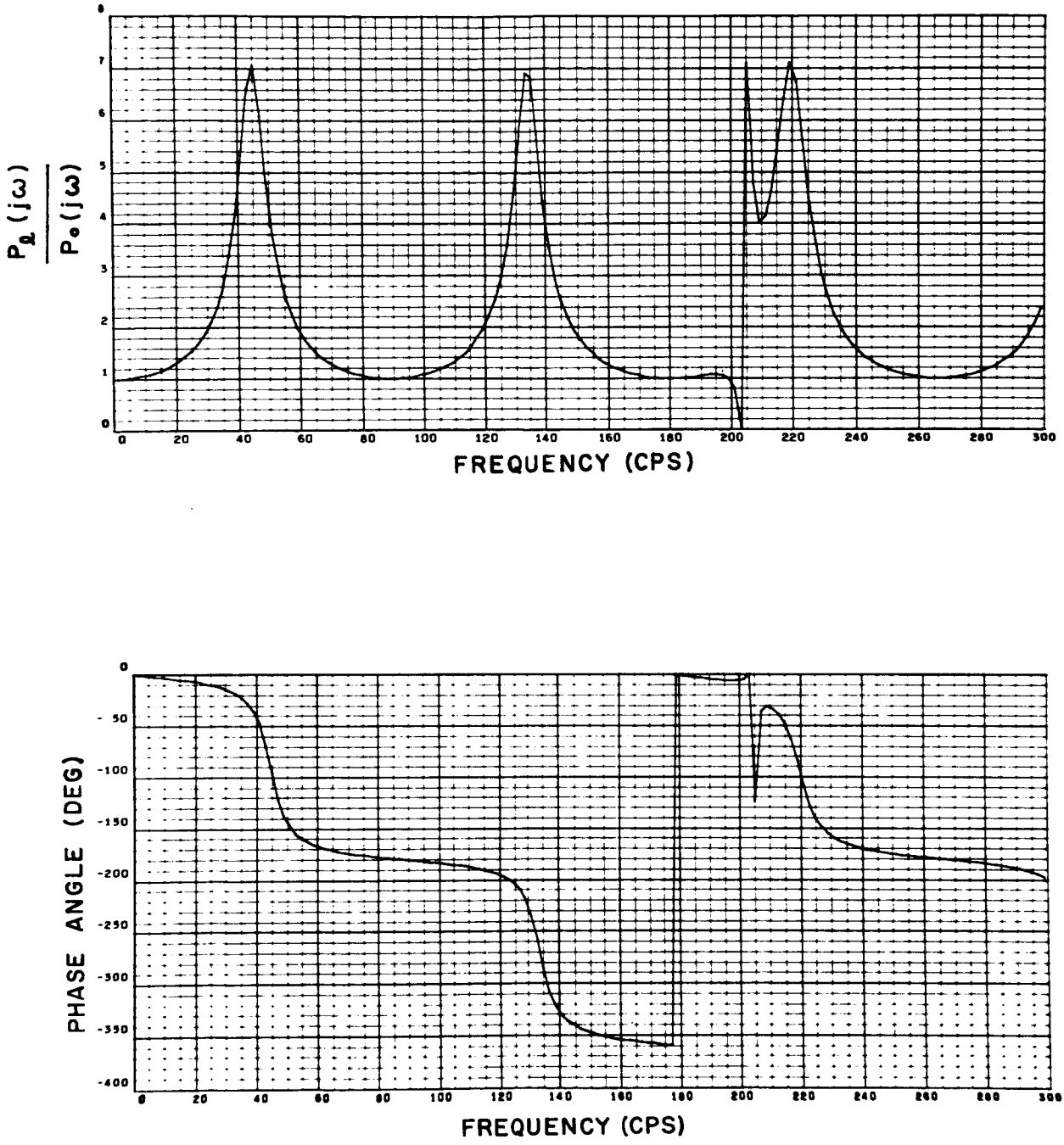

Figure A-7. The Ratio of Pressure Deviation at x = ℓ to Pressure Deviation at x = 0 for Outboard LH_2 Line, Frictionless and Including Pipe Vibration

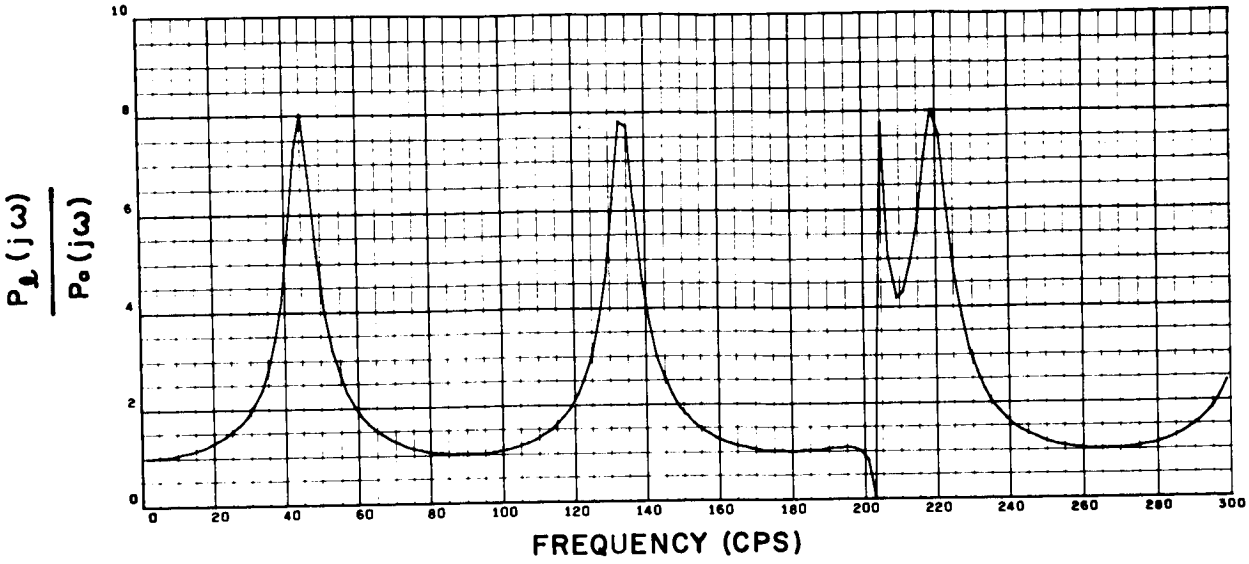

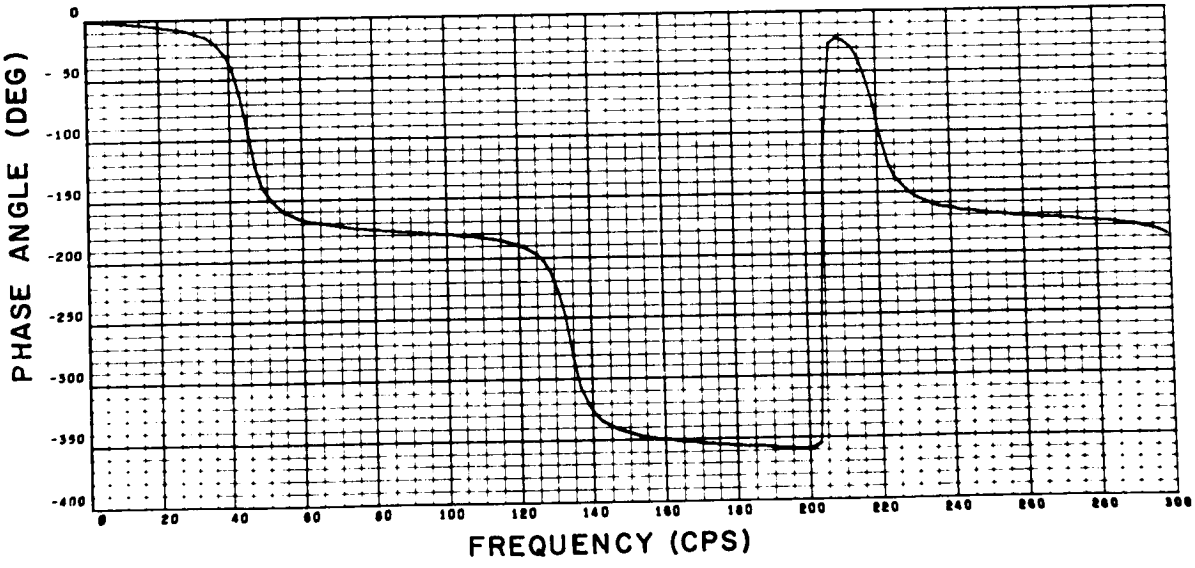

Figure A-8. The Ratio of Pressure Deviation at x = ℓ to Pressure Deviation at x = 0 for Outboard LH_2 Line, With Turbulent Resistance and Including Pipe Vibration

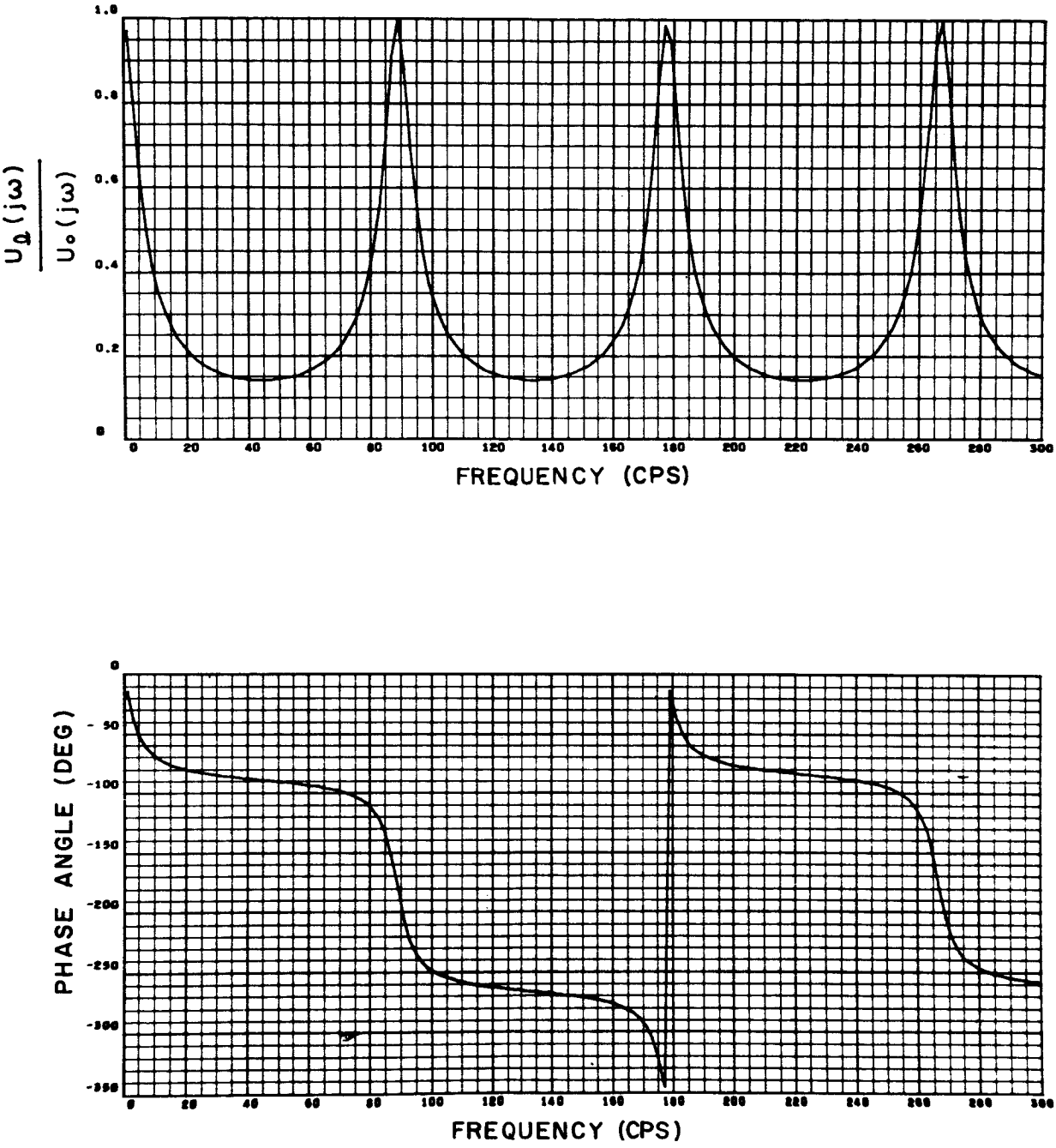

Figure A-9. The Ratio of Velocity Deviation at x = ℓ to Velocity Deviation at x = 0 for Outboard LH_2 Line, Frictionless and Without Pipe Vibration

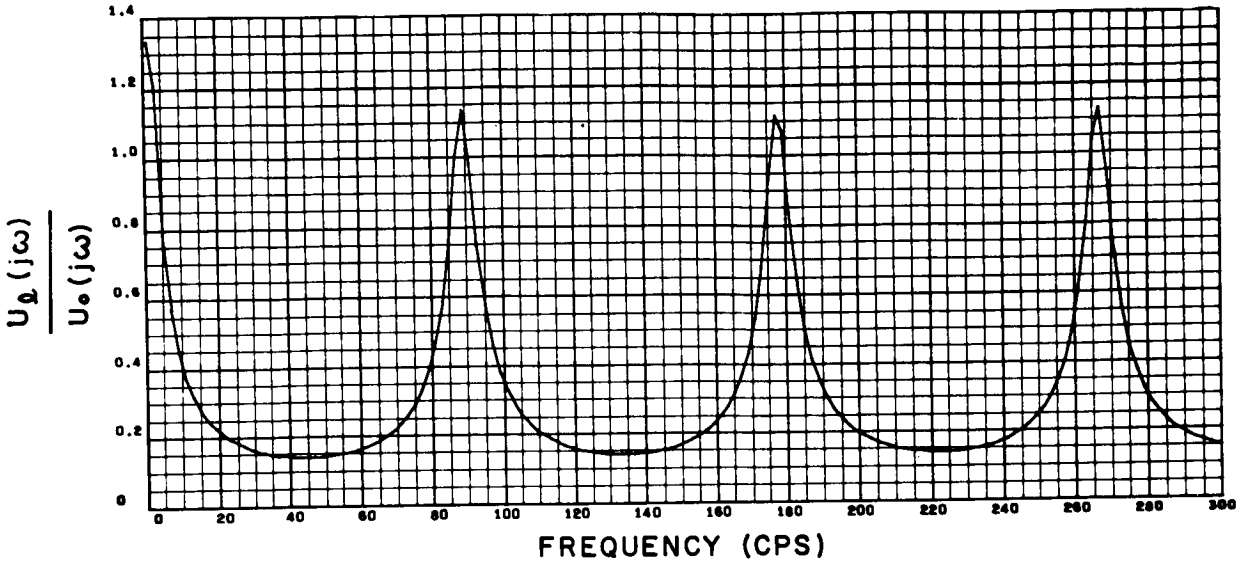

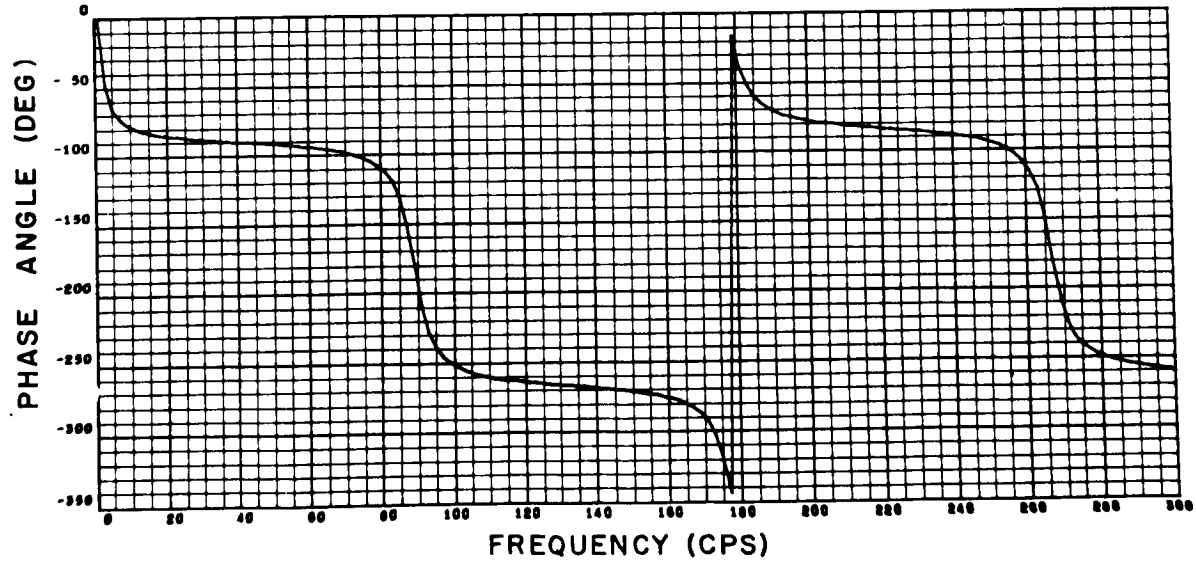

Figure A-10. The Ratio of Velocity Deviation at x = ℓ to Velocity Deviation at x = 0 for Outboard LH_2 Line, With Turbulent Resistance and Without Pipe Vibration

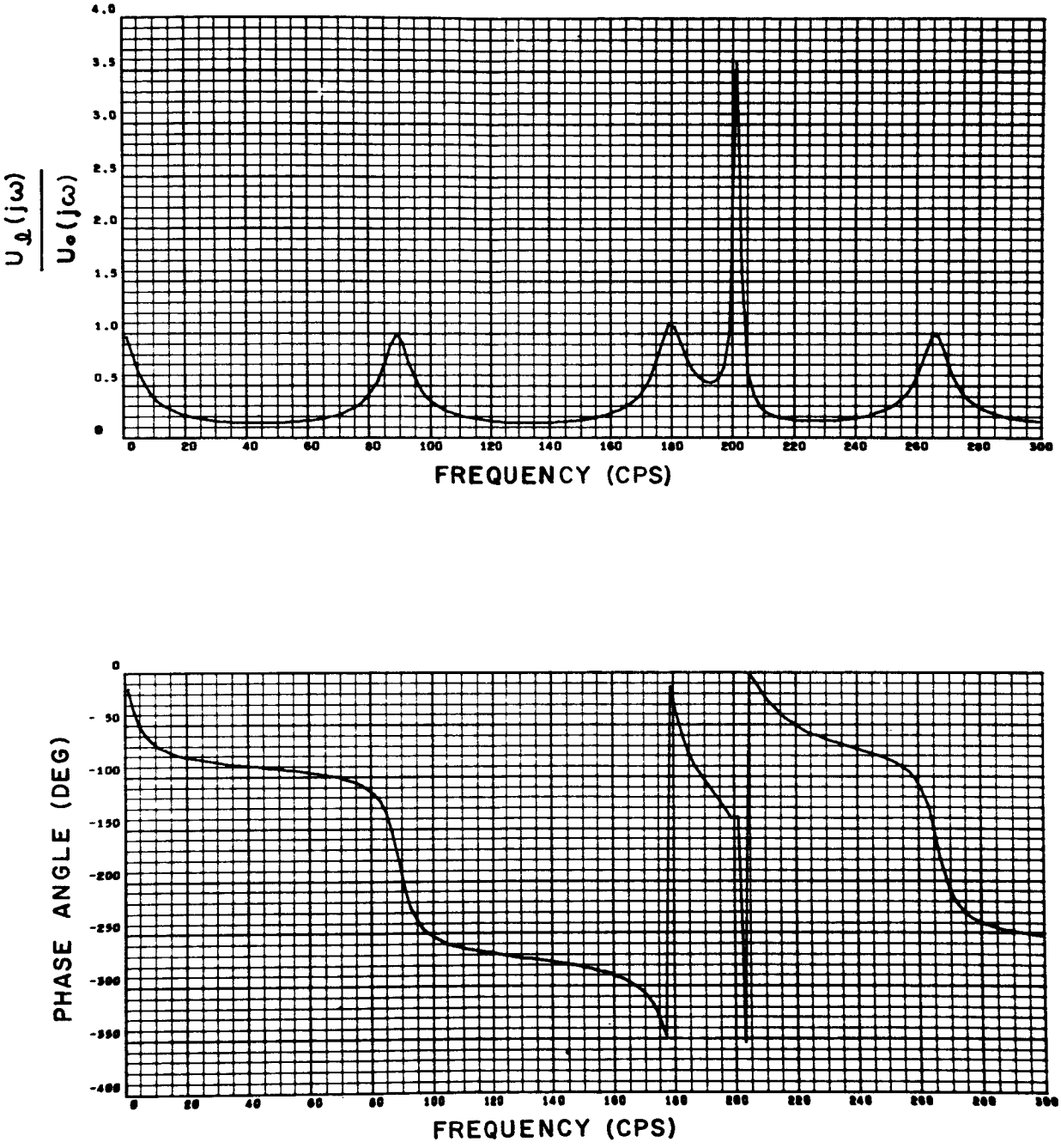

Figure A-11. The Ratio of Velocity Deviation at x = ℓ to Velocity Deviation at x = 0 for Outboard LH_2 Line, Frictionless and Including Pipe Vibration

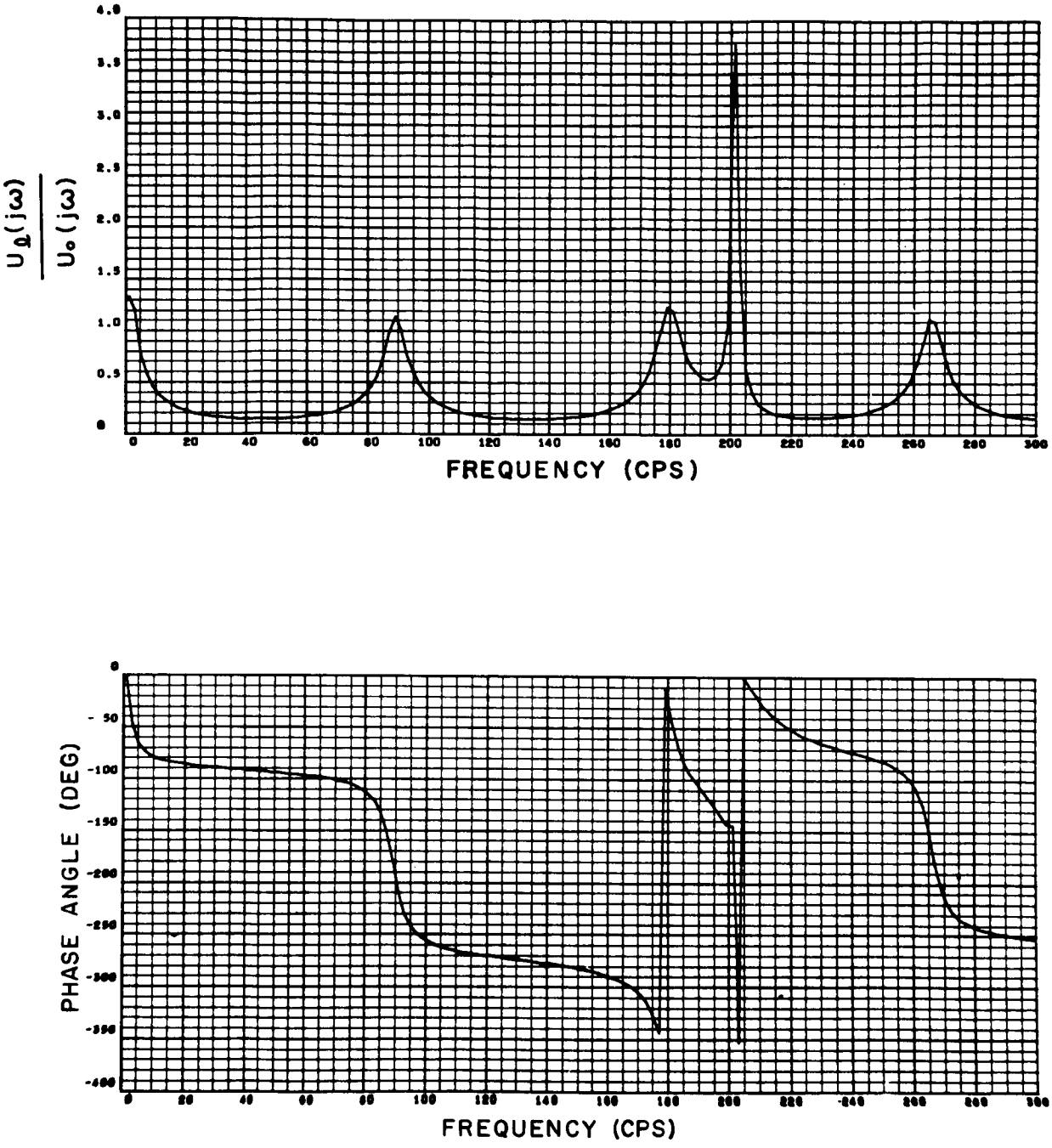

Figure A-12. The Ratio of Velocity Deviation at $x = \ell$ to Velocity Deviation at $x = 0$ for Outboard LH_2 Line, With Turbulent Resistance and Including Pipe Vibration

APPENDIX B. VELOCITY AND PRESSURE DATA

Velocity and pressure time histories for the center liquid hydrogen line on the Saturn S-II engine

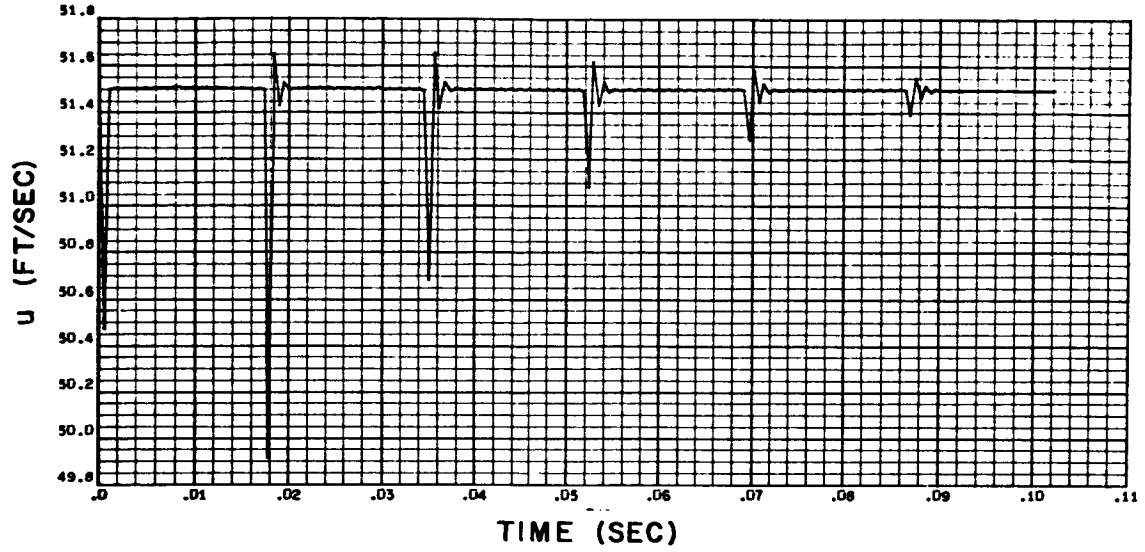

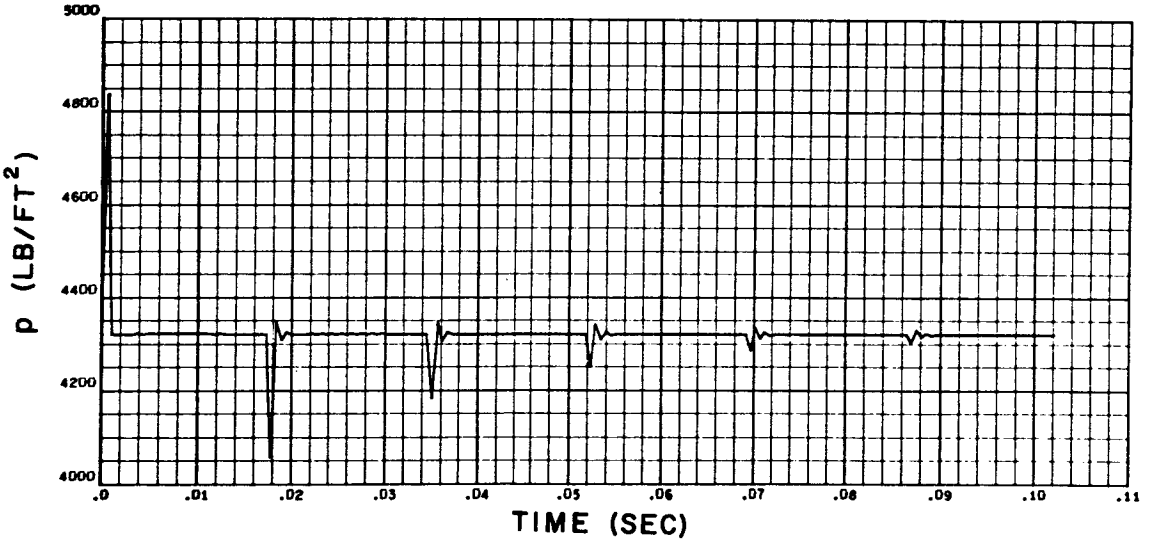

Figure B-1. Velocity and Pressure Time History at Right End of Feed Line, Impulse Disturbance 2 Percent of Steady-State Velocity

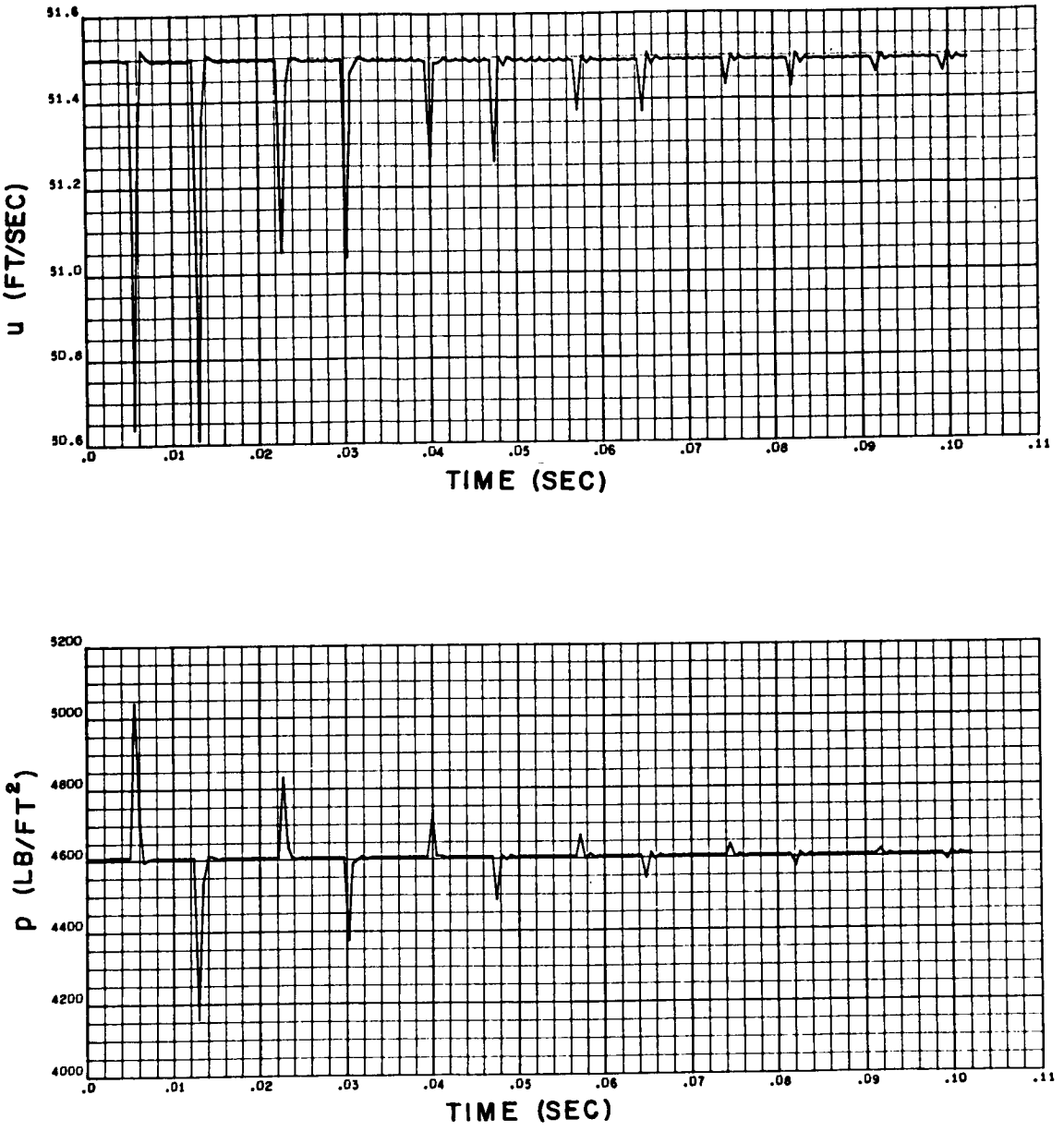

Figure B-2. Velocity and Pressure Time History at Midpoint of Feed Line, Impulse Disturbance 2 Percent of Steady-State Velocity

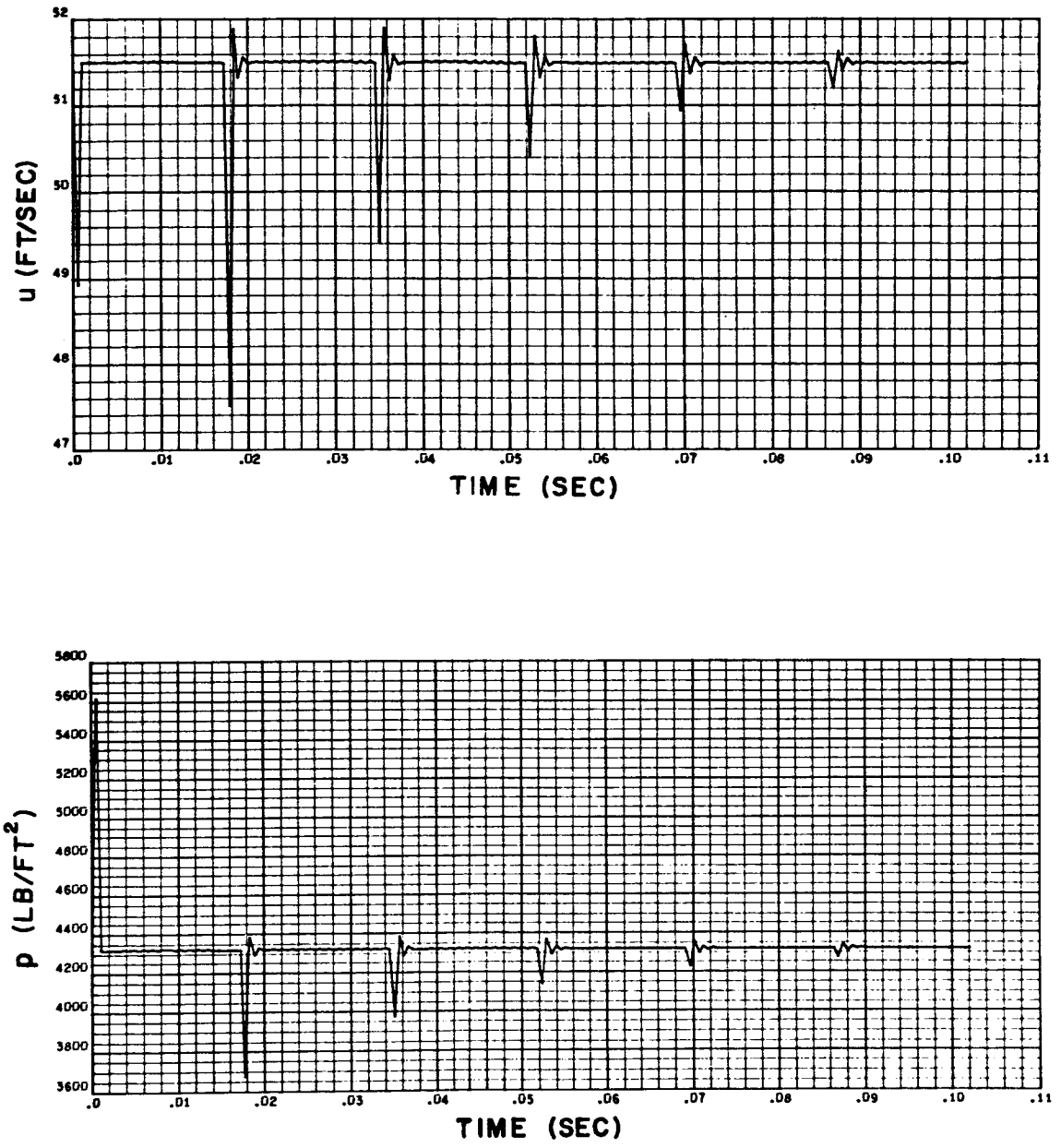

Figure B-3. Velocity and Pressure Time History at Right End of Feed Line, Impulse Disturbance 5 Percent of Steady-State Velocity

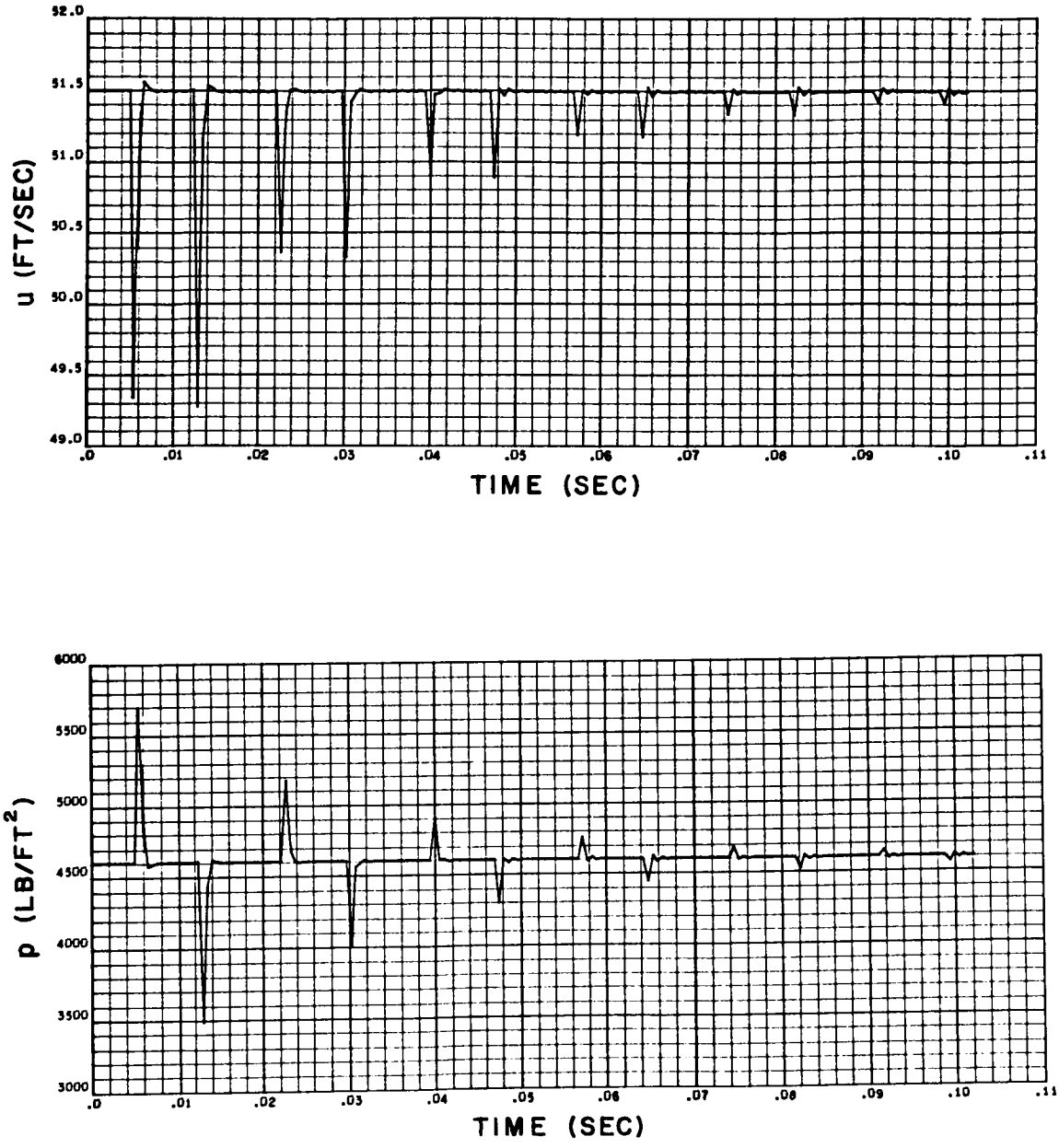

Figure B-4. Velocity and Pressure Time History at Midpoint of Feed Line, Impulse Disturbance 5 Percent of Steady-State Velocity

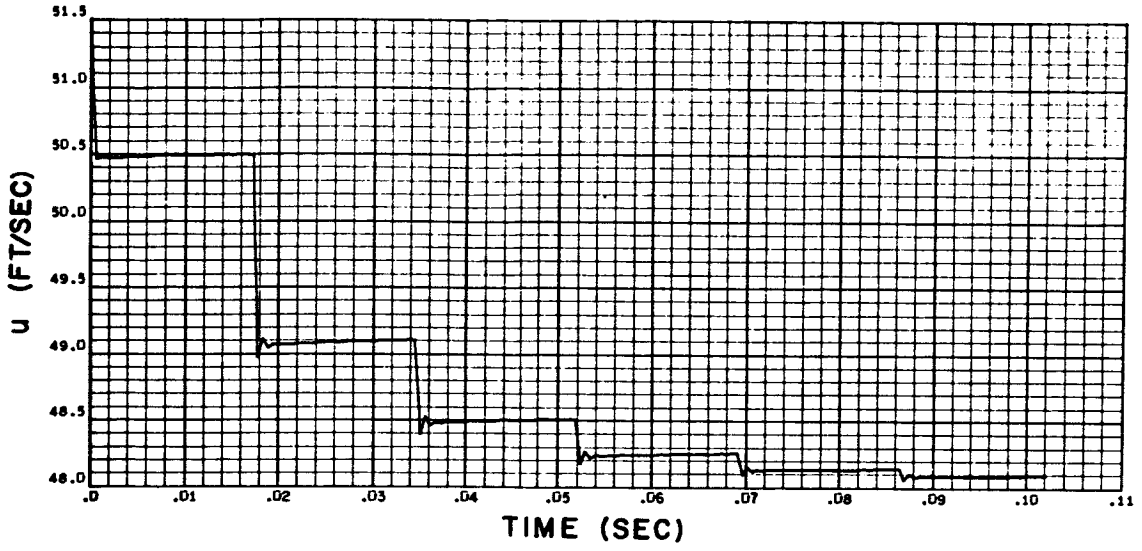

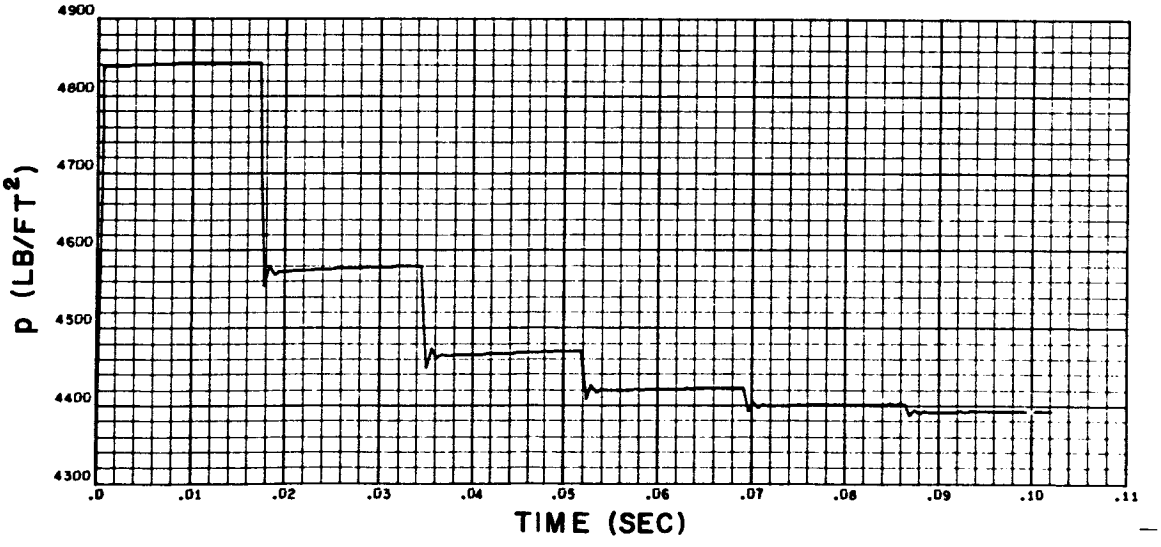

Figure B-5. Velocity and Pressure Time History at Right End of Feed Line, Step Disturbance 2 Percent of Steady-State Velocity

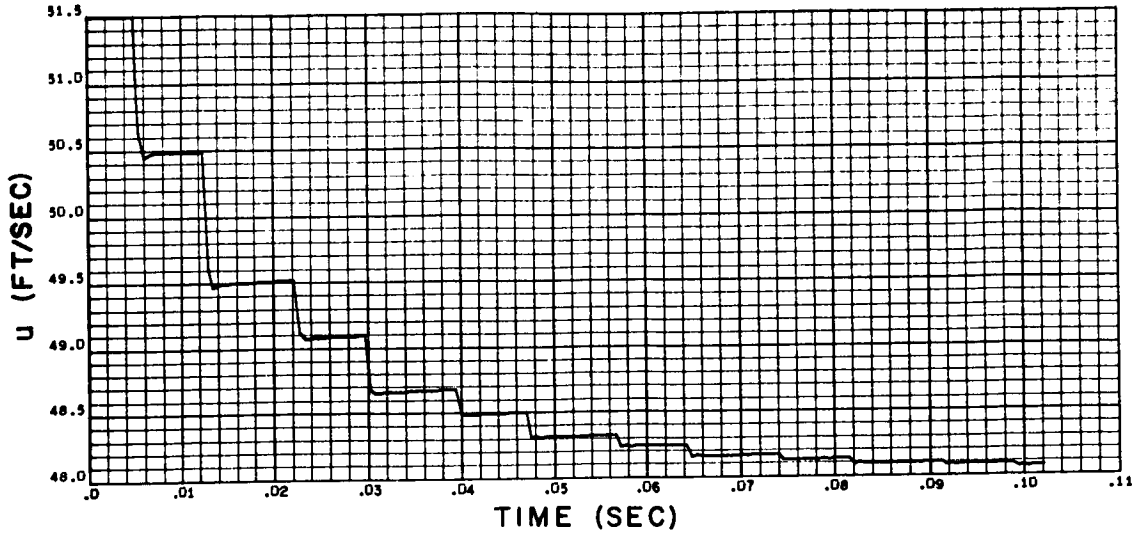

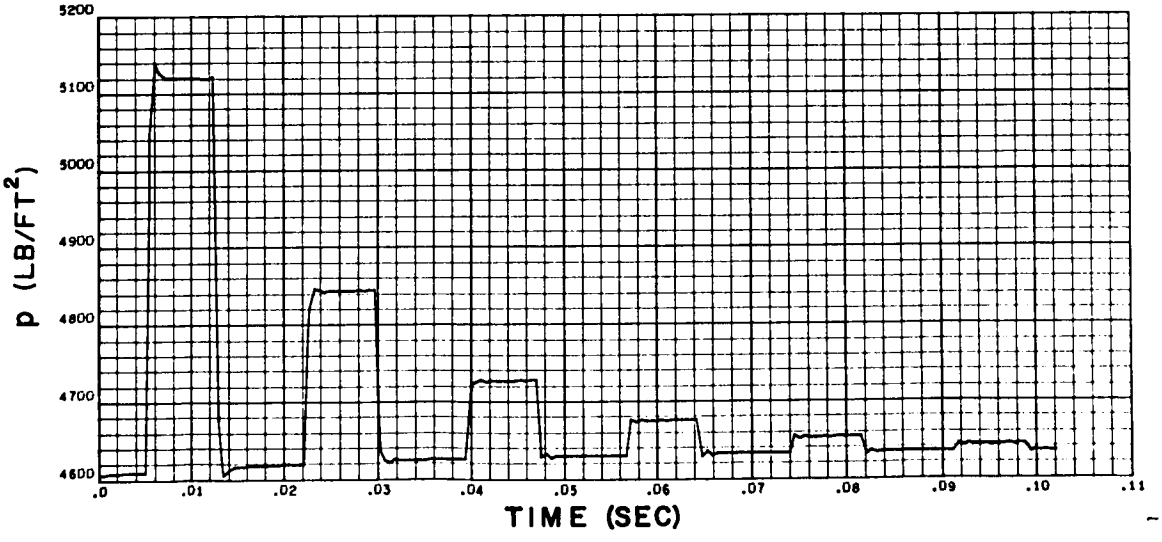

Figure B-6. Velocity and Pressure Time History at Midpoint of Feed Line, Step Disturbance 2 Percent of Steady-State Velocity

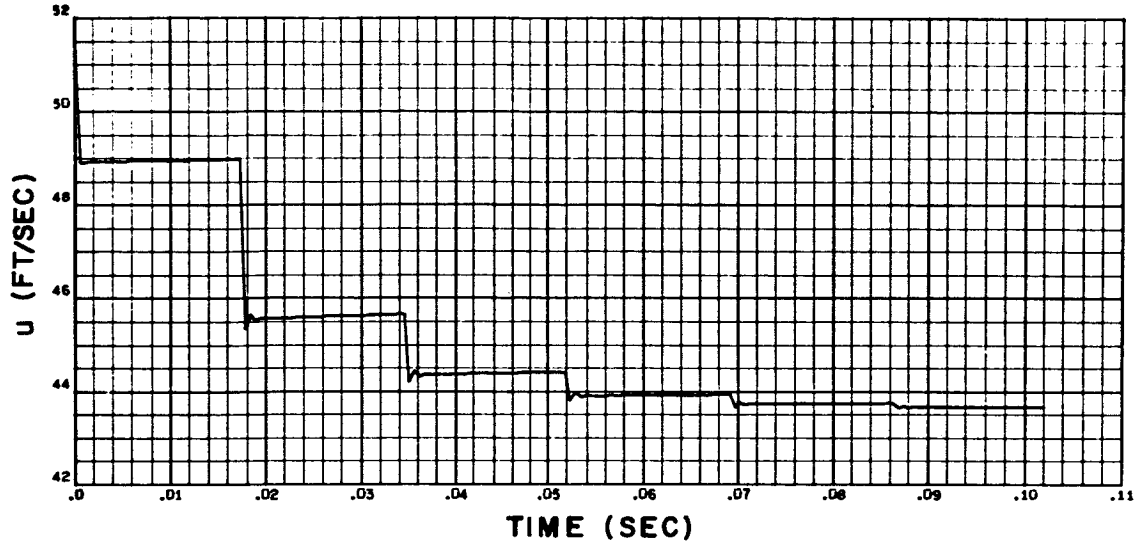

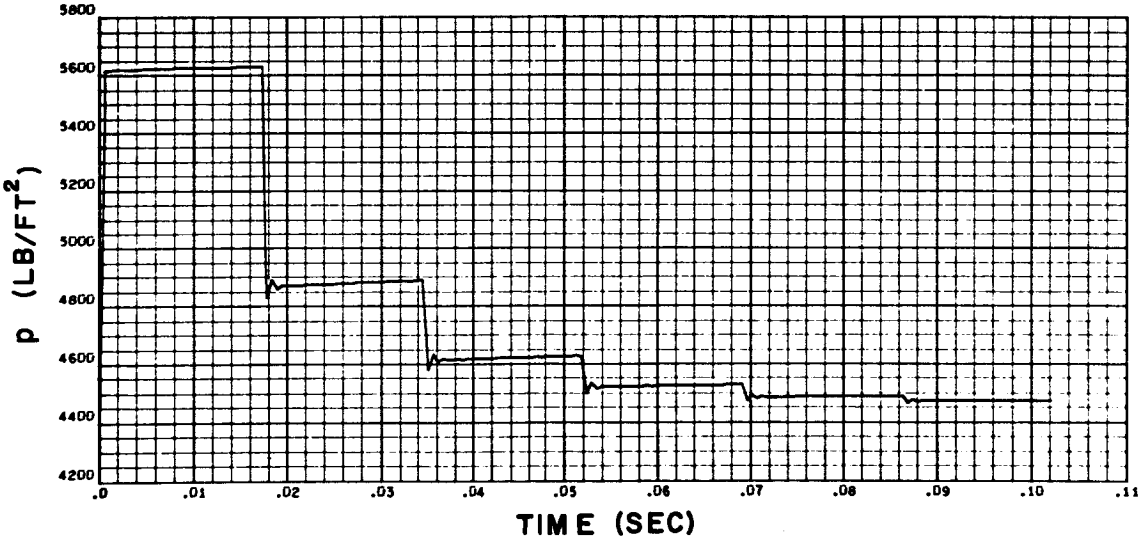

Figure B-7. Velocity and Pressure Time History at Right End of Feed Line, Step Distrubance 5 Percent of Steady-State Velocity

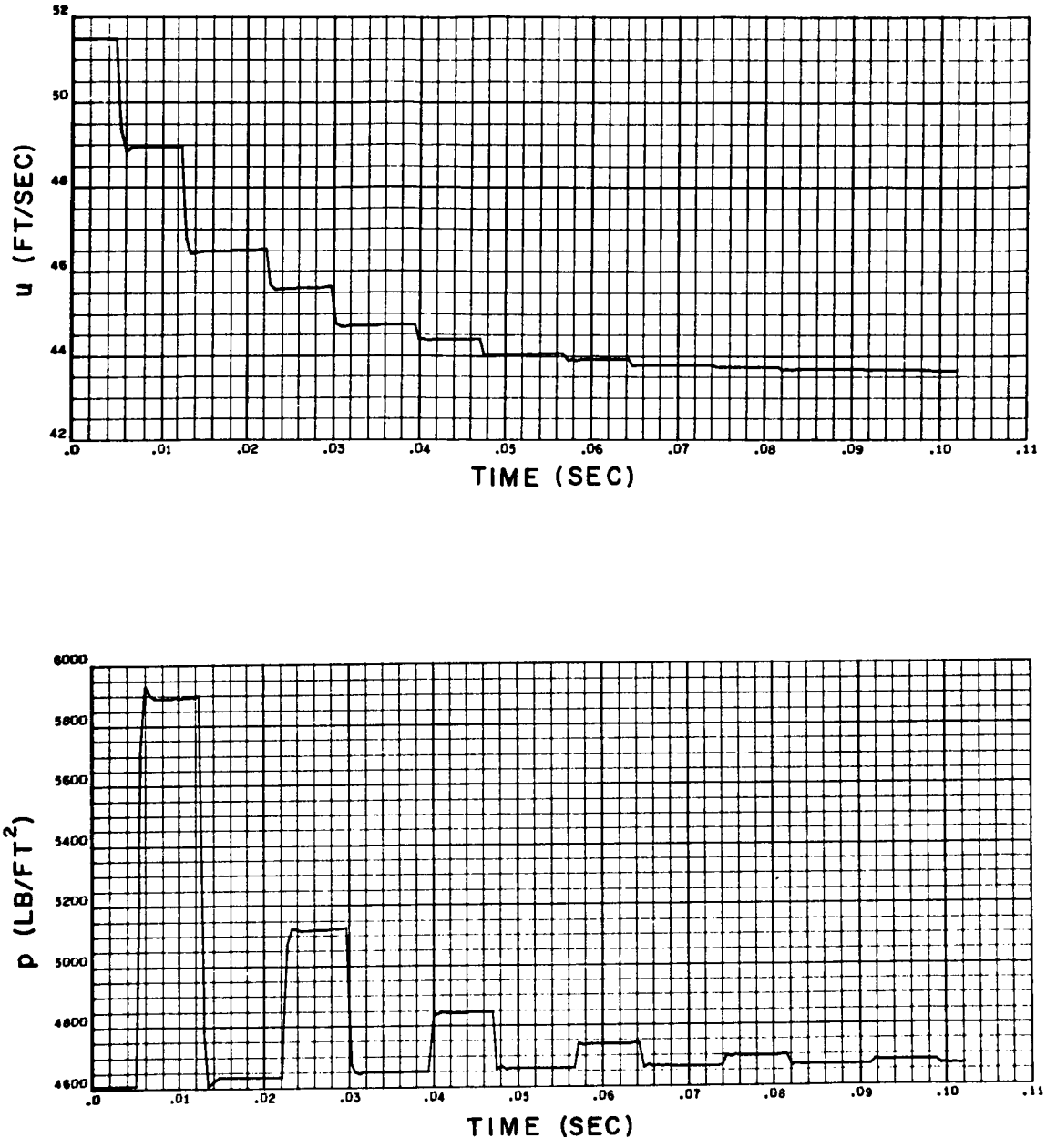

Figure B-8. Velocity and Pressure Time History at Midpoint of Feed Line, Step Disturbance 5 Percent of Steady-State Velocity

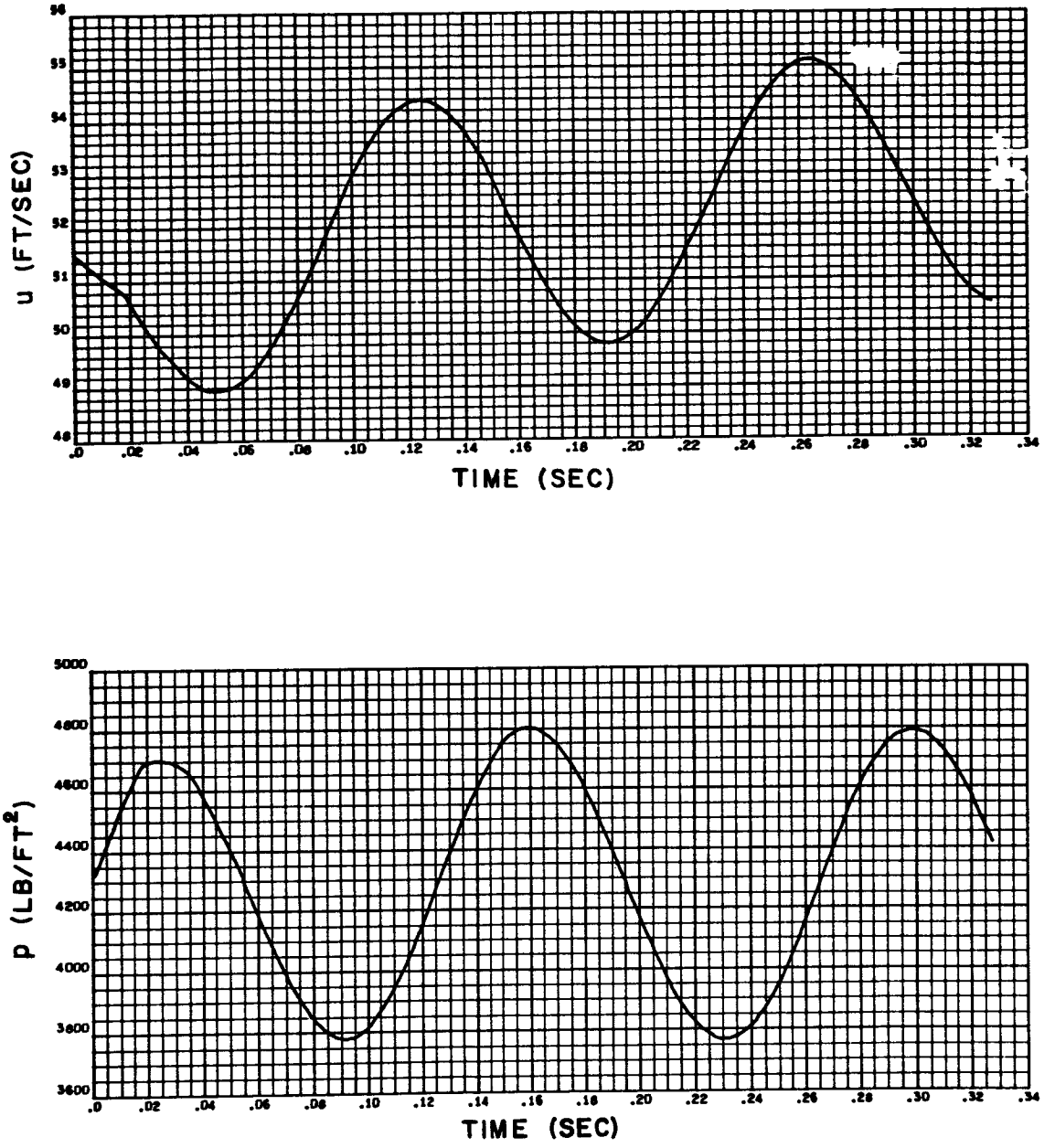

Figure B-9. Velocity and Pressure Time History at Right End of Feed Line Under Sinusoidal Disturbance, Amplitude 2 Percent of Steady-State Velocity, Frequency 7.20 cps

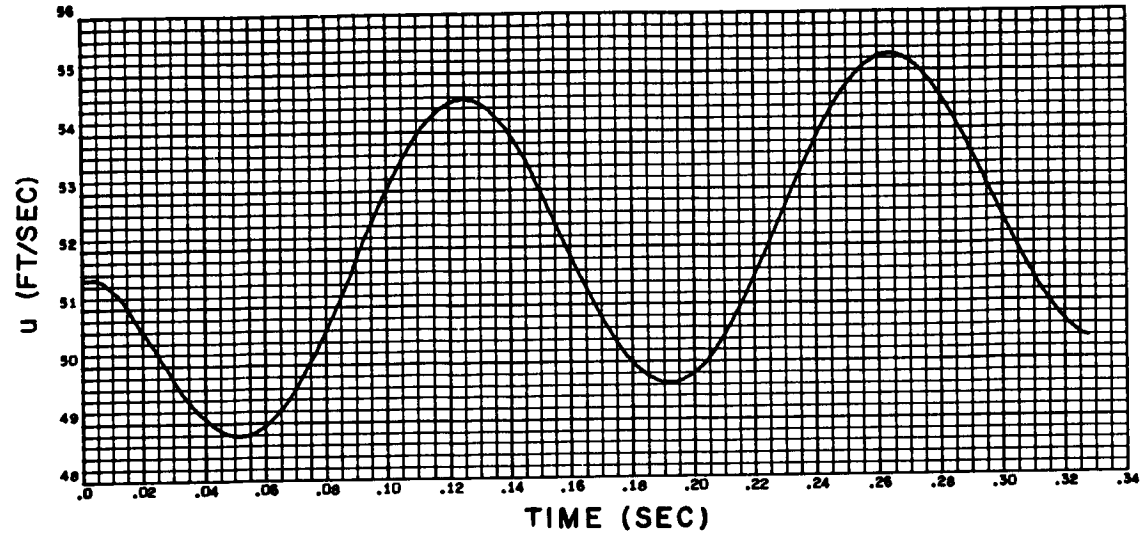

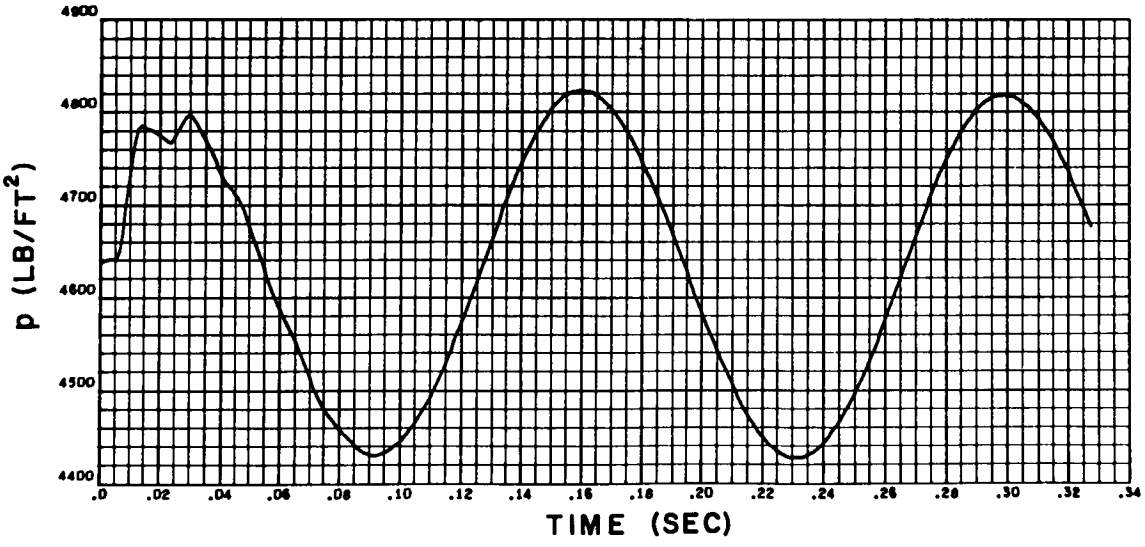

Figure B-10. Velocity and Pressure Time History at Midpoint of Feed Line Under Sinusoidal Disturbance, Amplitude 2 Percent of Steady-State Velocity, Frequency 7.20 cps

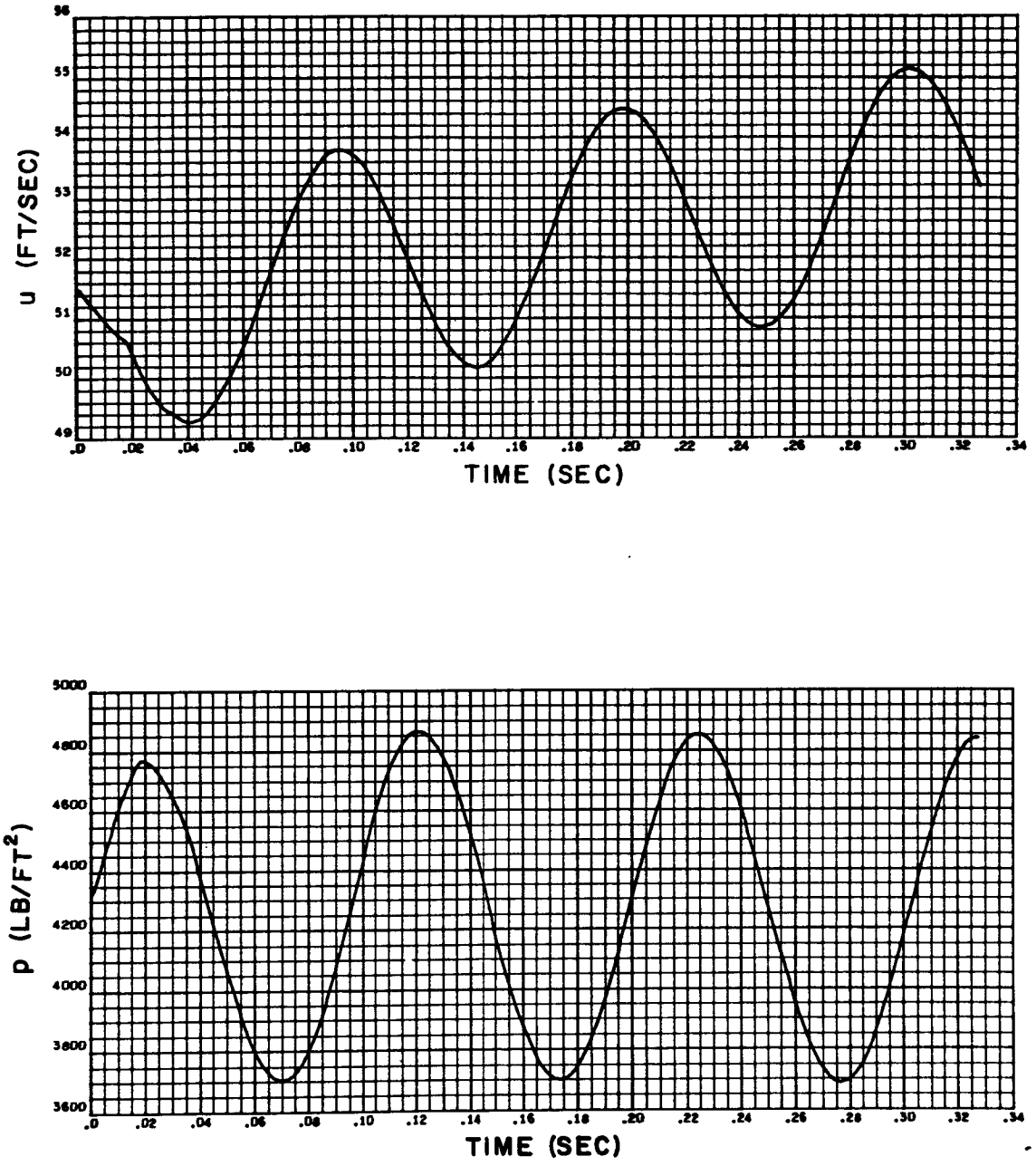

Figure B-11. Velocity and Pressure Time History at Right End of Feed Line Under Sinusoidal Disturbance, Amplitude 2 Percent of Steady-State Velocity, Frequency 9.70 cps

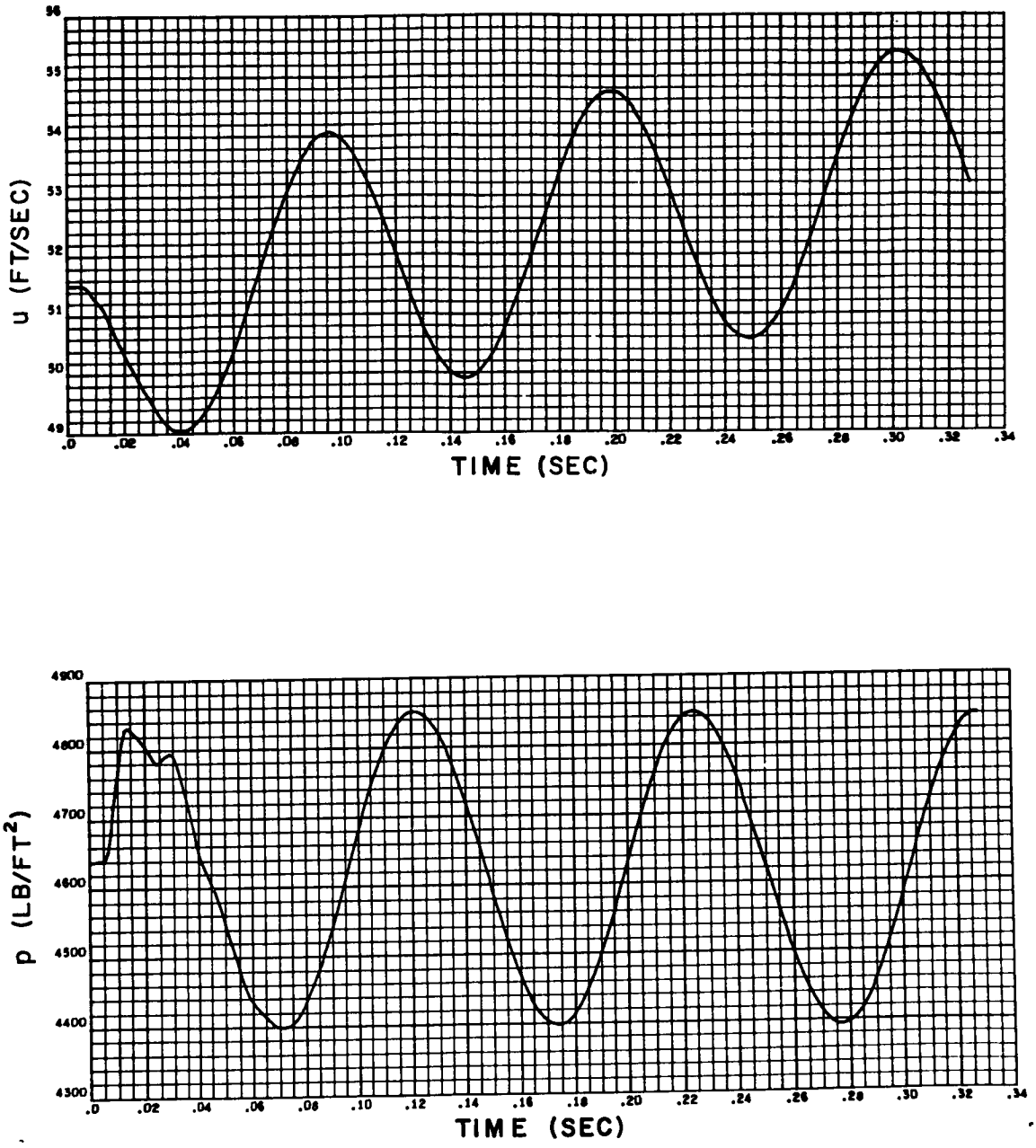

Figure B-12. Velocity and Pressure Time History at Midpoint of Feed Line Under Sinusoidal Disturbance, Amplitude 2 Percent of Steady-State Velocity, Frequency 9.70 cps

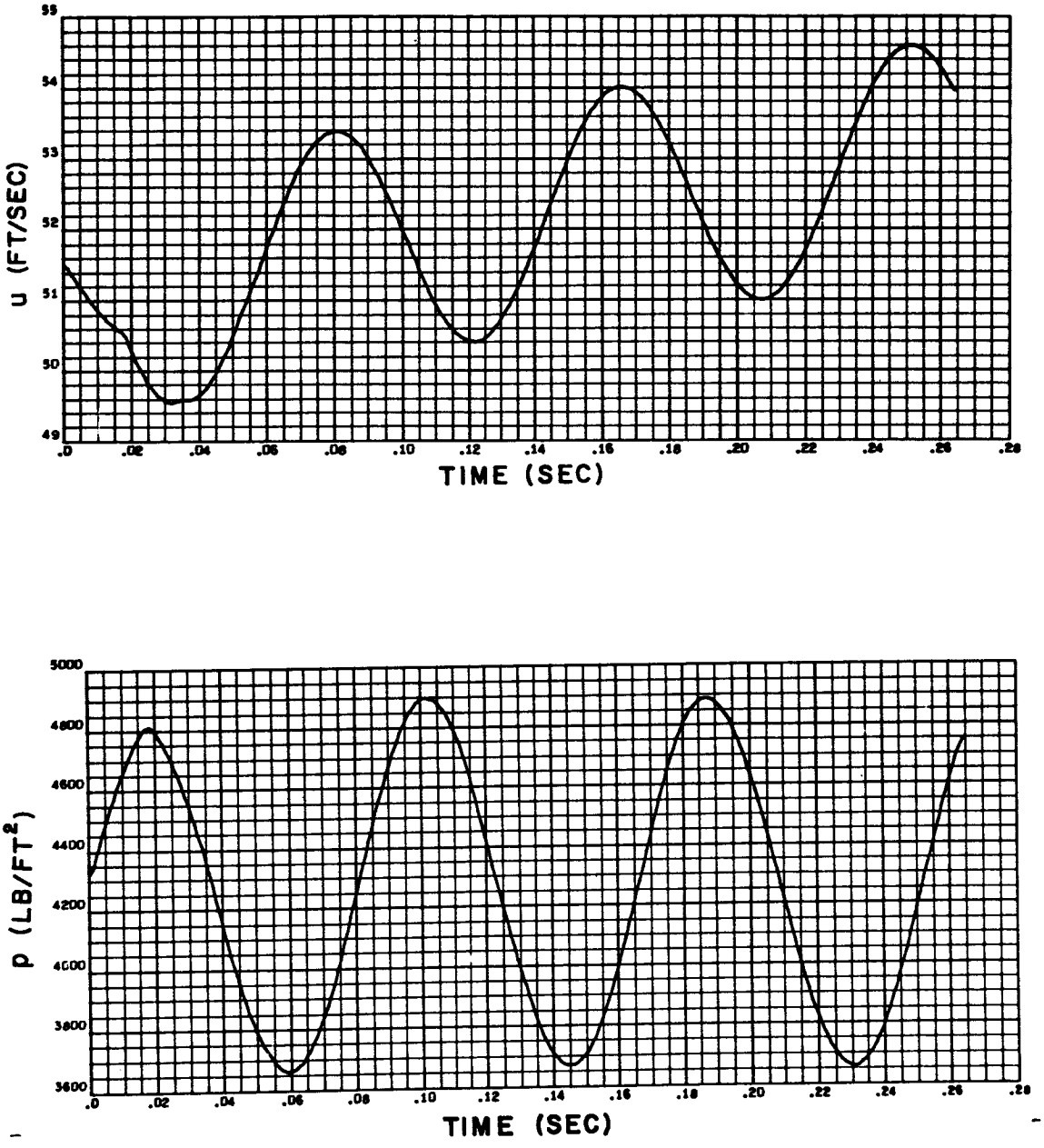

Figure B-13. Velocity and Pressure Time History at Right End of Feed Line Under Sinusoidal Disturbance, Amplitude 2 Percent of Steady-State Velocity, Frequency 11.70 cps

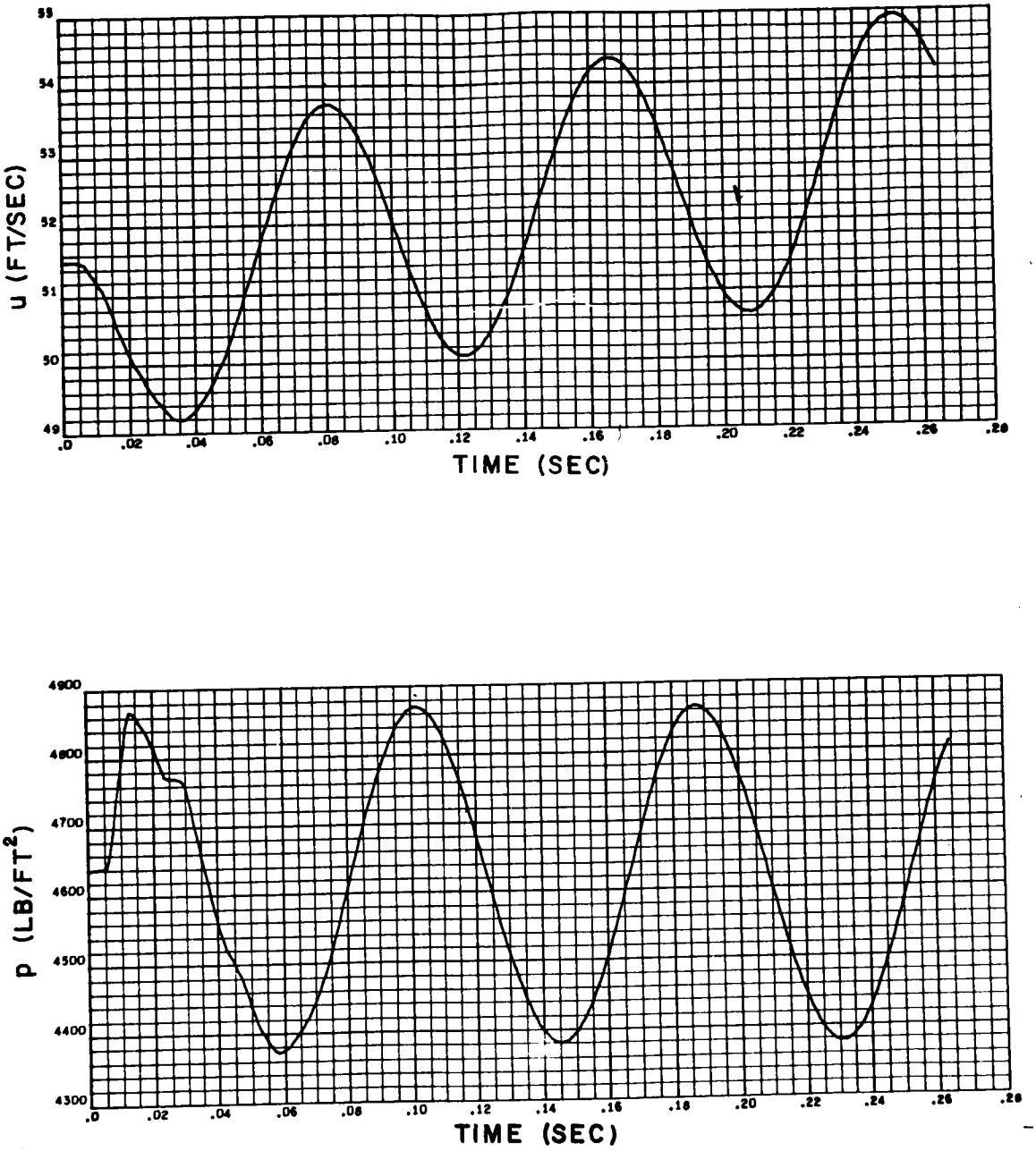

Figure B-14. Velocity and Pressure Time History at Midpoint of Feed Line Under Sinusoidal Disturbance, Amplitude 2 Percent of Steady-State Velocity, Frequency 11.70 cps

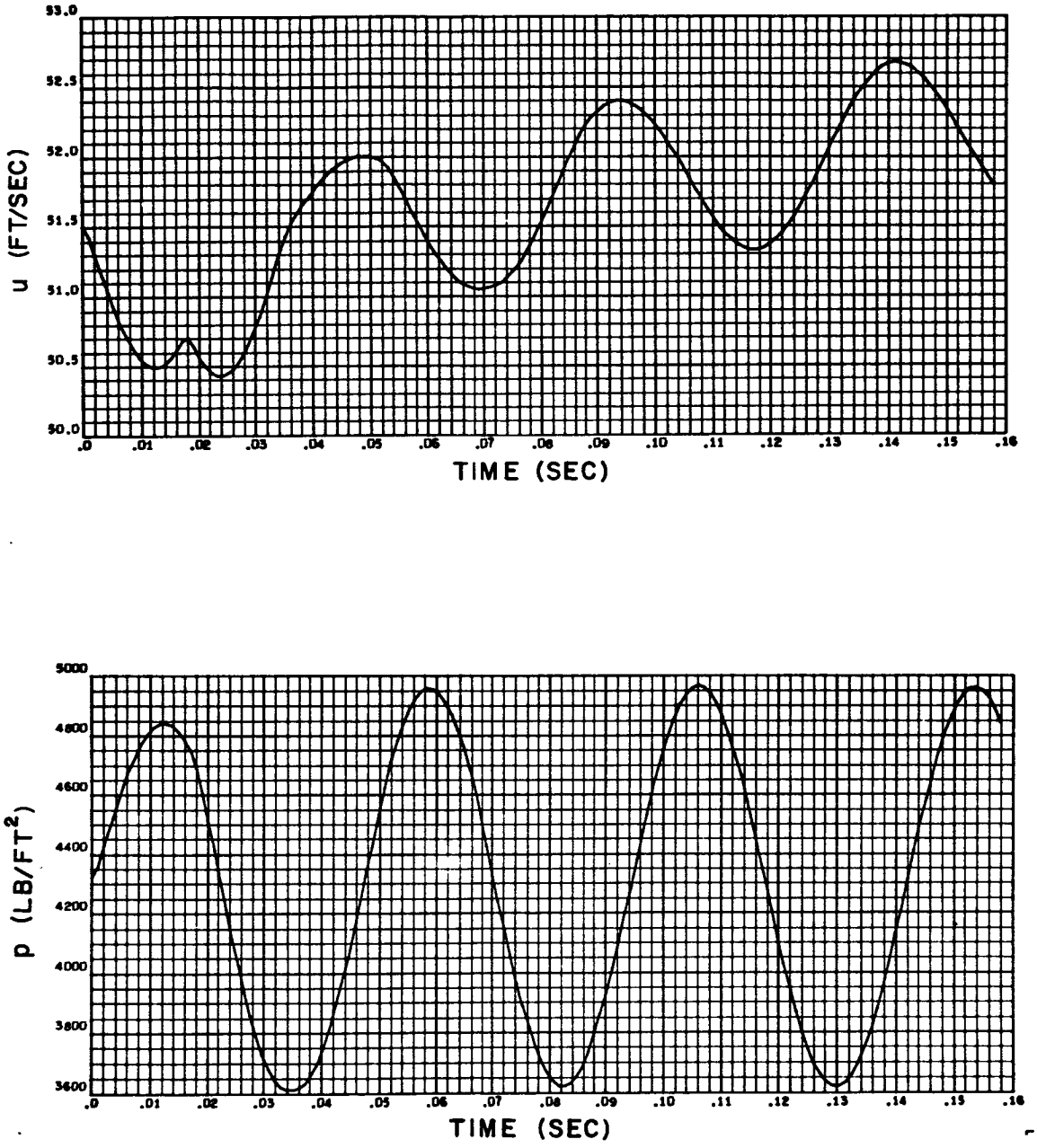

Figure B-15. Velocity and Pressure Time History at Right End of Feed Line Under Sinusoidal Disturbance, Amplitude 2 Percent of Steady-State Velocity, Frequency 21.11 cps

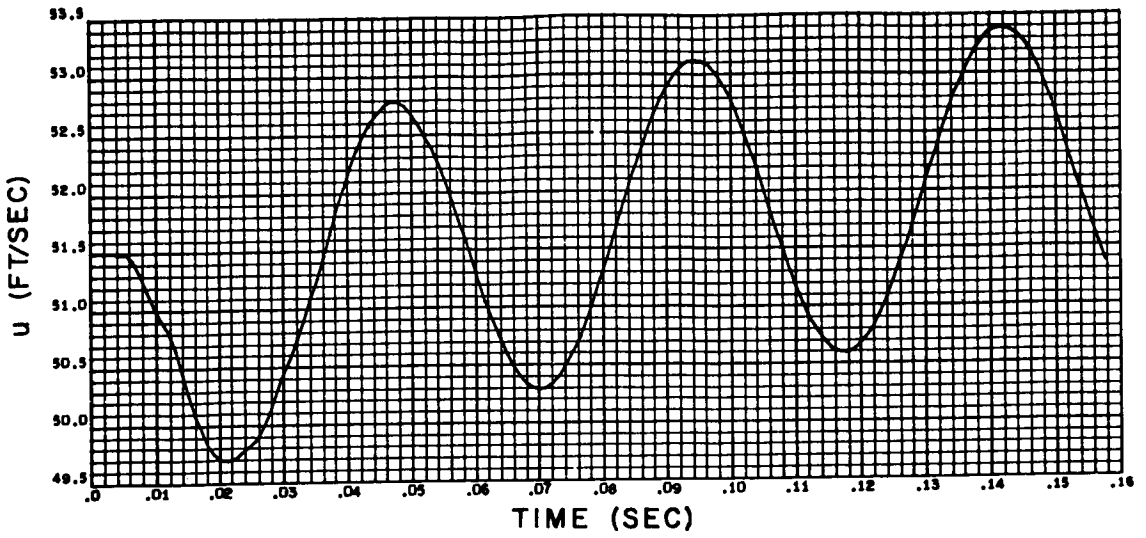

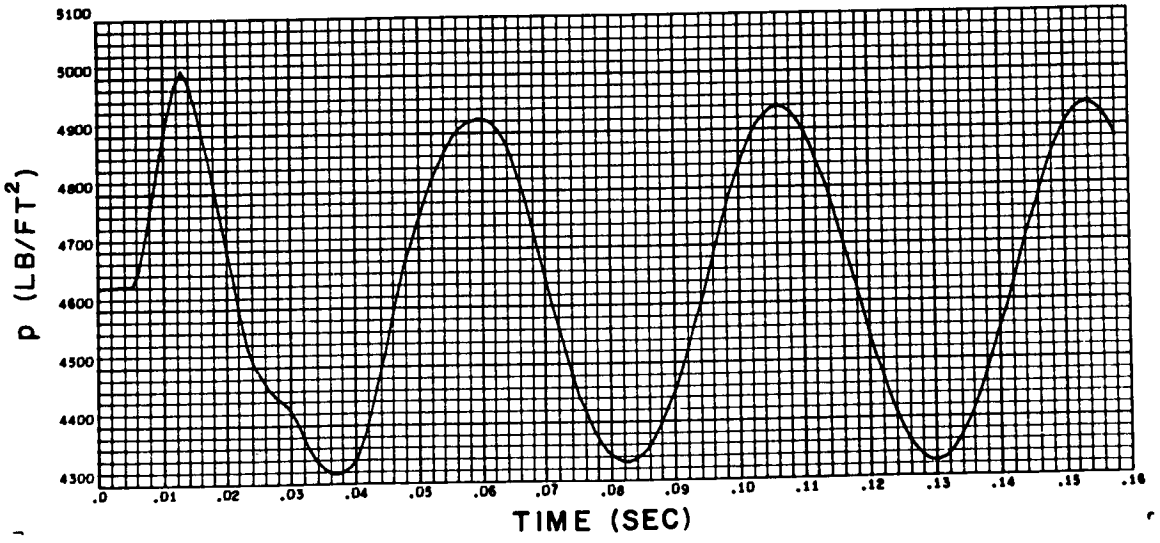

Figure B-16. Velocity and Pressure Time History at Midpoint of Feed Line Under Sinusoidal Disturbance, Amplitude 2 Percent of Steady-State Velocity, Frequency 21.11 cps

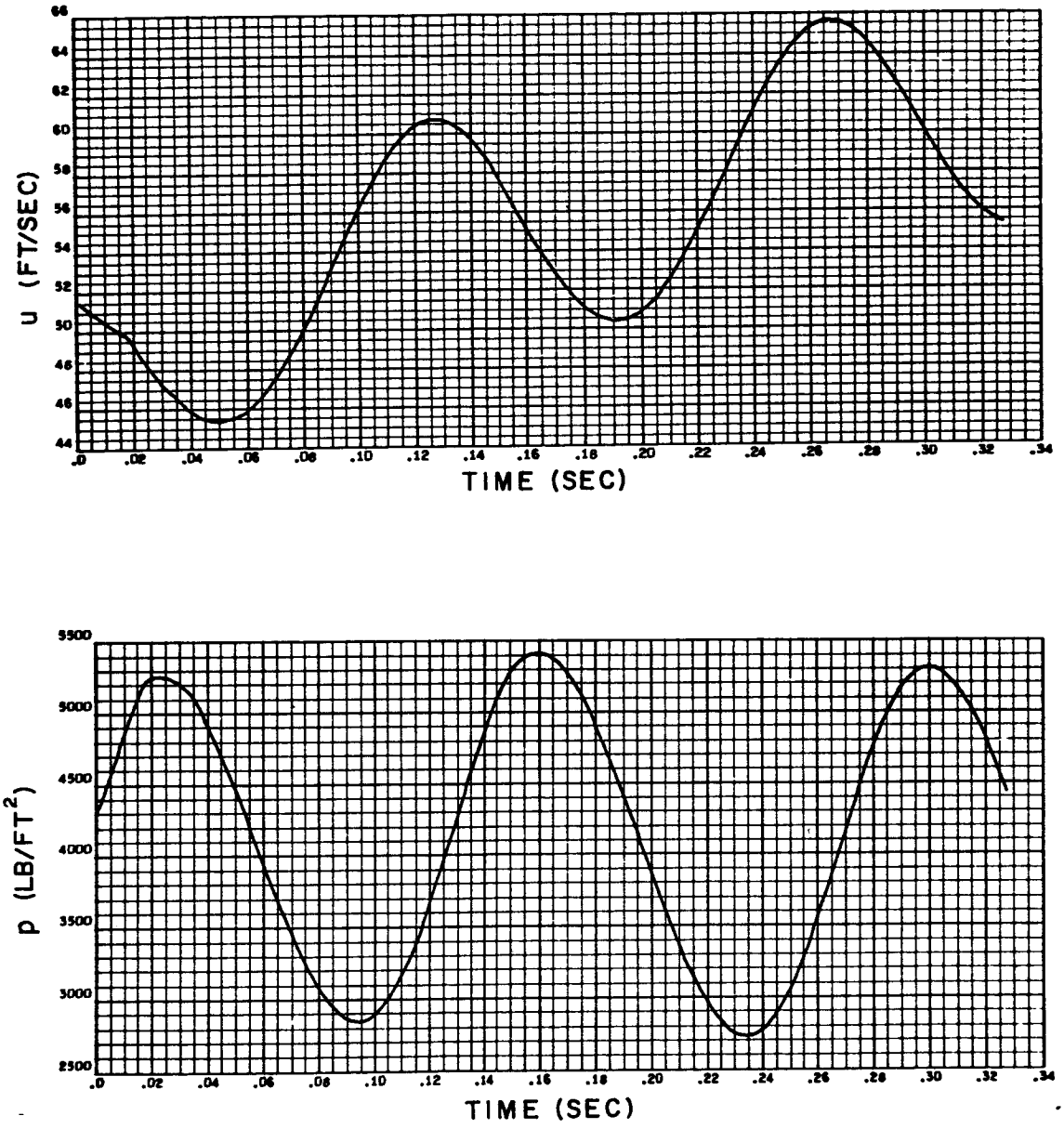

Figure B-17. Velocity and Pressure Time History at Right End of Feed Line Under Sinusoidal Disturbance, Amplitude 5 Percent of Steady-State Velocity, Frequency 7.20 cps

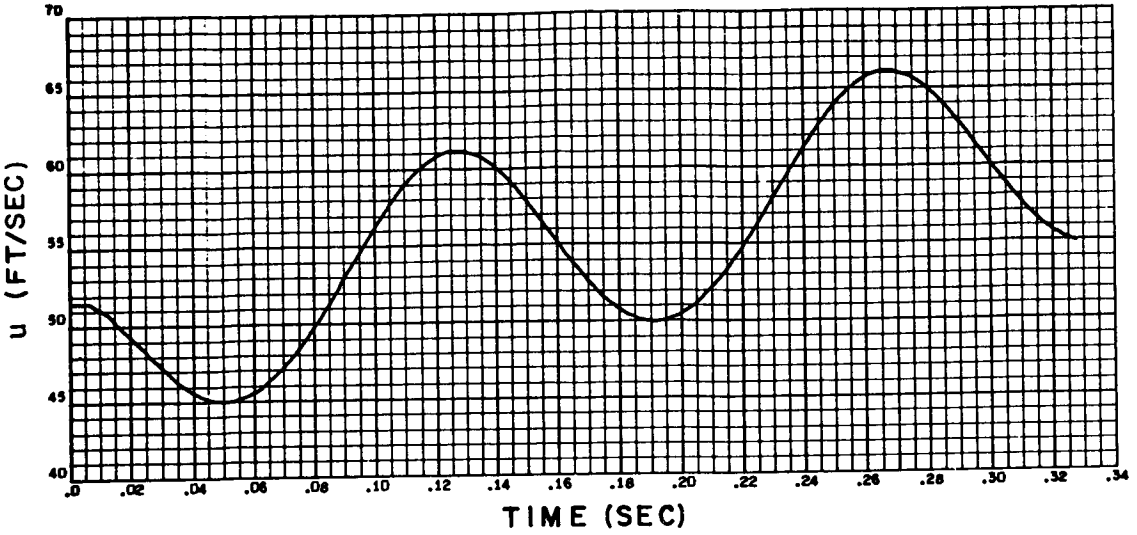

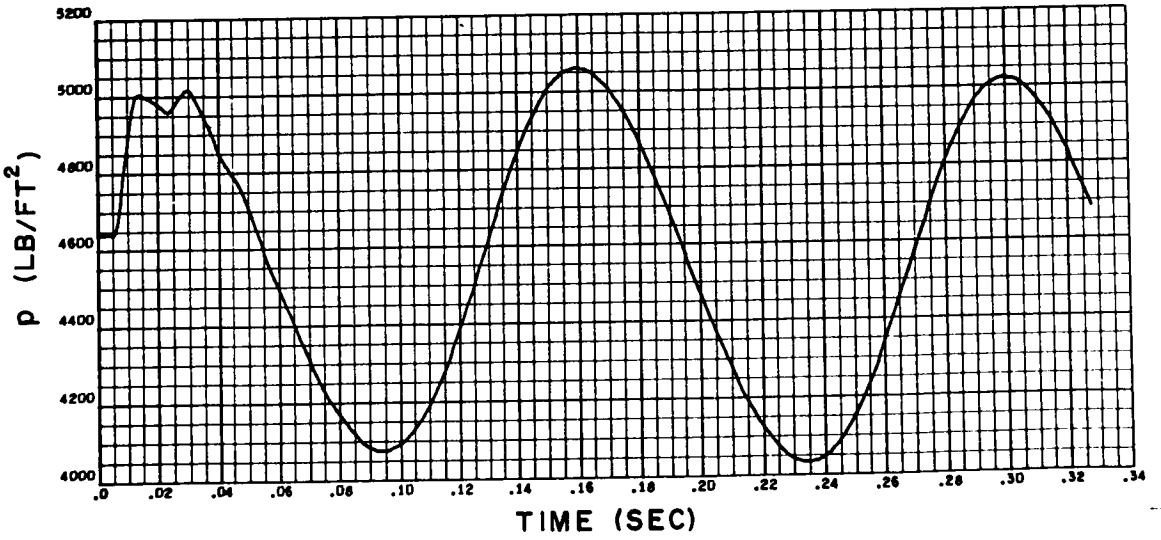

Figure B-18. Velocity and Pressure Time History at Midpoint of Feed Line Under Sinusoidal Disturbance, Amplitude 5 Percent of Steady-State Velocity, Frequency 7.20 cps

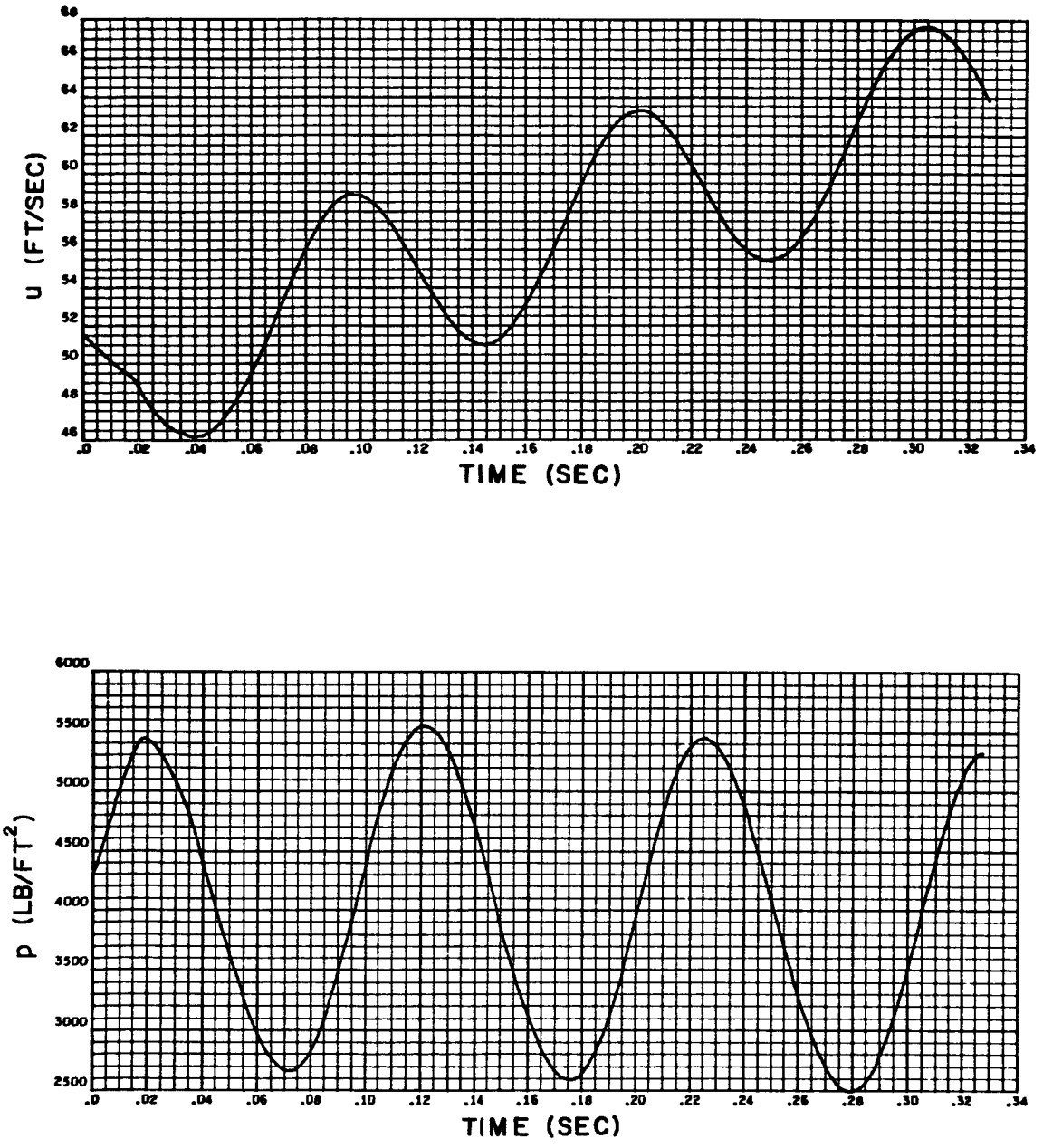

Figure B-19. Velocity and Pressure Time History at Right End of Feed Line Under Sinusoidal Disturbance, Amplitude 5 Percent of Steady-State Velocity, Frequency 9.70 cps

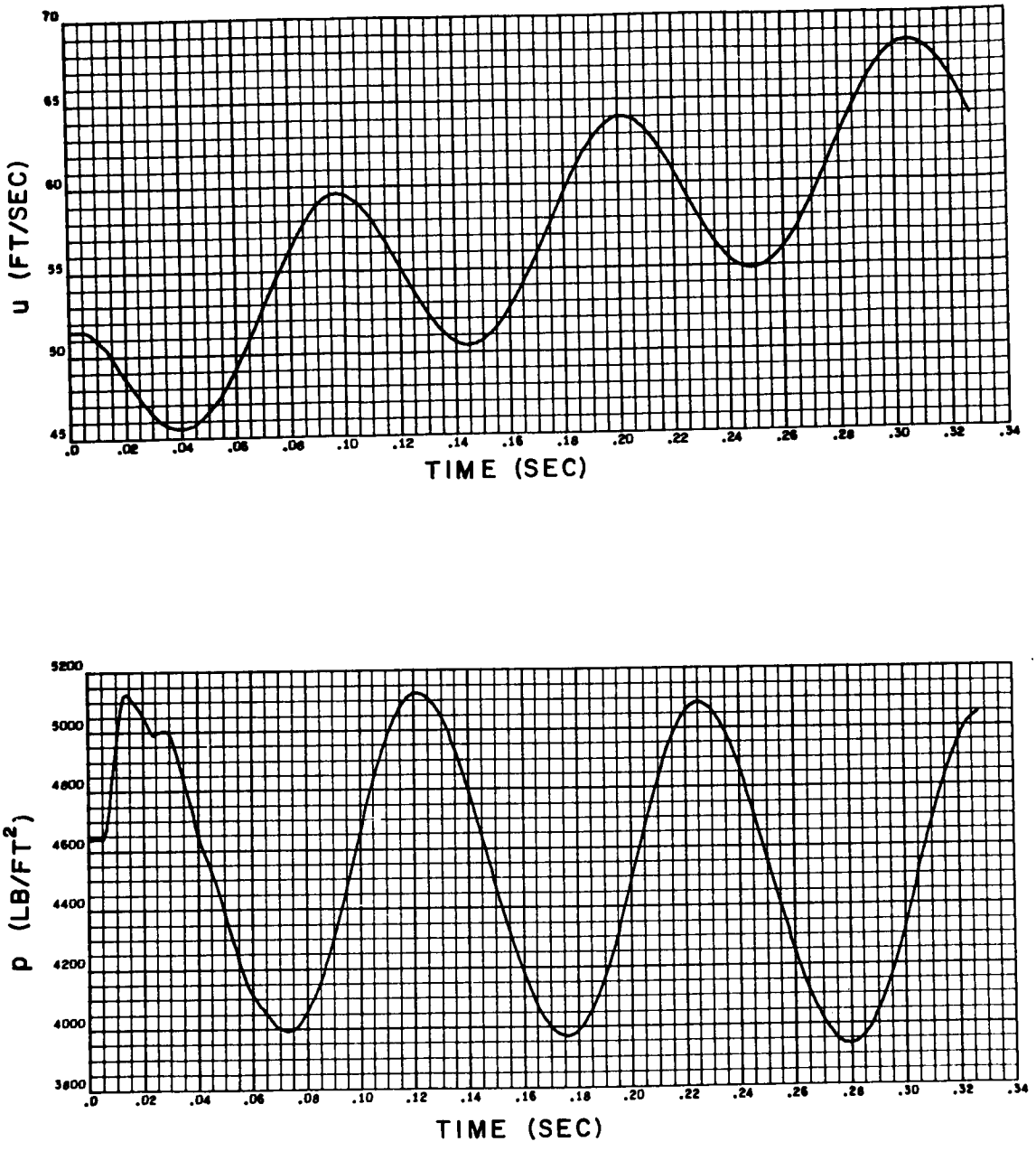

Figure B-20. Velocity and Pressure Time History at Midpoint of Feed Line Under Sinusoidal Disturbance, Amplitude 5 Percent of Steady-State Velocity, Frequency 9,70 cps

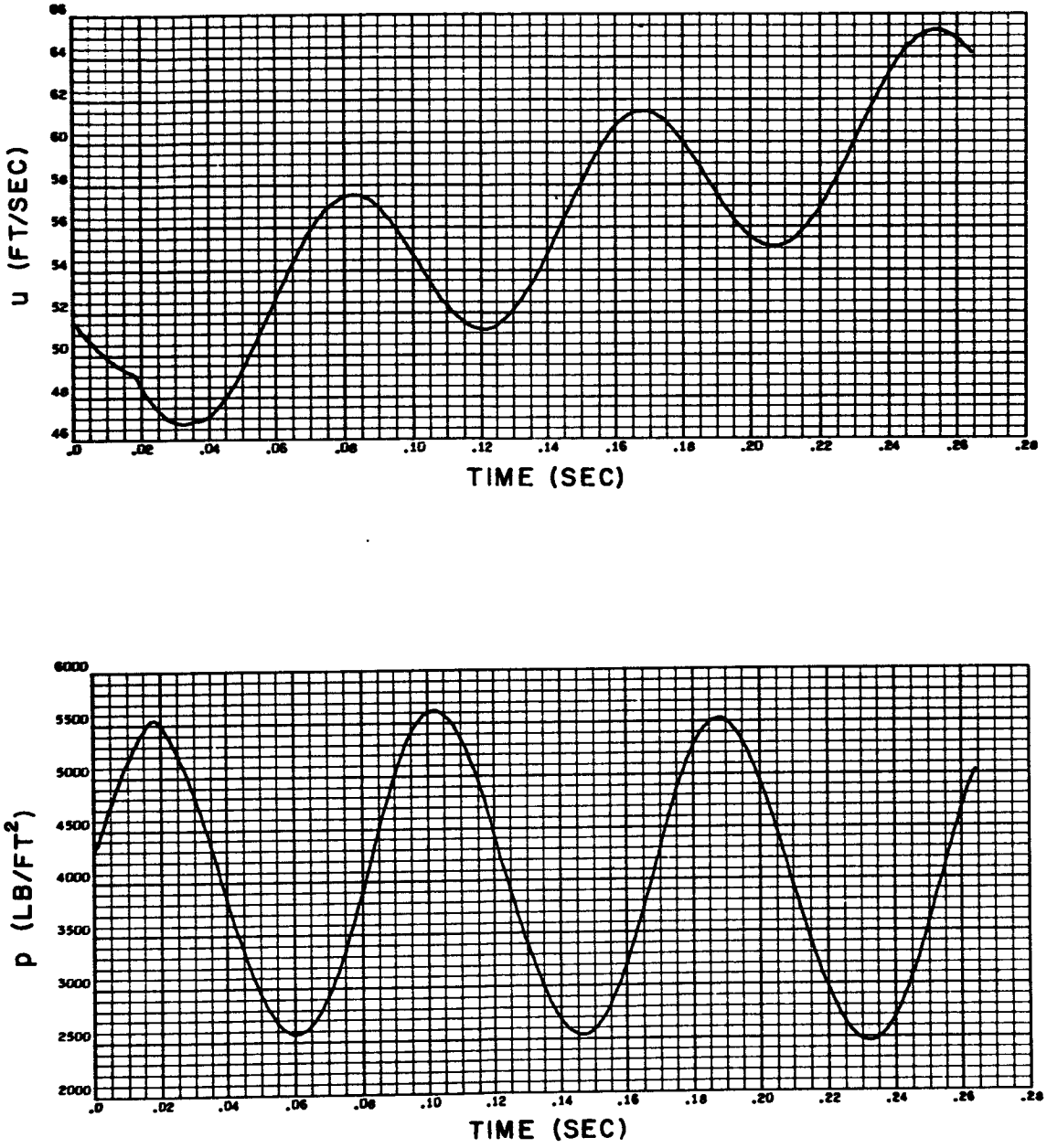

Figure B-21. Velocity and Pressure Time History at Right End of Feed Line Under Sinusoidal Disturbance, Amplitude 5 Percent of Steady-State Velocity, Frequency 11.70 cps

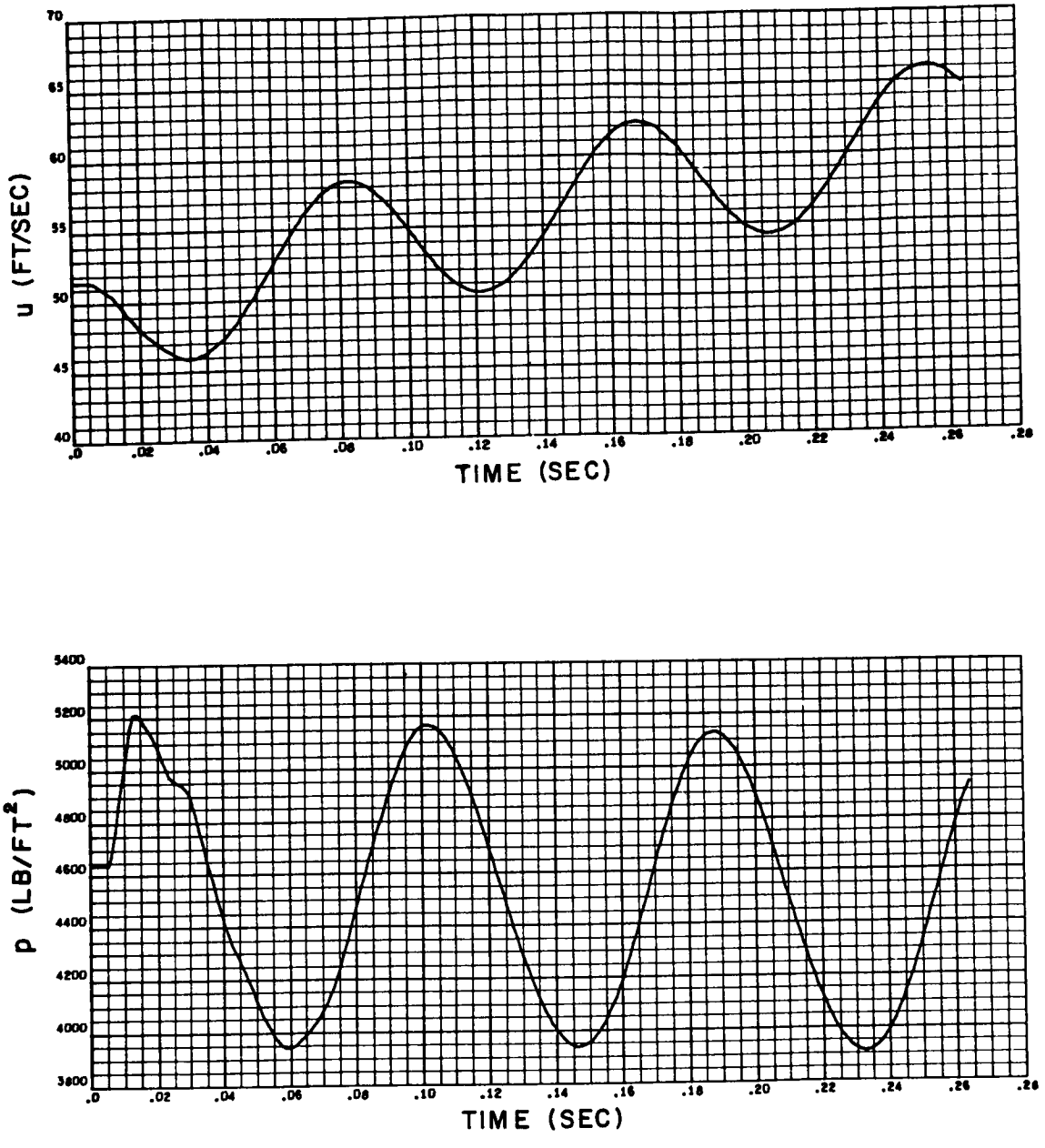

Figure B-22. Velocity and Pressure Time History at Midpoint of Feed Line Under Sinusoidal Disturbance, Amplitude 5 Percent of Steady-State Velocity, Frequency 11.70 cps

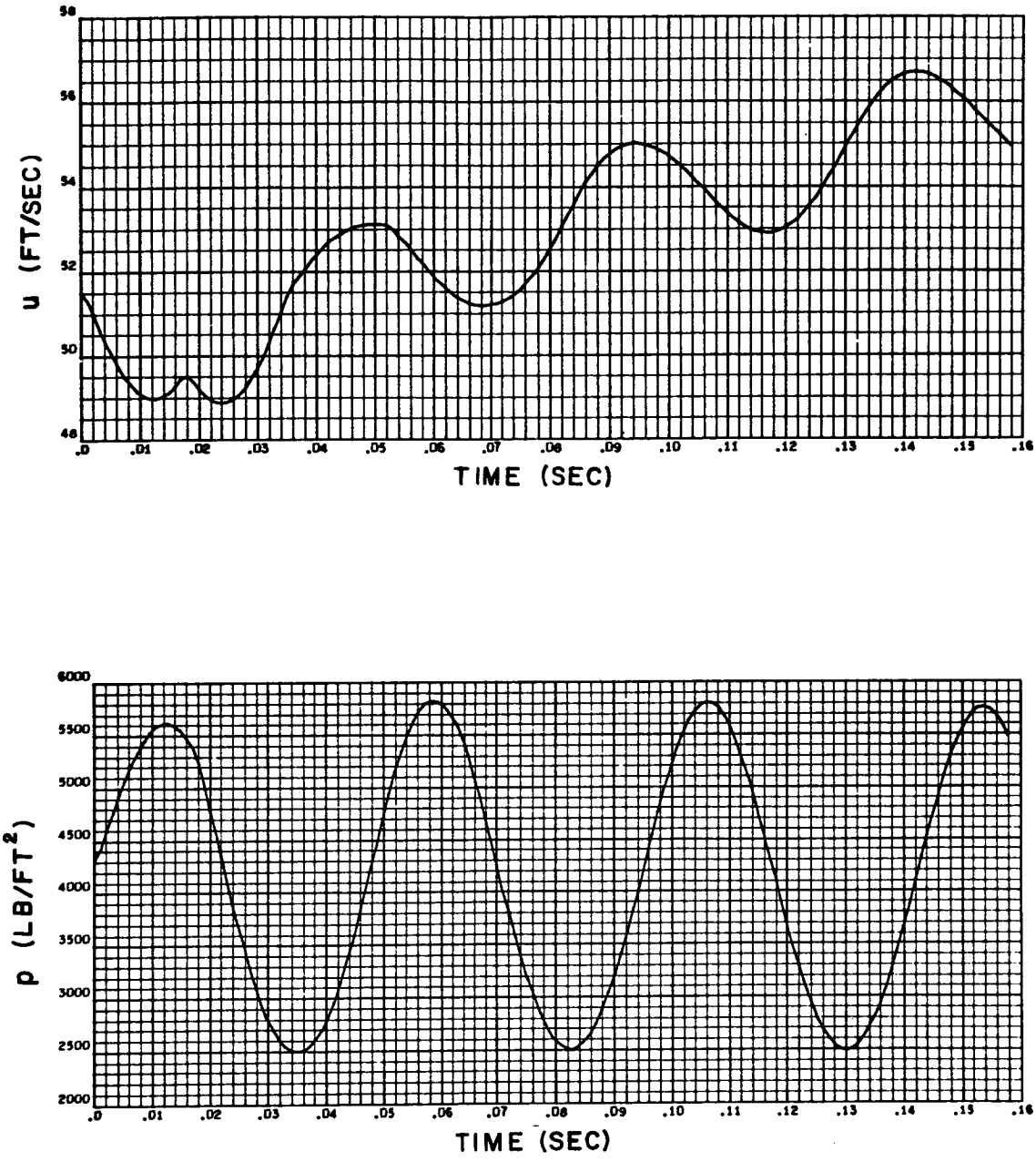

Figure B-23. Velocity and Pressure Time History at Right End of Feed Line Under Sinusoidal Disturbance, Amplitude 5 Percent of Steady-State Velocity, Frequency 21.11 cps

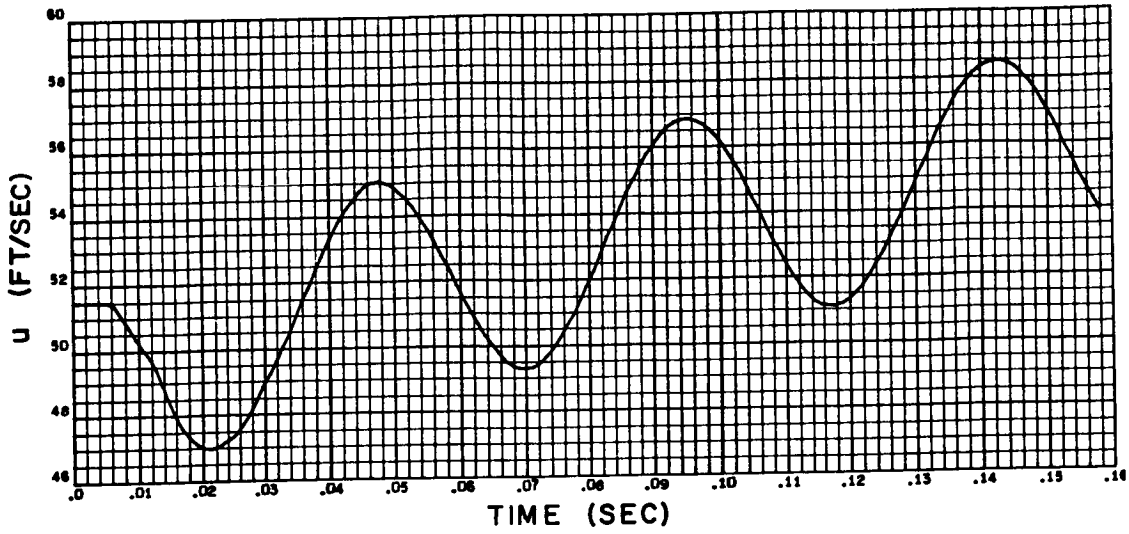

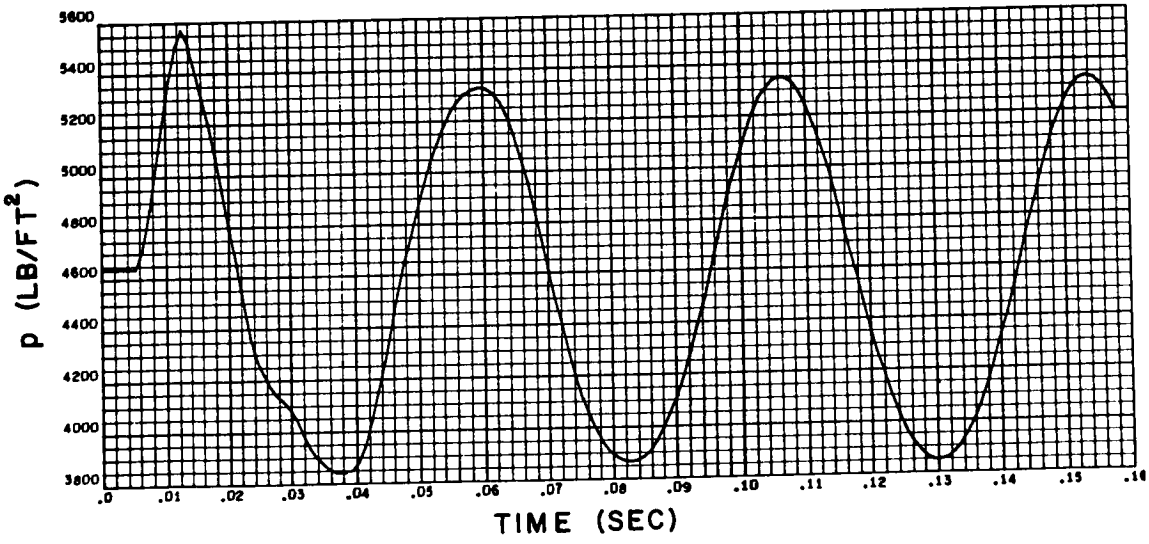

Figure B-24. Velocity and Pressure Time History at Midpoint of Feed Line Under Sinusoidal Disturbance, Amplitude 5 Percent of Steady-State Velocity, Frequency 21.11 cps

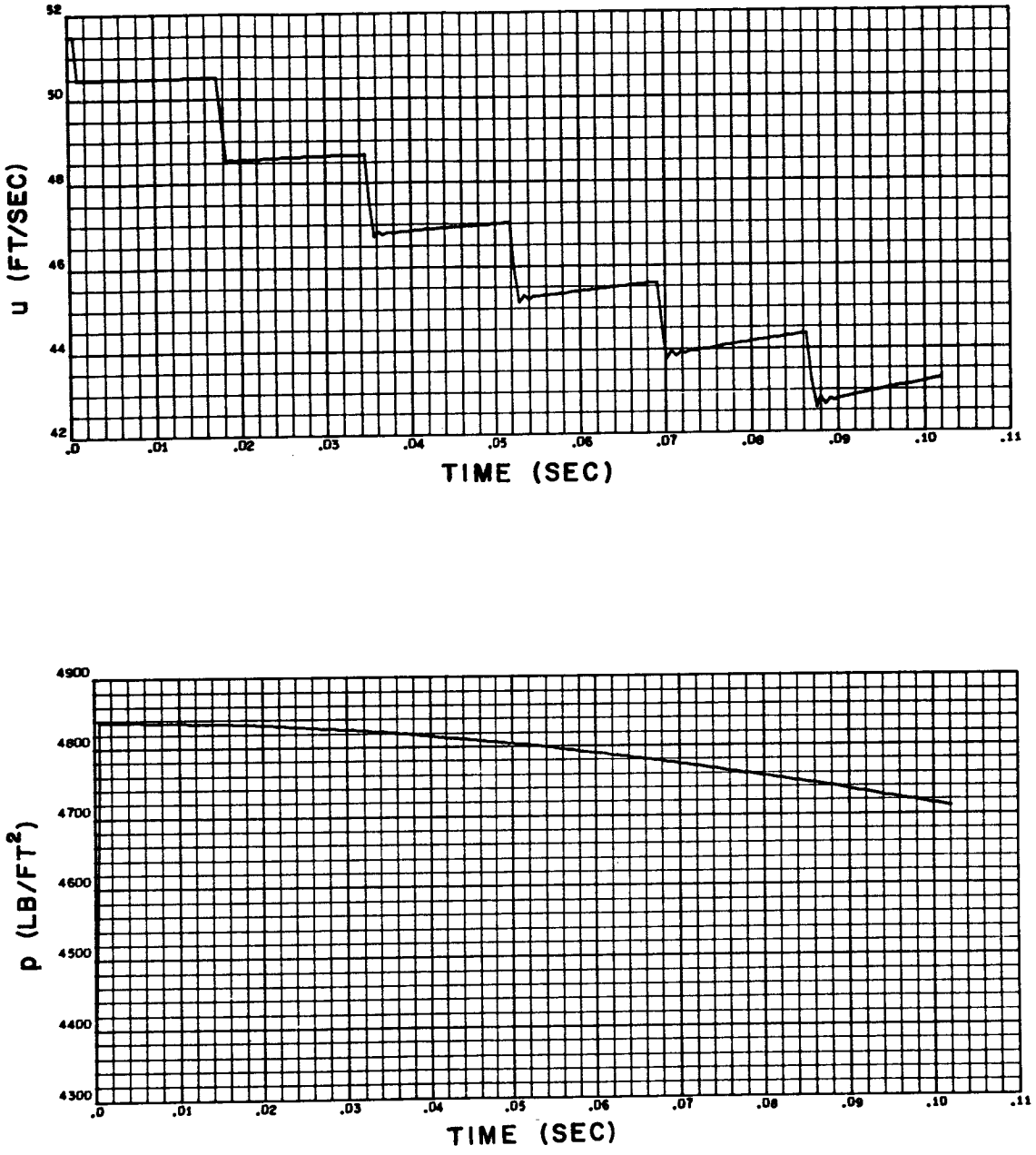

Figure B-25. Velocity and Pressure Time History at Right End of Feed Line With Air Chamber, Impulse Disturbance 2 Percent of Steady-State Velocity

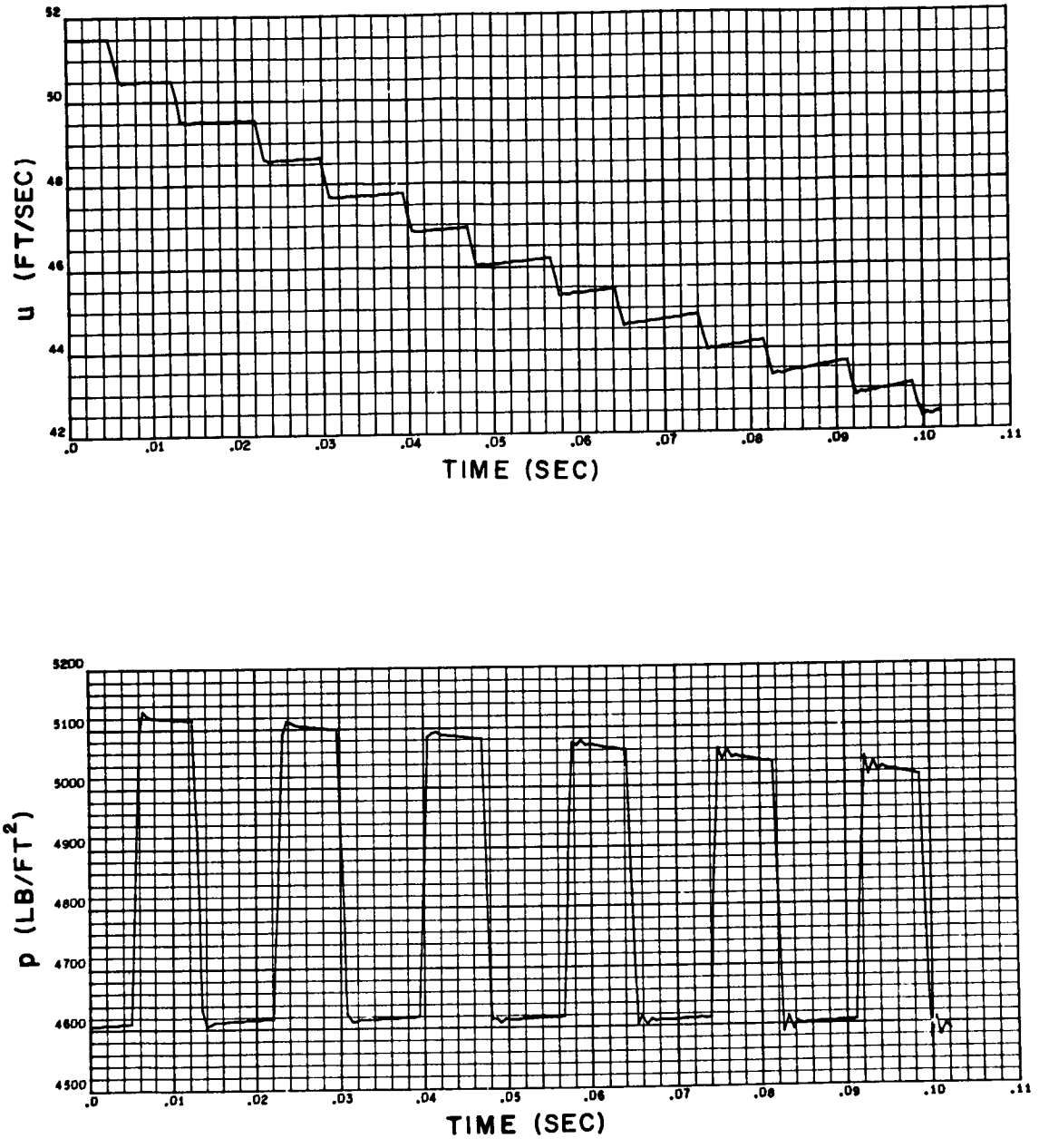

Figure B-26. Velocity and Pressure Time History at Midpoint of Feed Line With Air Chamber, Impulse Disturbance 2 Percent of Steady-State Velocity

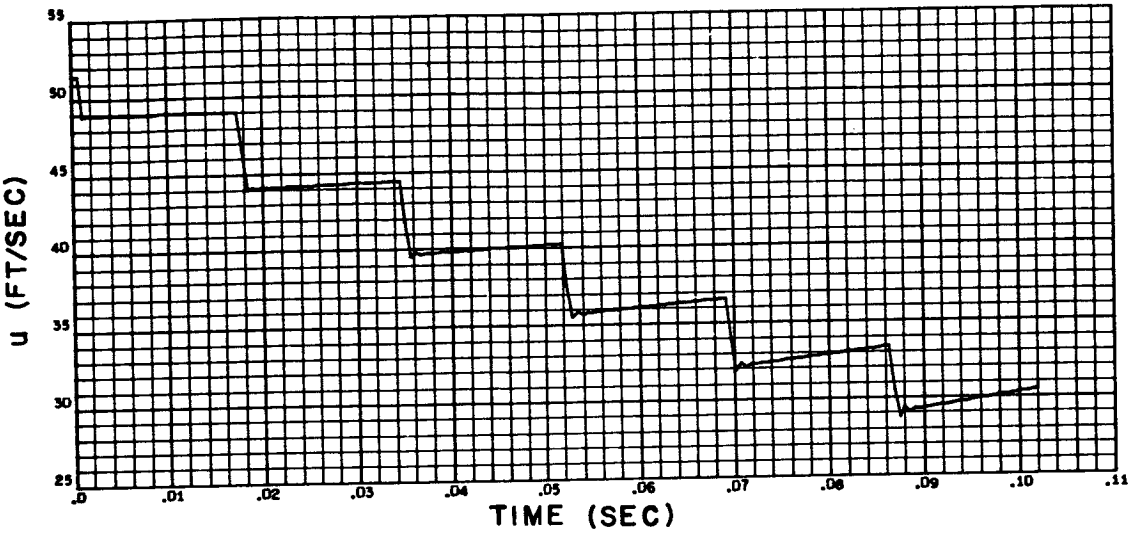

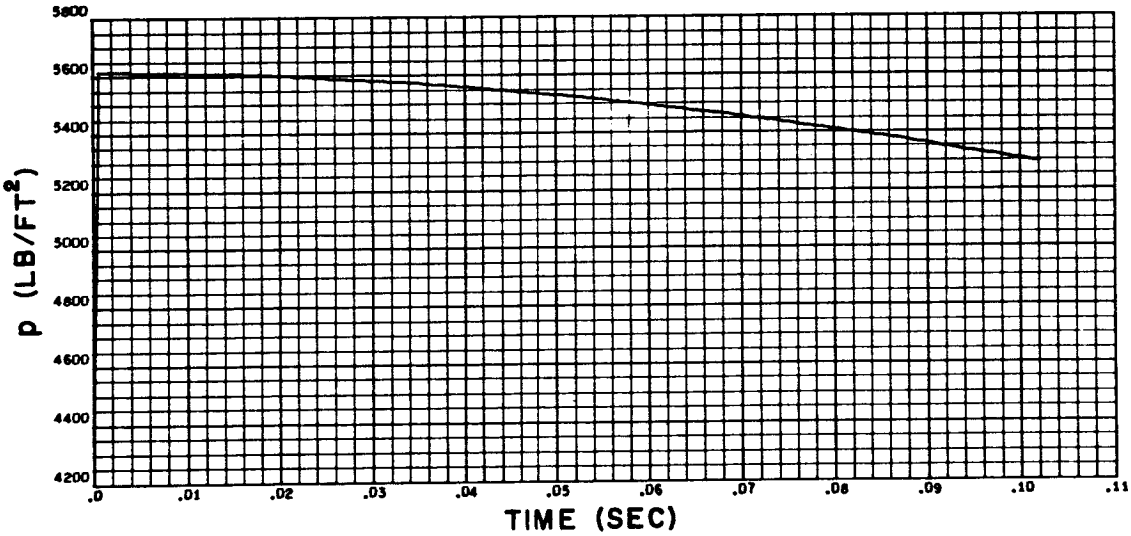

Figure B-27. Velocity and Pressure Time History at Right End of Feed Line With Air Chamber, Impulse Disturbance 5 Percent of Steady-State Velocity

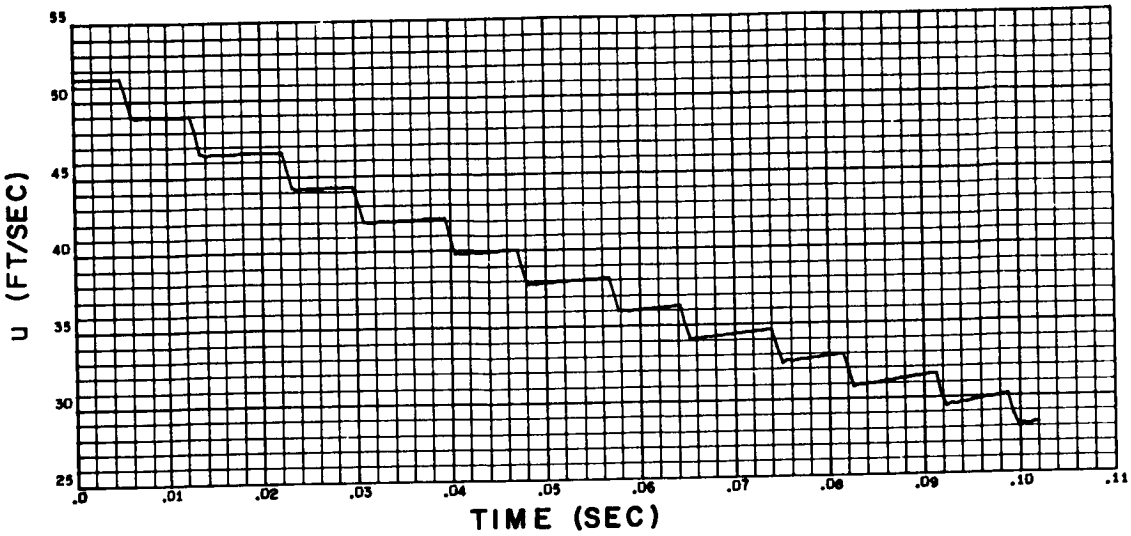

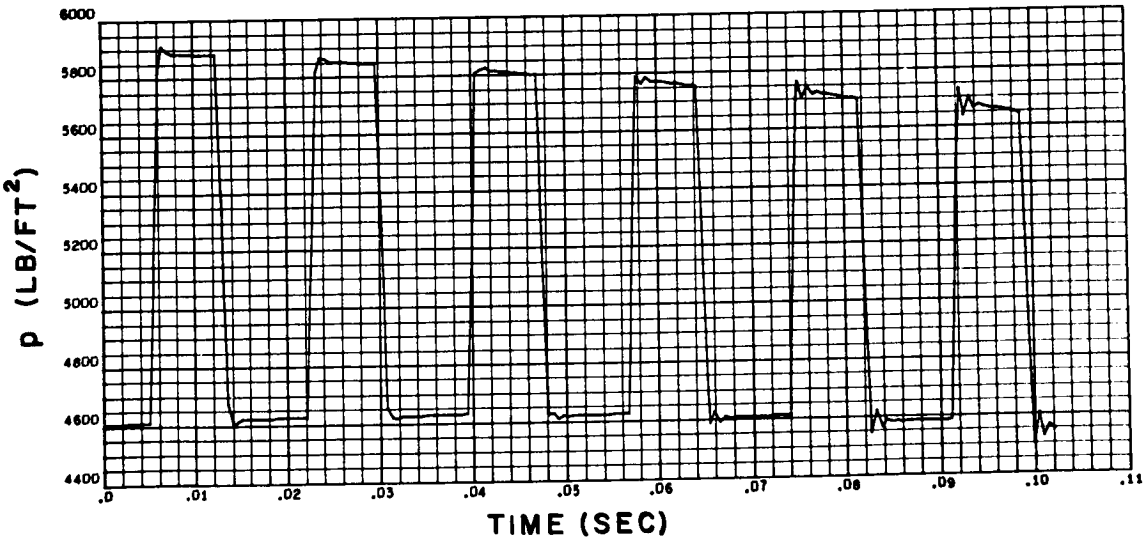

Figure B-28. Velocity and Pressure Time History at Midpoint of Feed Line With Air Chamber, Impulse Disturbance 5 Percent of Steady-State Velocity

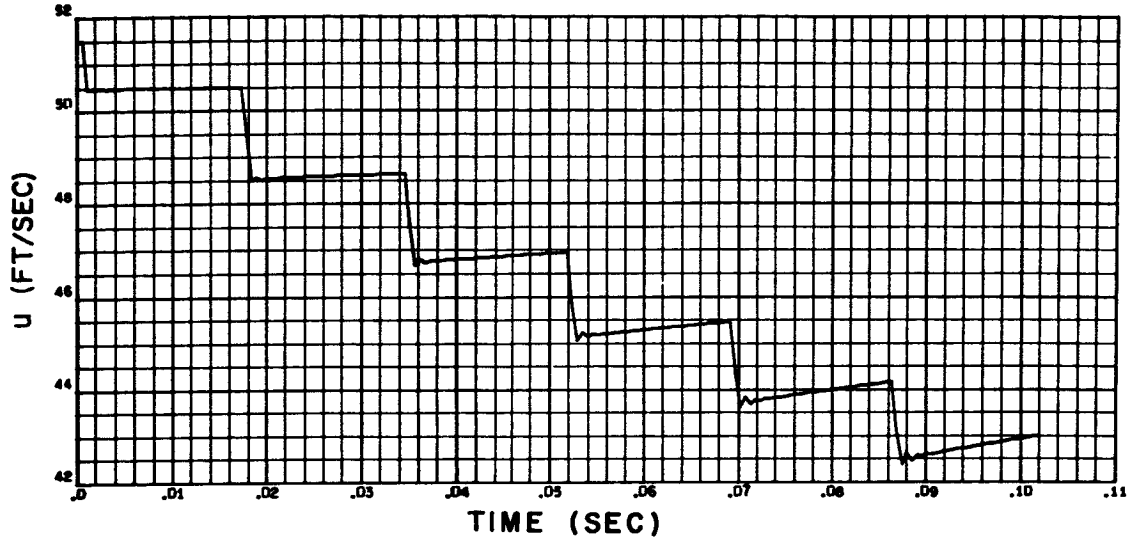

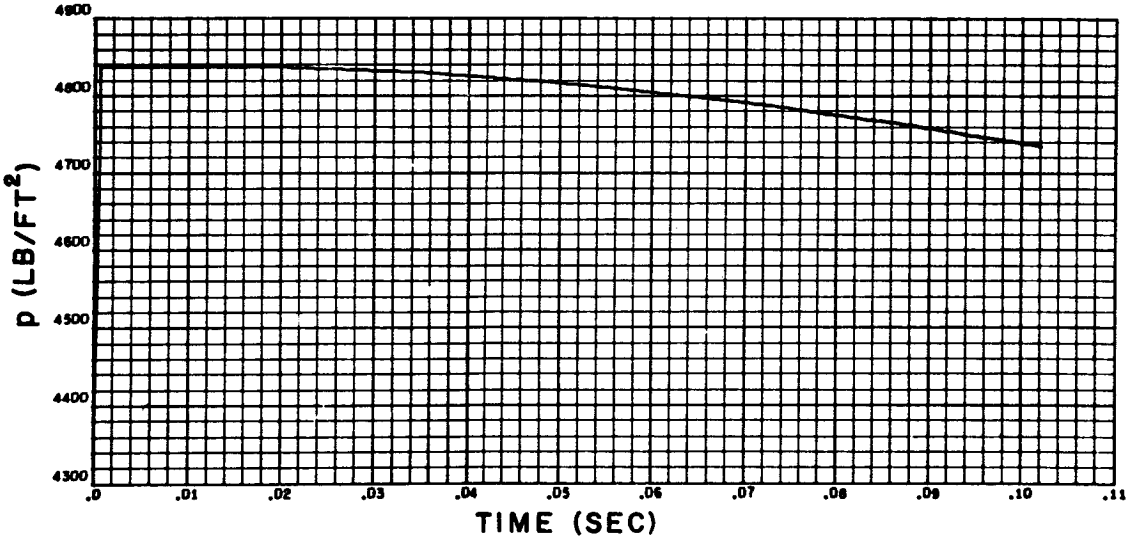

Figure B-29. Velocity and Pressure Time History at Right End of Feed Line With Air Chamber, Step Disturbance 2 Percent of Steady-State Velocity

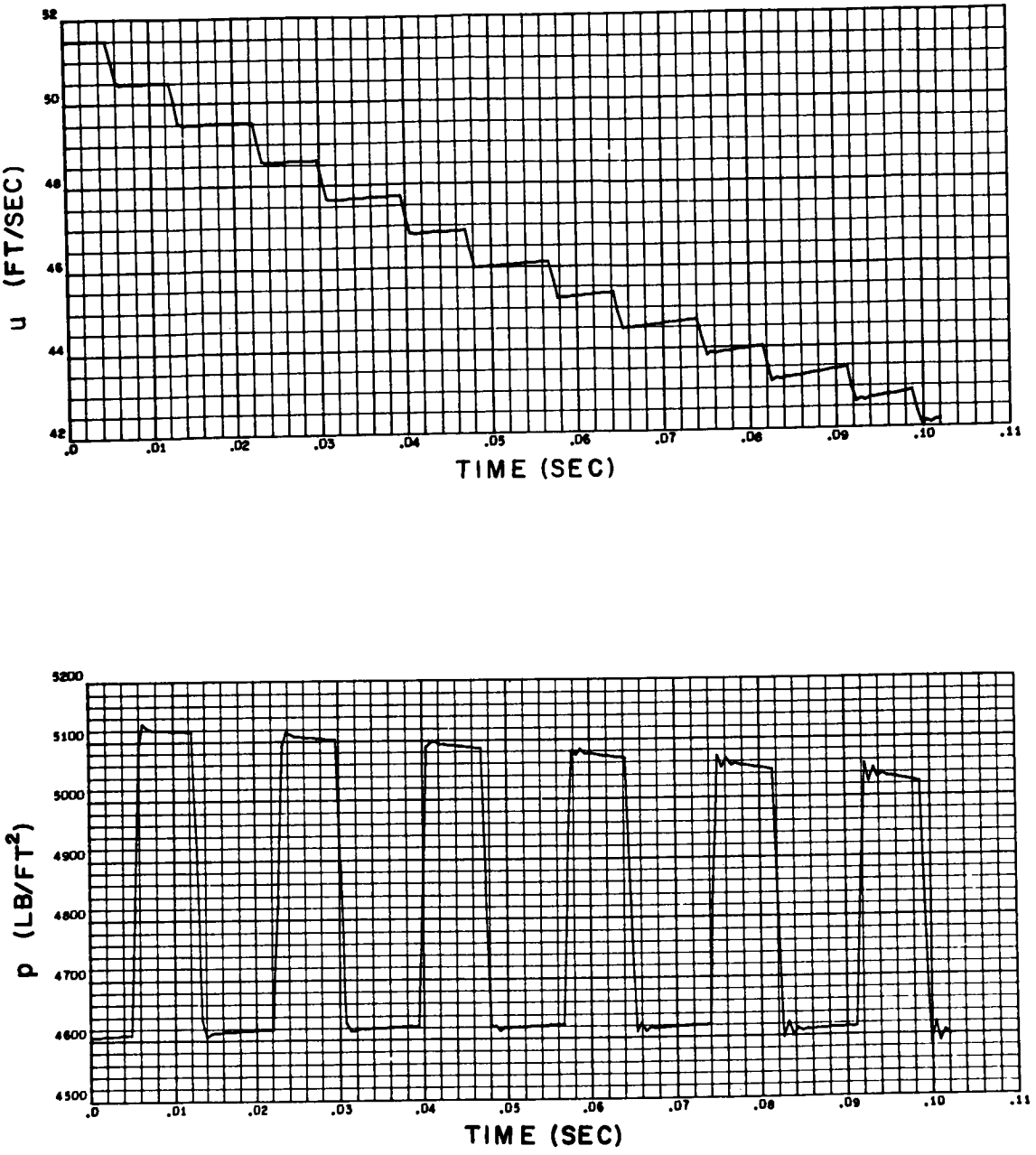

Figure B-30. Velocity and Pressure Time History at Midpoint of Feed Line With Air Chamber, Step Disturbance 2 Percent of Steady-State Velocity

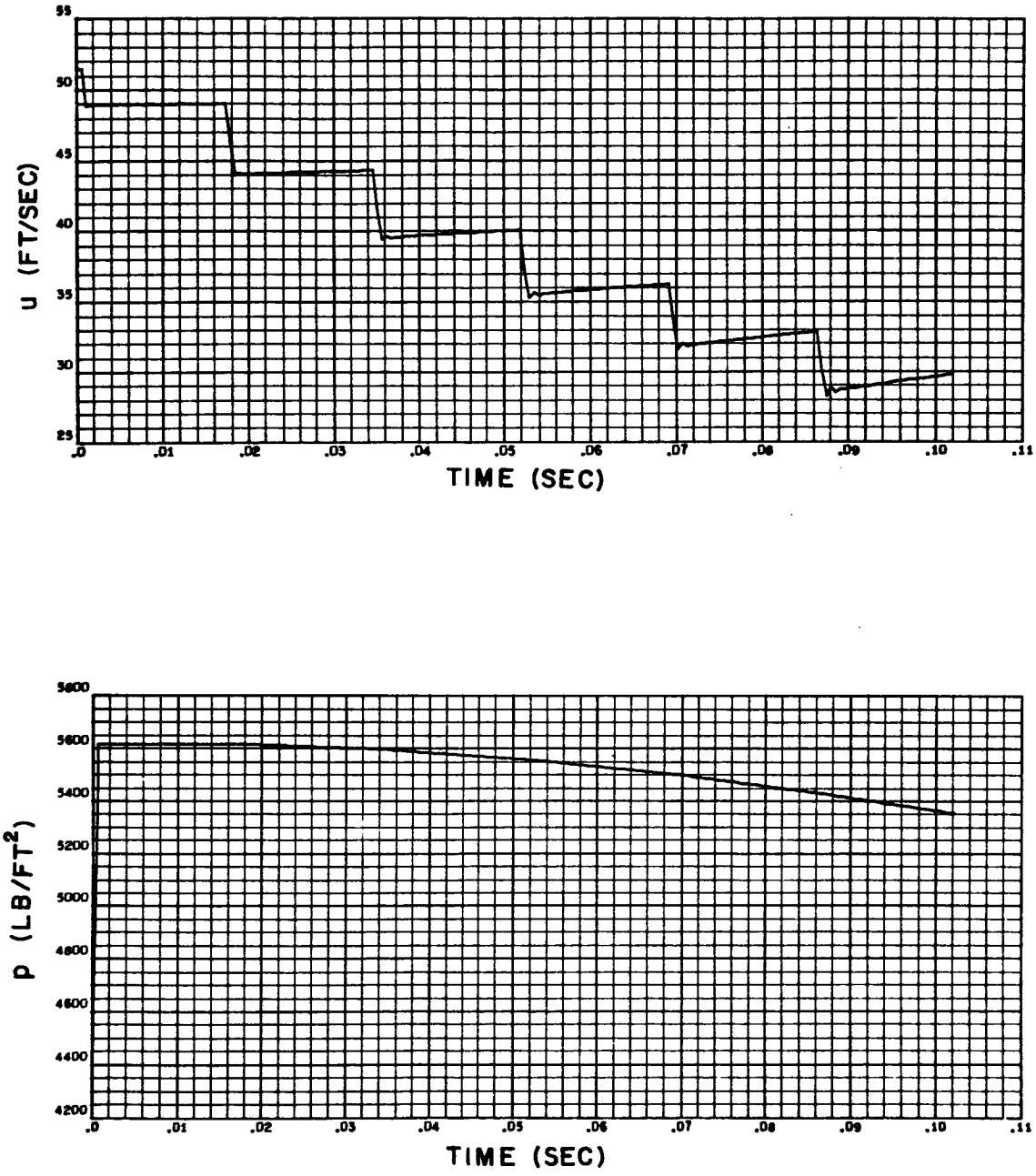

Figure B-31. Velocity and Pressure Time History at Right End of Feed Line With Air Chamber, Step Disturbance 5 Percent of Steady-State Velocity

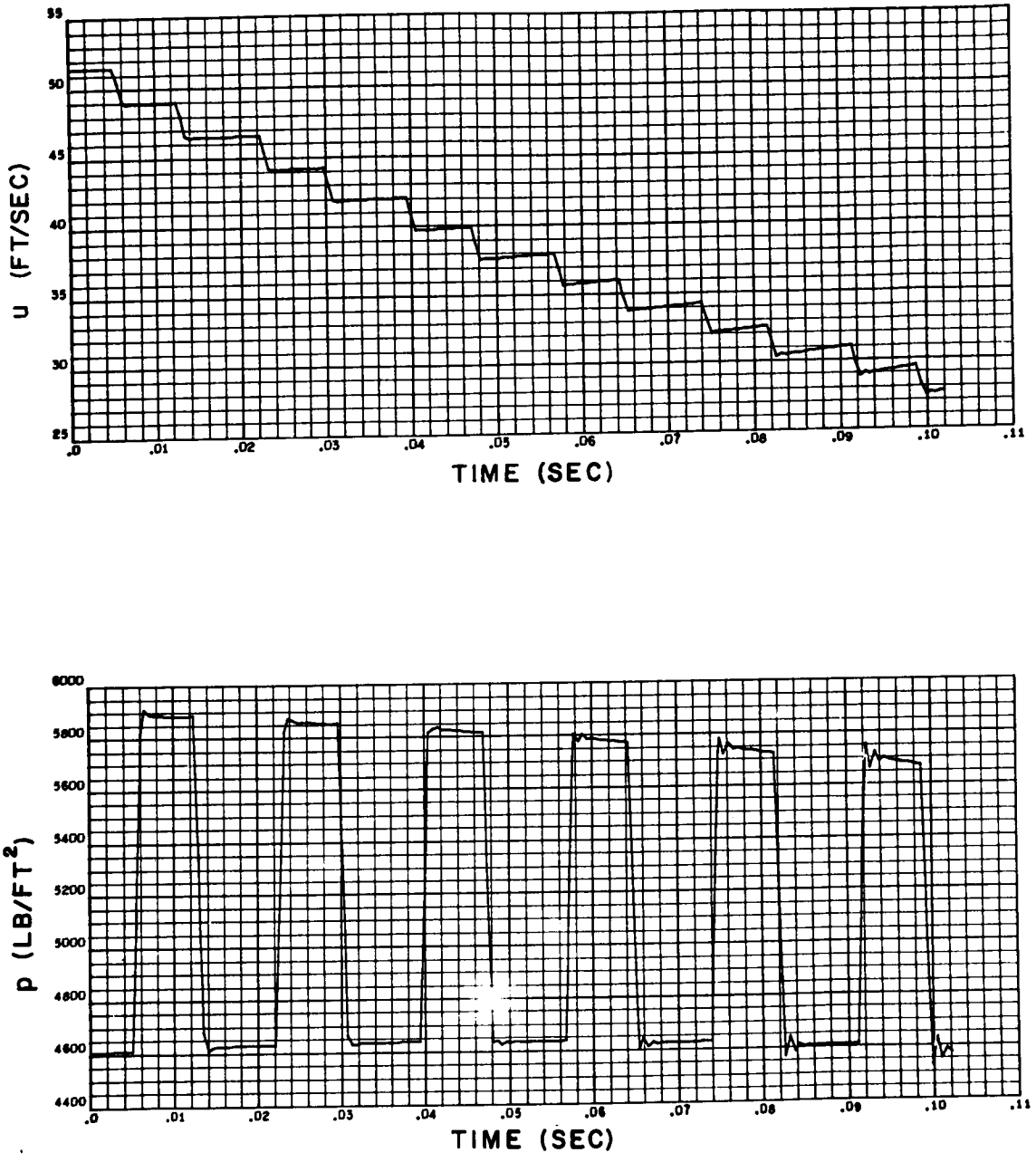

Figure B-32. Velocity and Pressure Time History at Midpoint of Feed Line With Air Chamber, Step Disturbance 5 Percent of Steady-State Velocity

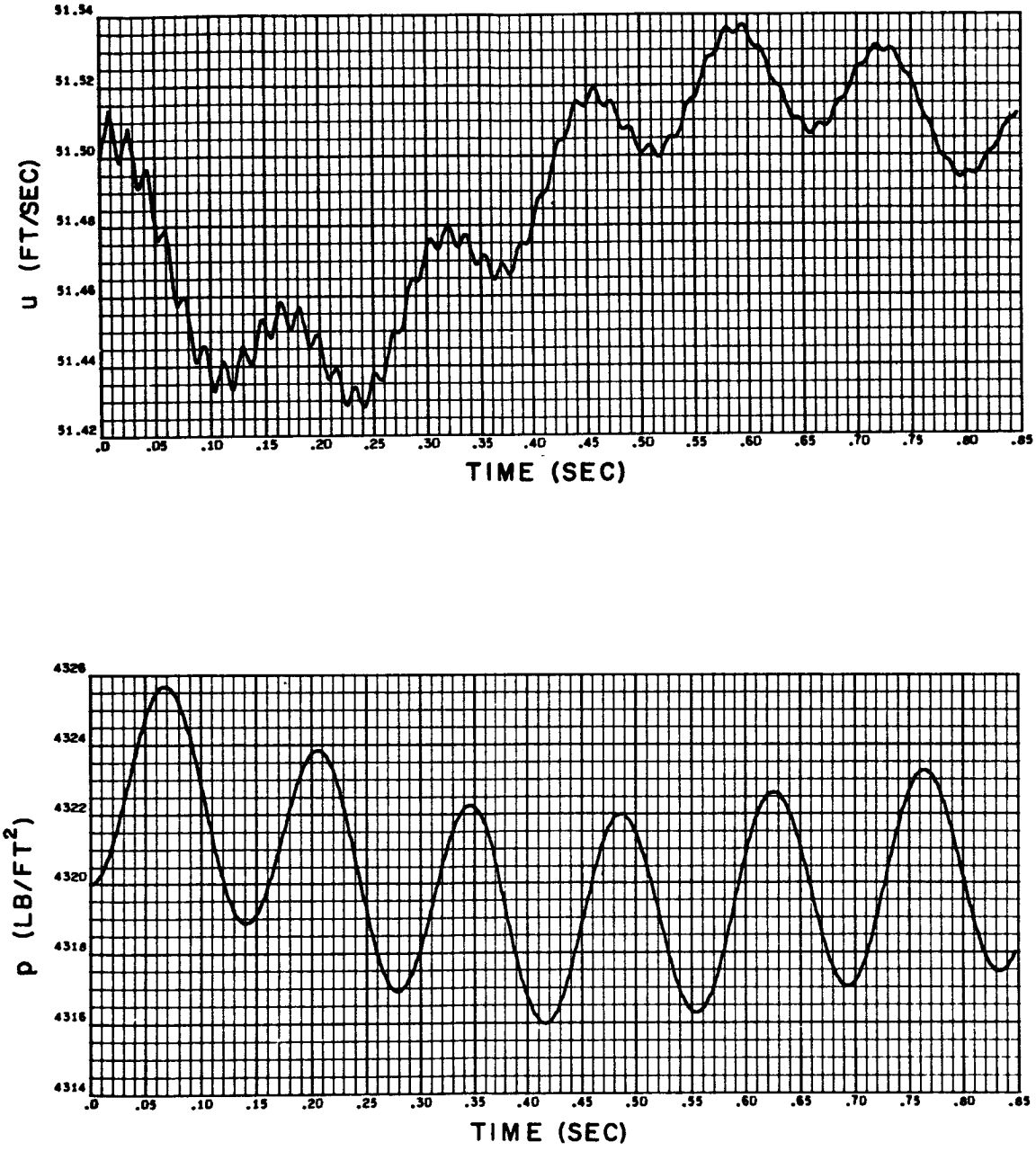

Figure B-33. Velocity and Pressure Time History at Right End of Feed Line With Air Chamber Under Sinusoidal Disturbance, Amplitude 2 Percent of Steady-State Velocity, Frequency 7.20 cps

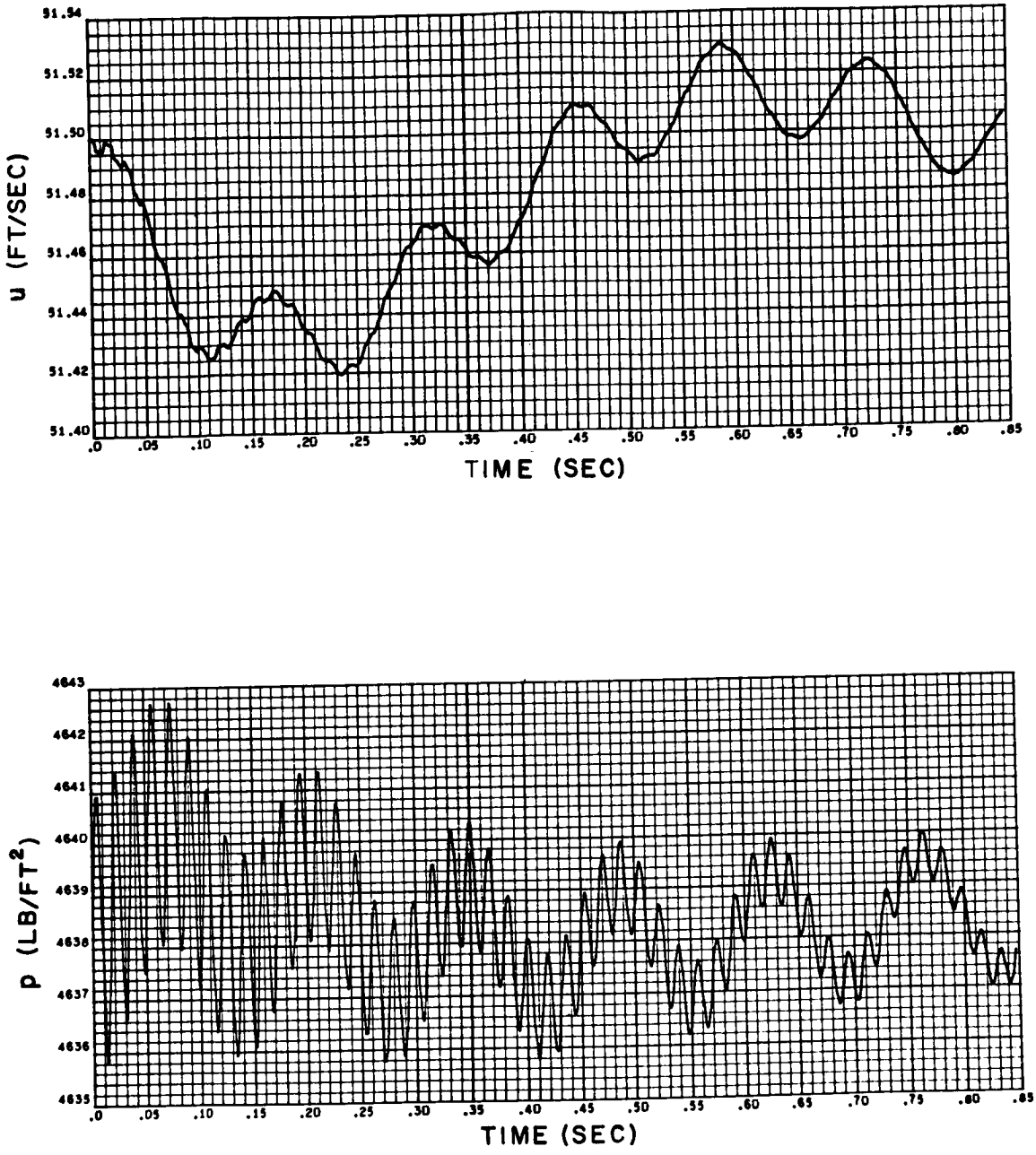

Figure B-34. Velocity and Pressure Time History at Midpoint of Feed Line With Air Chamber Under Sinusoidal Disturbance Amplitude 2 Percent of Steady-State Velocity, Frequency 7.20 cps

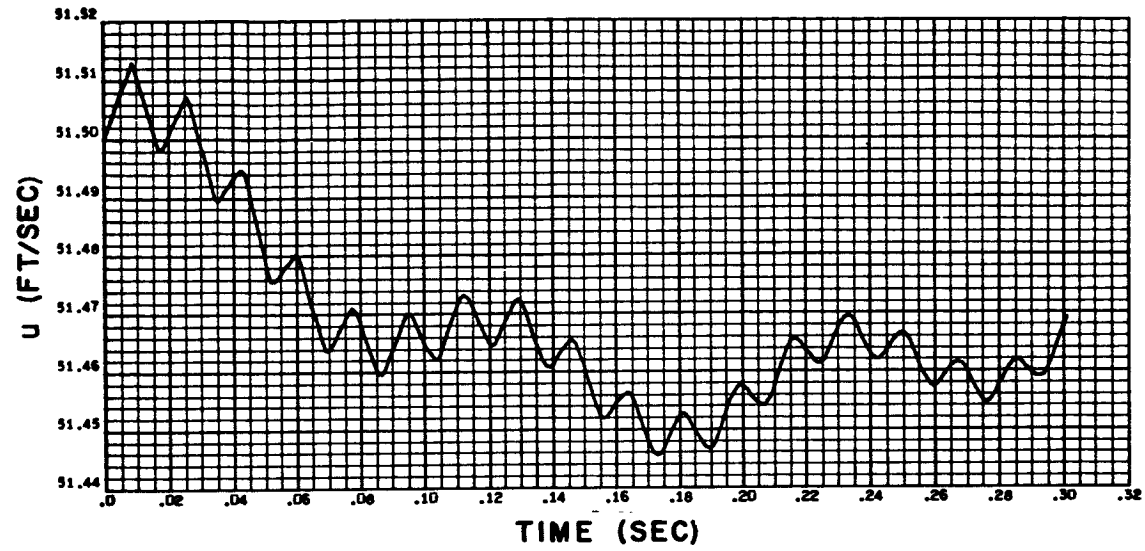

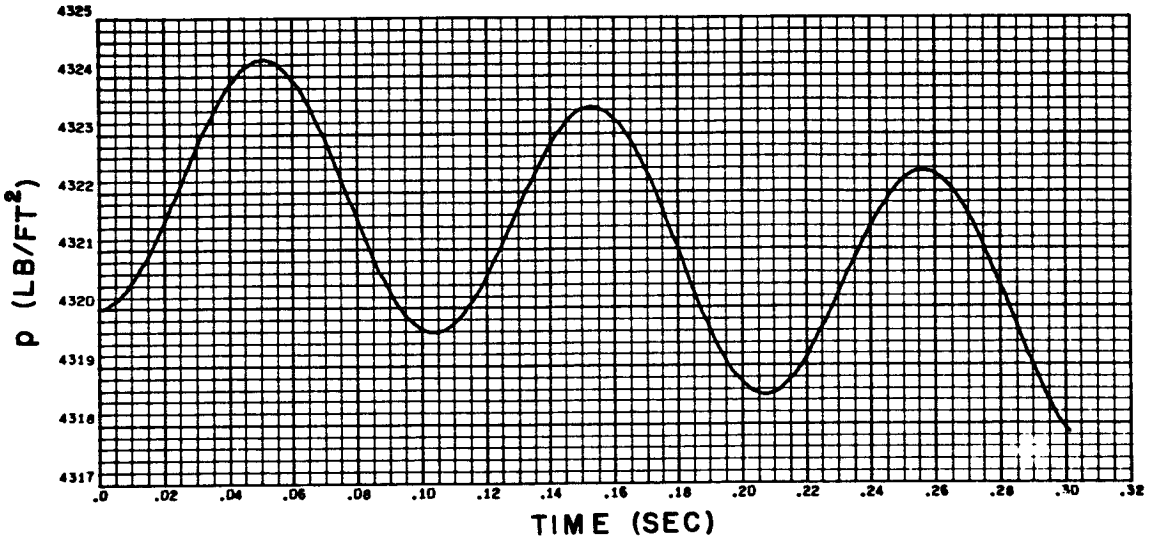

Figure B-35. Velocity and Pressure Time History at Right End of Feed Line With Air Chamber Under Sinusoidal Disturbance, Amplitude 2 Percent of Steady-State Velocity, Frequency 9.70 cps

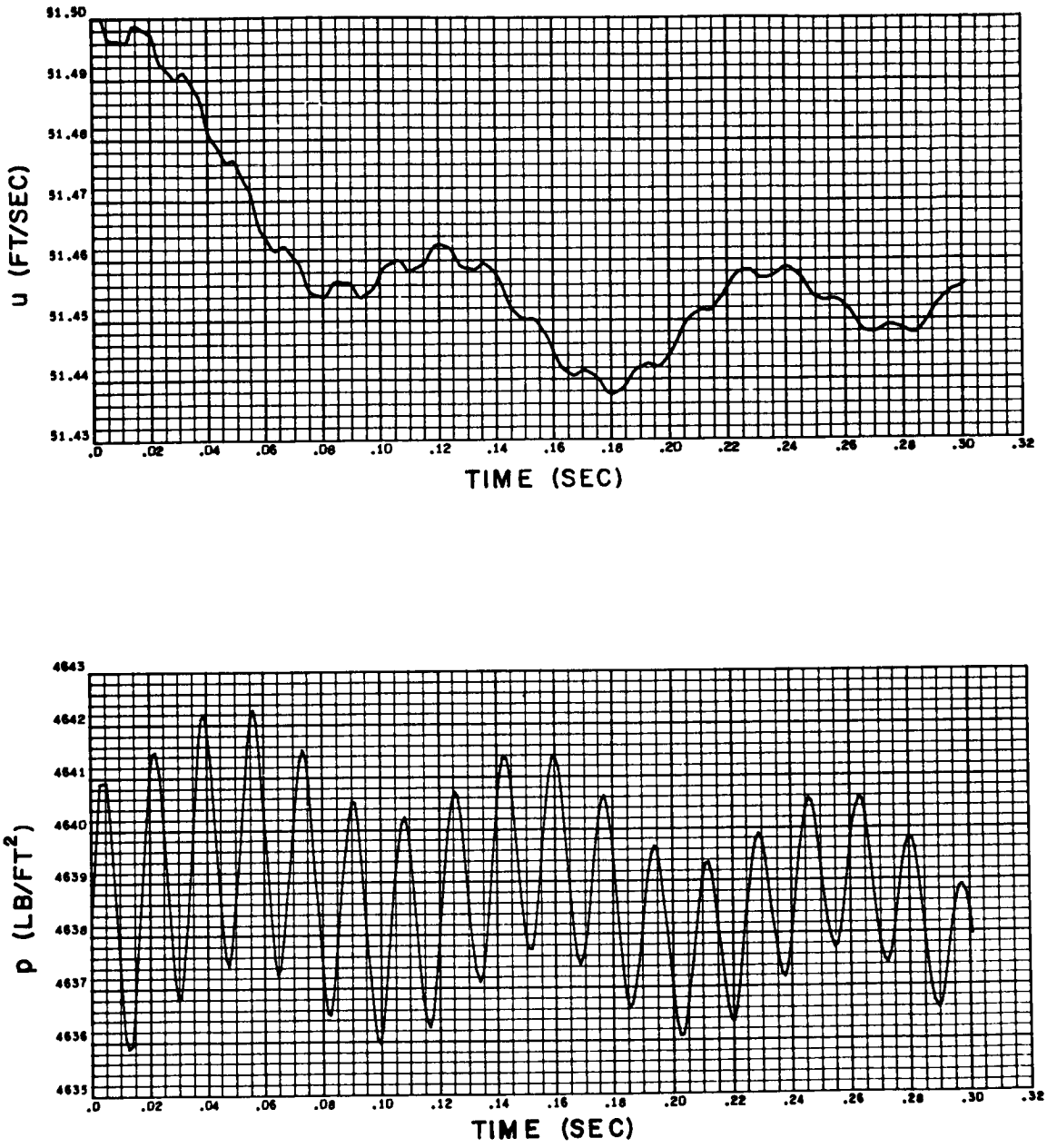

Figure B-36. Velocity and Pressure Time History at Midpoint of Feed Line With Air Chamber Under Sinusoidal Disturbance, Amplitude 2 Percent of Steady-State Velocity, Frequency 9.70 cps

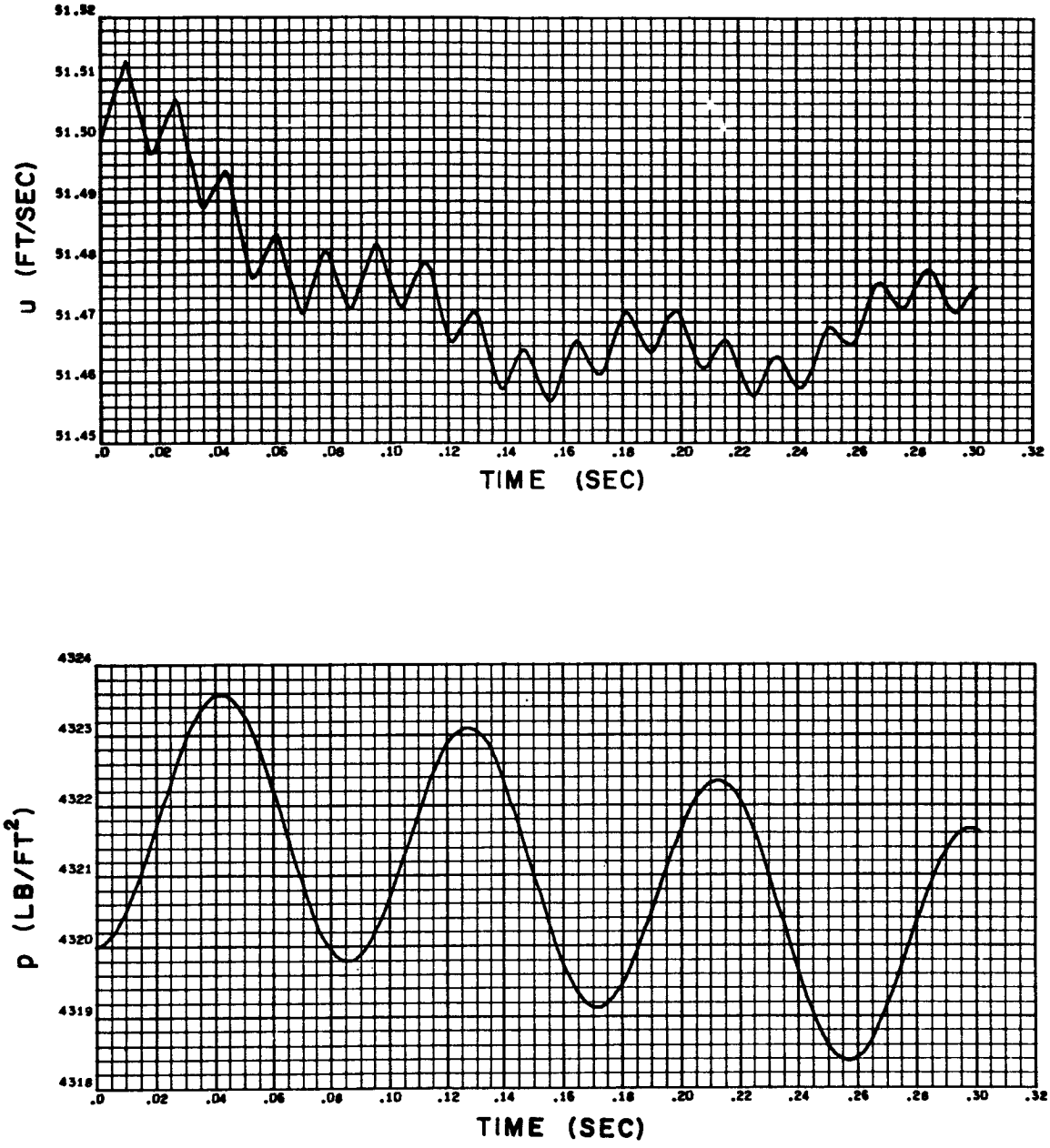

Figure B-37. Velocity and Pressure Time History at Right End of Feed Line With Air Chamber Under Sinusoidal Disturbances, Amplitude 2 Percent of Steady-State Velocity, Frequency 11.70 cps

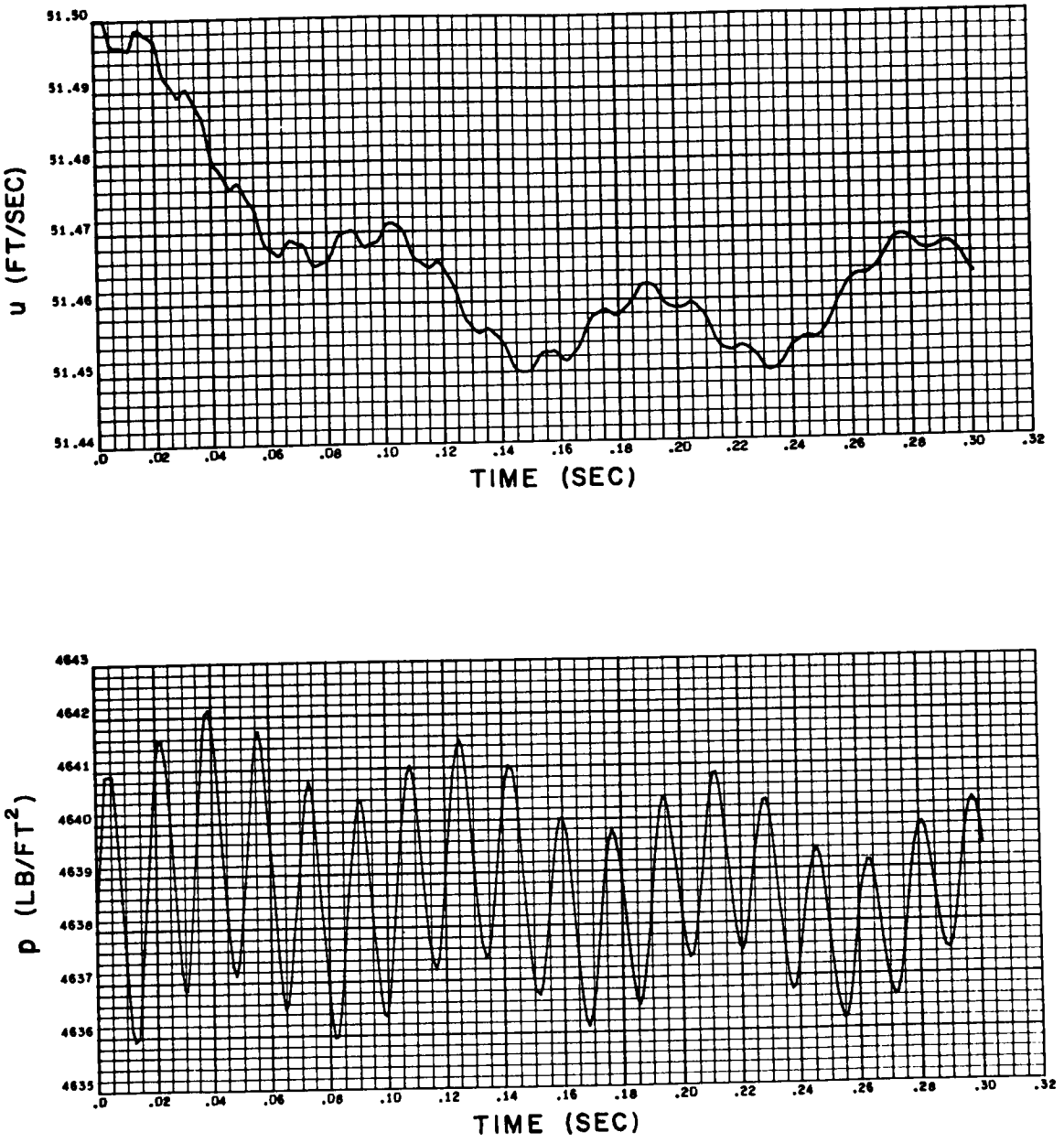

Figure B-38. Velocity and Pressure Time History at Midpoint of Feed Line With Air Chamber Under Sinusoidal Disturbance, Amplitude 2 Percent of Steady-State Velocity, Frequency 11.70 cps

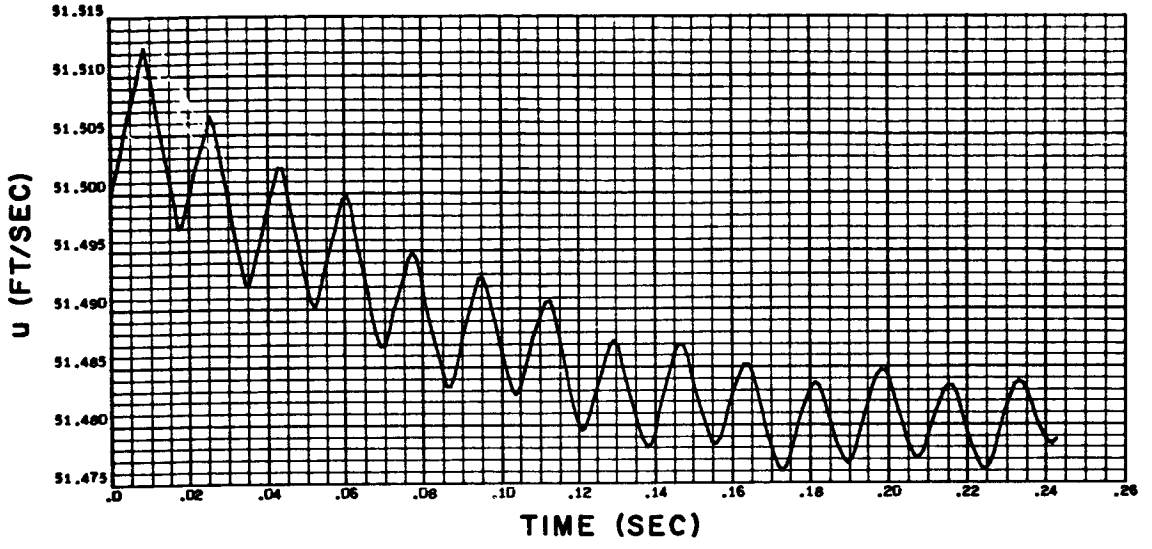

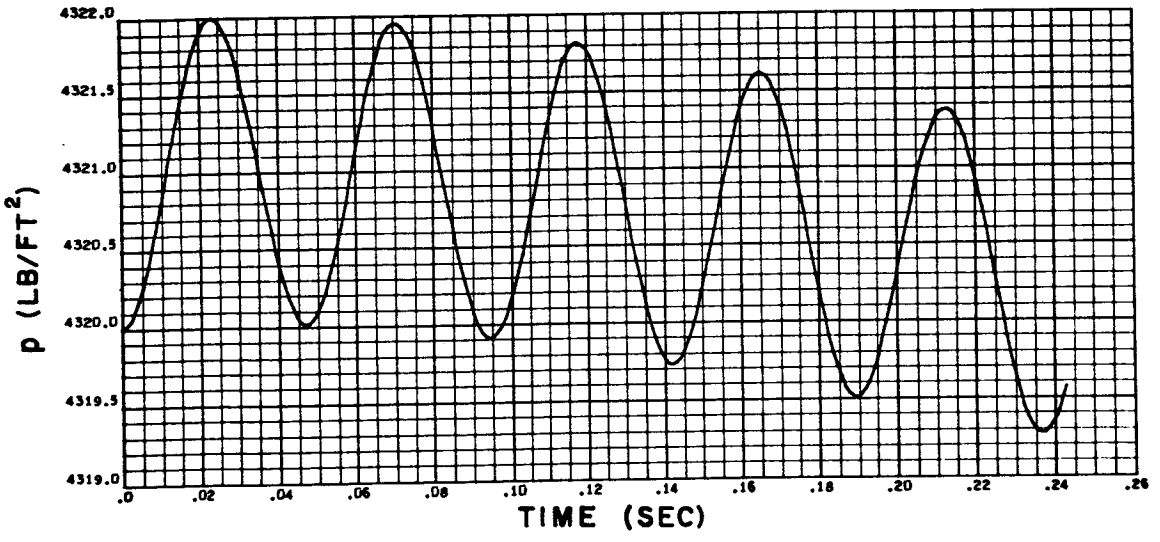

Figure B-39. Velocity and Pressure Time History at Right End of Feed Line With Air Chamber Under Sinusoidal Disturbance, Amplitude 2 Percent of Steady-State Velocity, Frequency 21.11 cps

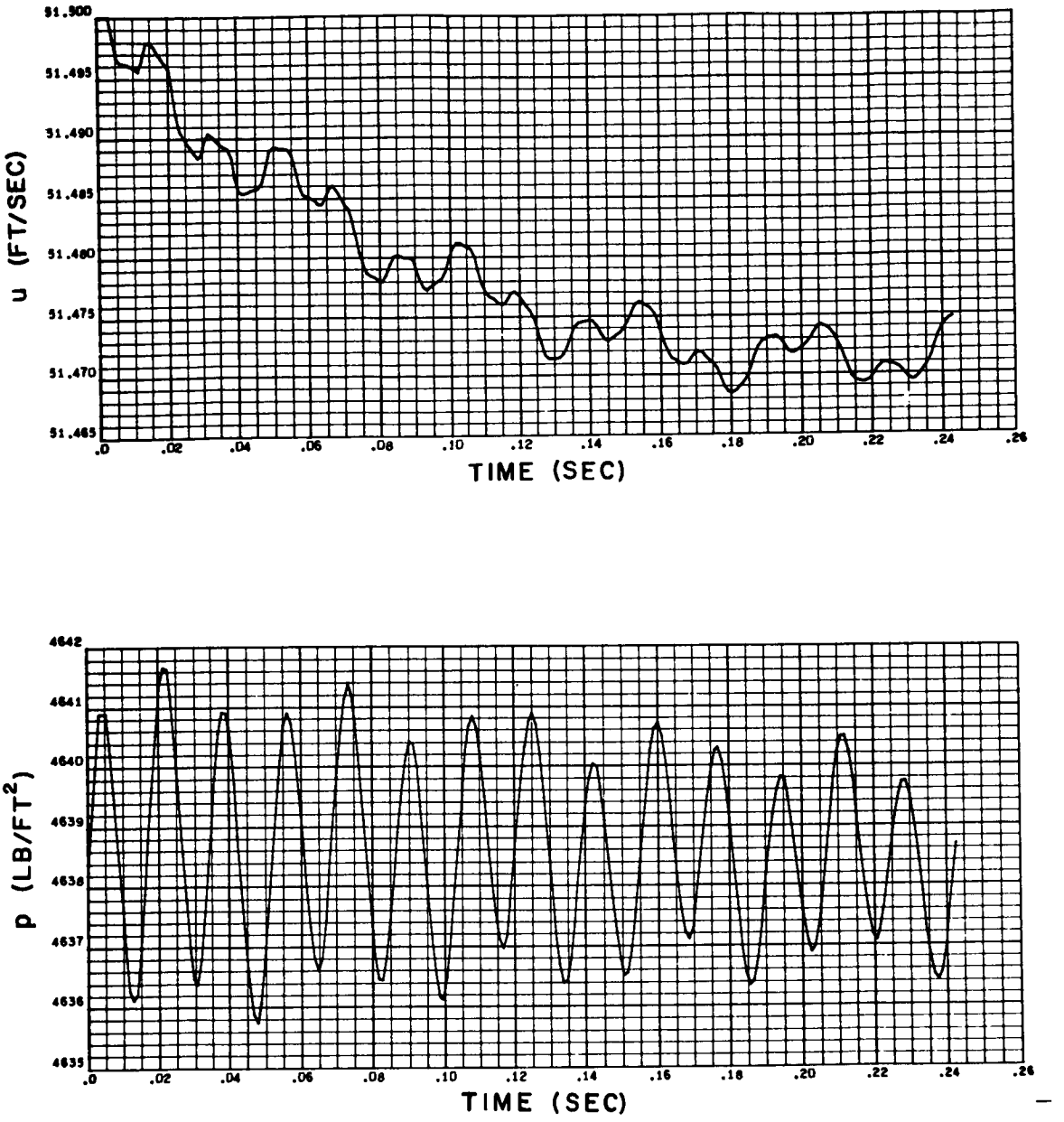

Figure B-40. Velocity and Pressure Time History at Midpoint of Feed Line With Air Chamber Under Sinusoidal Disturbance, Amplitude 2 Percent of Steady-State Velocity, Frequency 21.11 cps

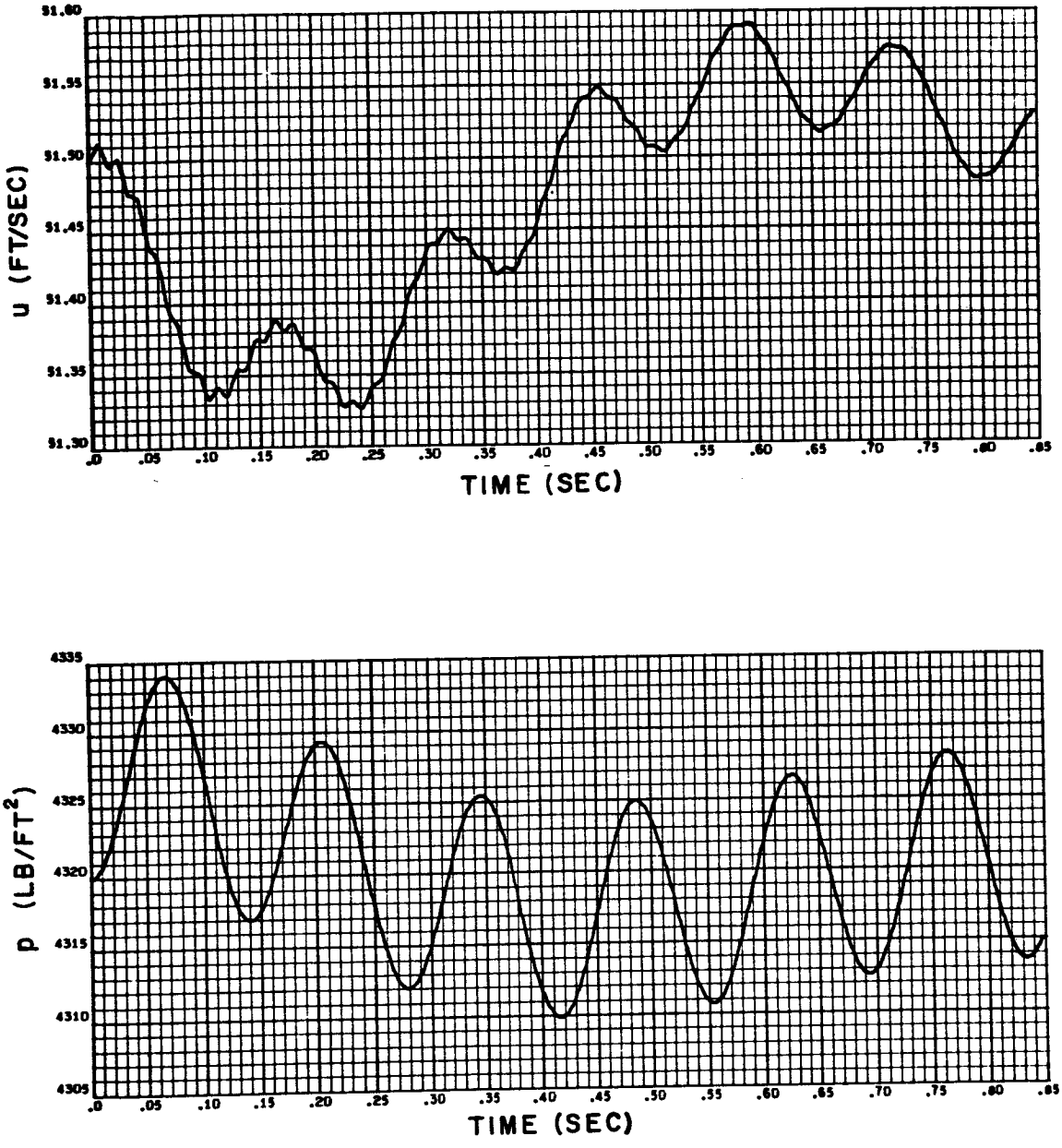

Figure B-41. Velocity and Pressure Time History at Right End of Feed Line With Air Chamber Under Sinusoidal Disturbance, Amplitude 5 Percent of Steady-State Velocity, Frequency 7.20 cps

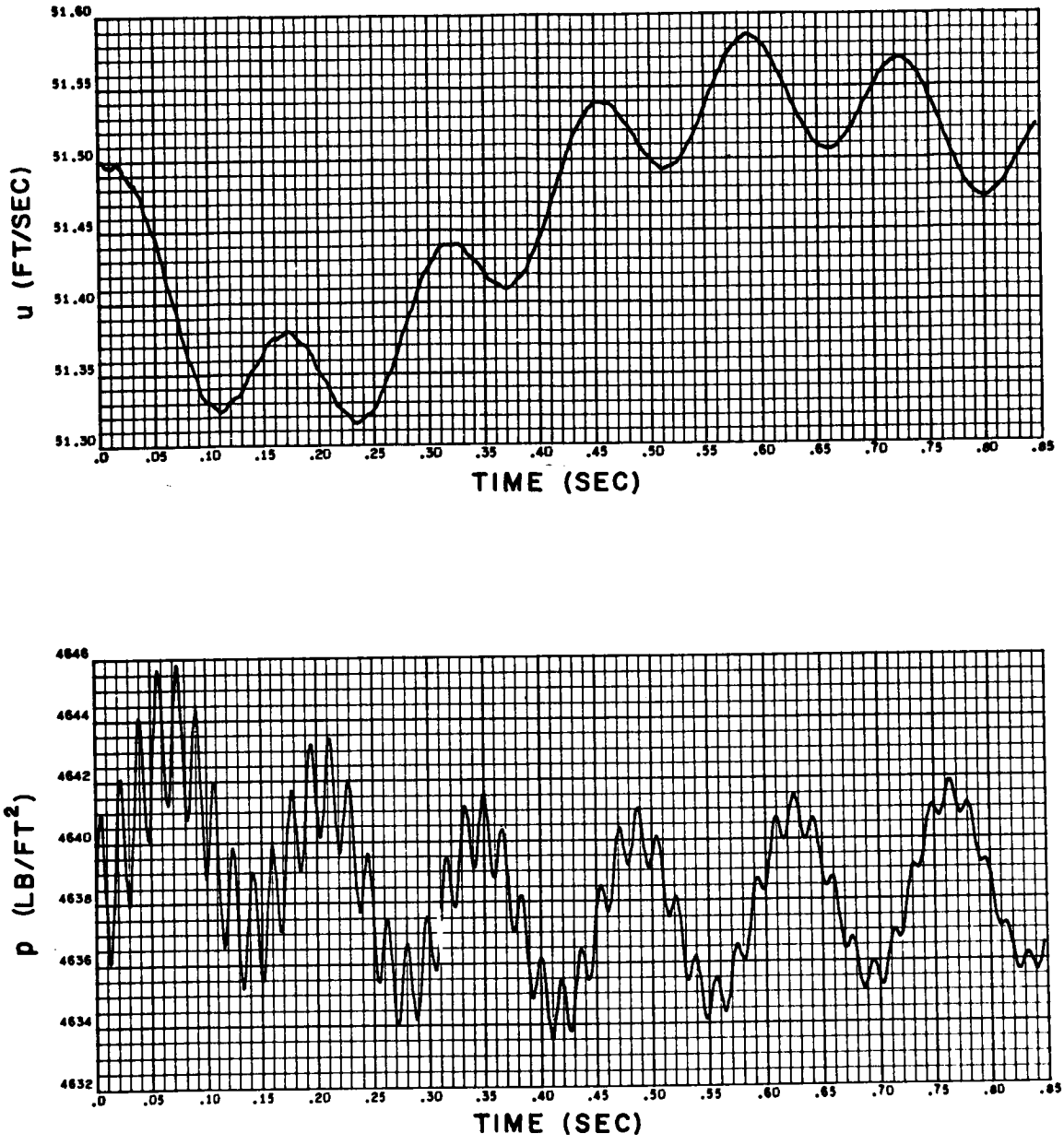

Figure B-42. Velocity and Pressure Time History at Midpoint of Feed Line With Air Chamber Under Sinusoidal Disturbance, Amplitude 5 Percent of Steady-State Velocity, Frequency 7.20 cps

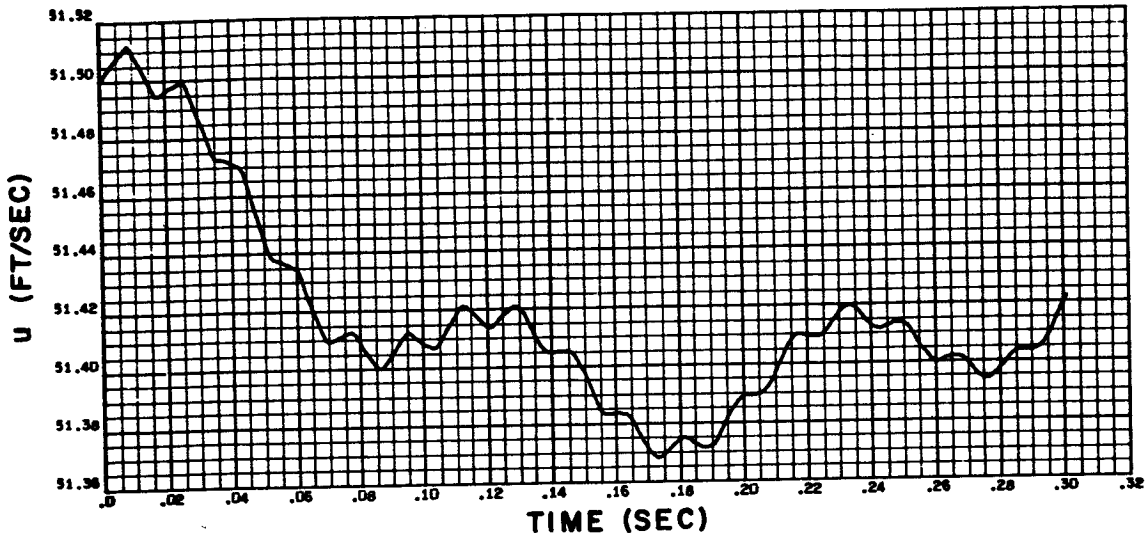

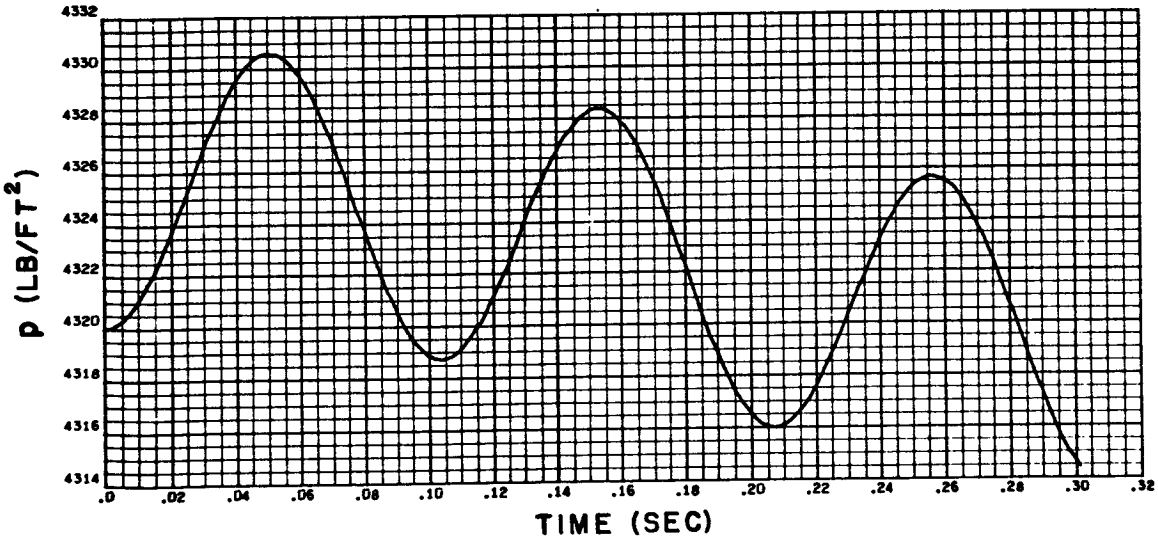

Figure B-43. Velocity and Pressure Time History at Right End of Feed Line With Air Chamber Under Sinusoidal Disturbance, Amplitude 5 Percent of Steady-State Velocity, Frequency 9.70 cps

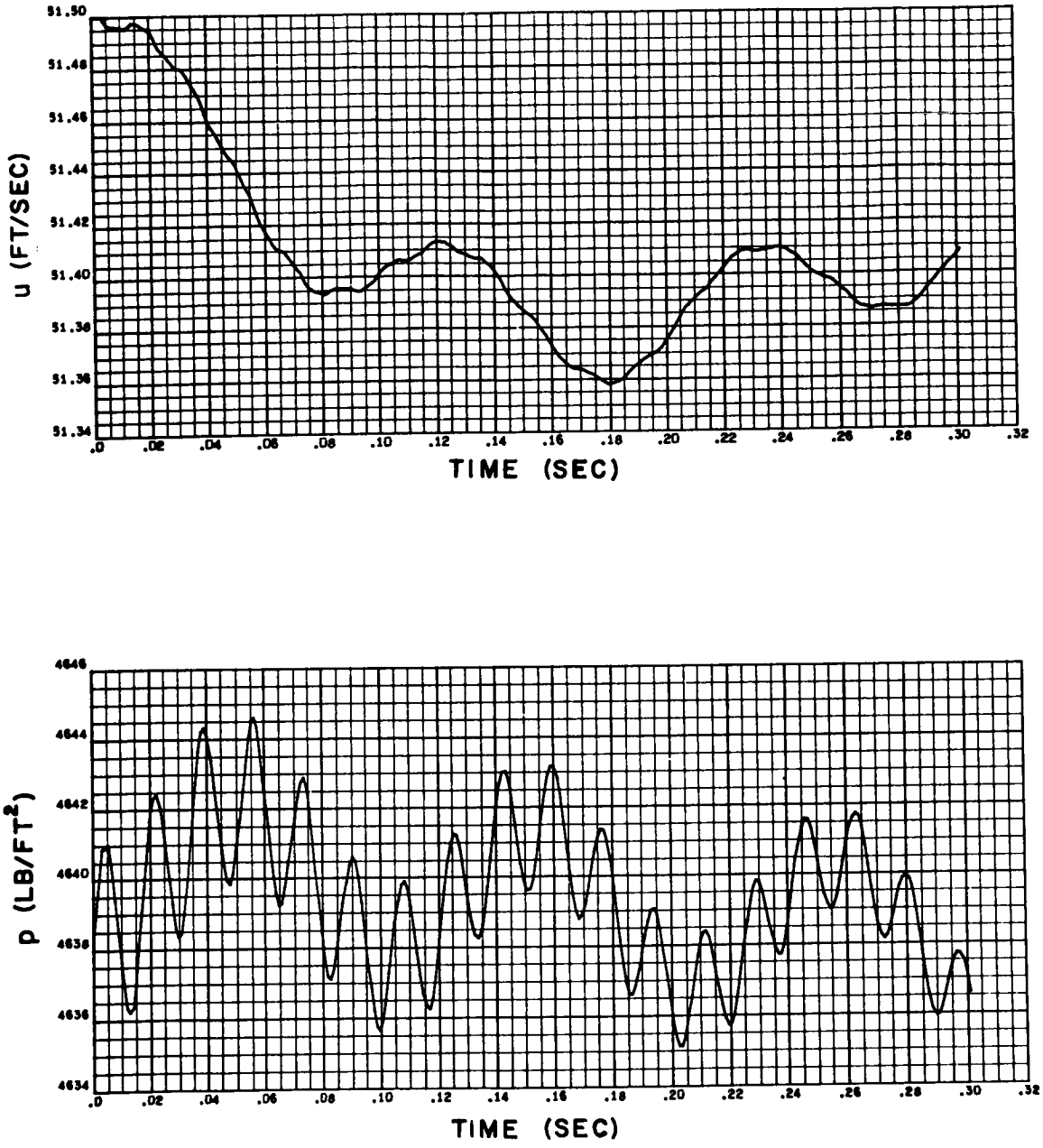

Figure B-44. Velocity and Pressure Time History at Midpoint of Feed Line With Air Chamber Under Sinusoidal Disturbance, Amplitude 5 Percent of Steady-State Velocity, Frequency 9.70 cps

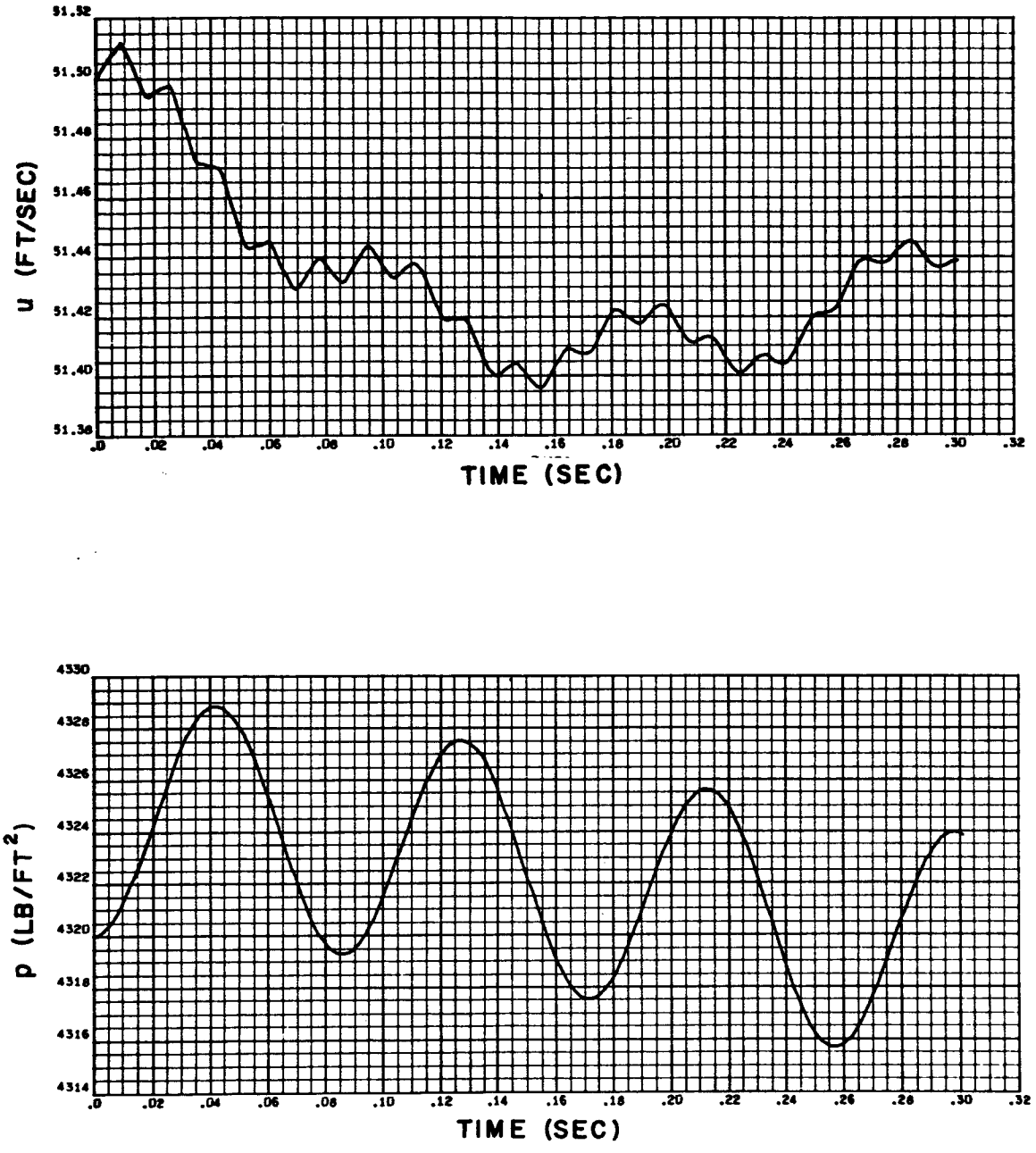

Figure B-45. Velocity and Pressure Time History at Right End of Feed Line With Air Chamber Under Sinusoidal Disturbance, Amplitude 5 Percent of Steady-State Velocity, Frequency 11.70 cps

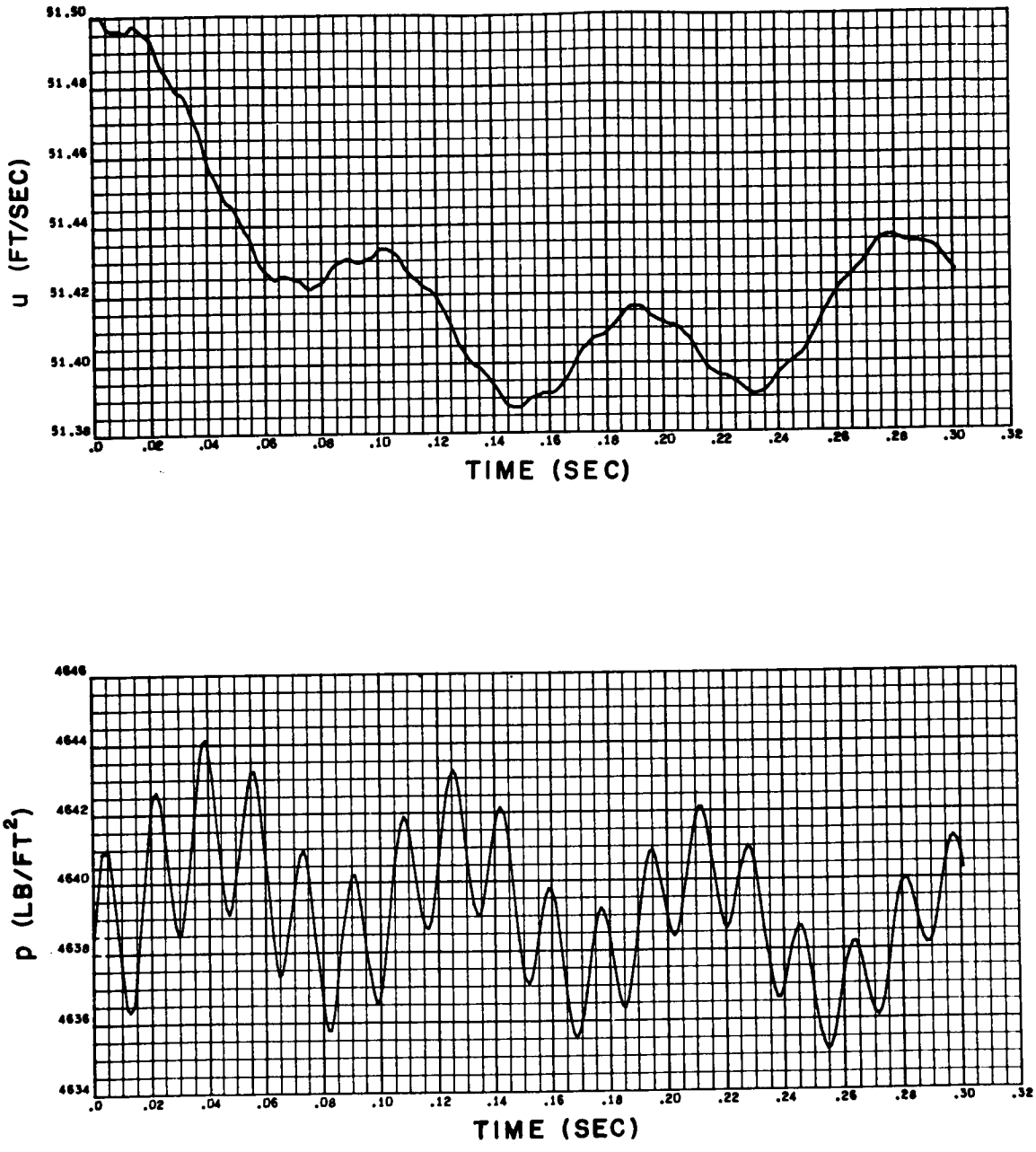

Figure B-46. Velocity and Pressure Time History at Midpoint of Feed Line With Air Chamber Under Sinusoidal Disturbance, Amplitude 5 Percent of Steady-State Velocity, Frequency 11.70 cps

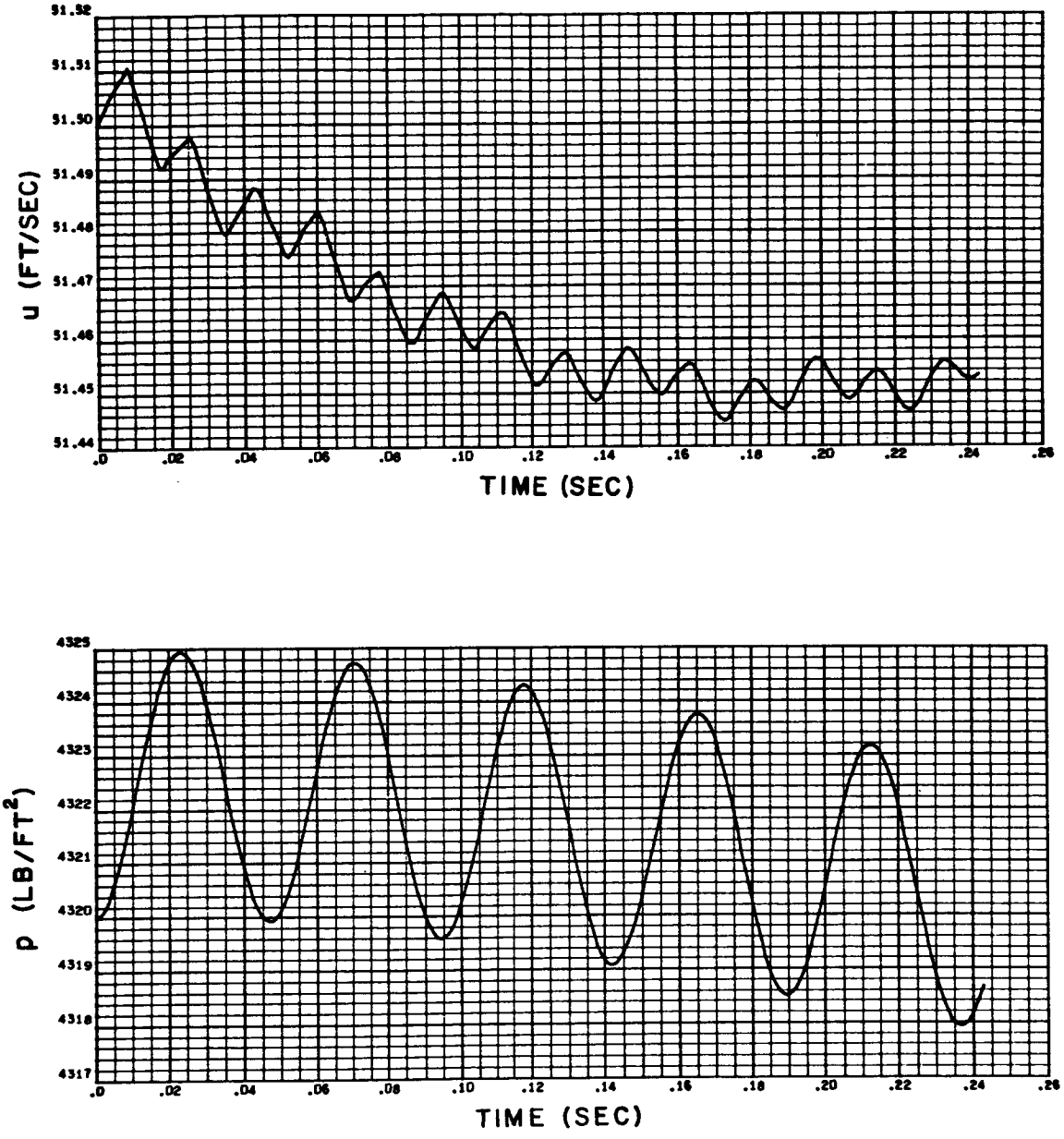

Figure B-47. Velocity and Pressure Time History at Right End of Feed Line With Air Chamber Under Sinusoidal Disturbance, Amplitude 5 Percent of Steady-State Velocity, Frequency 21.11 cps

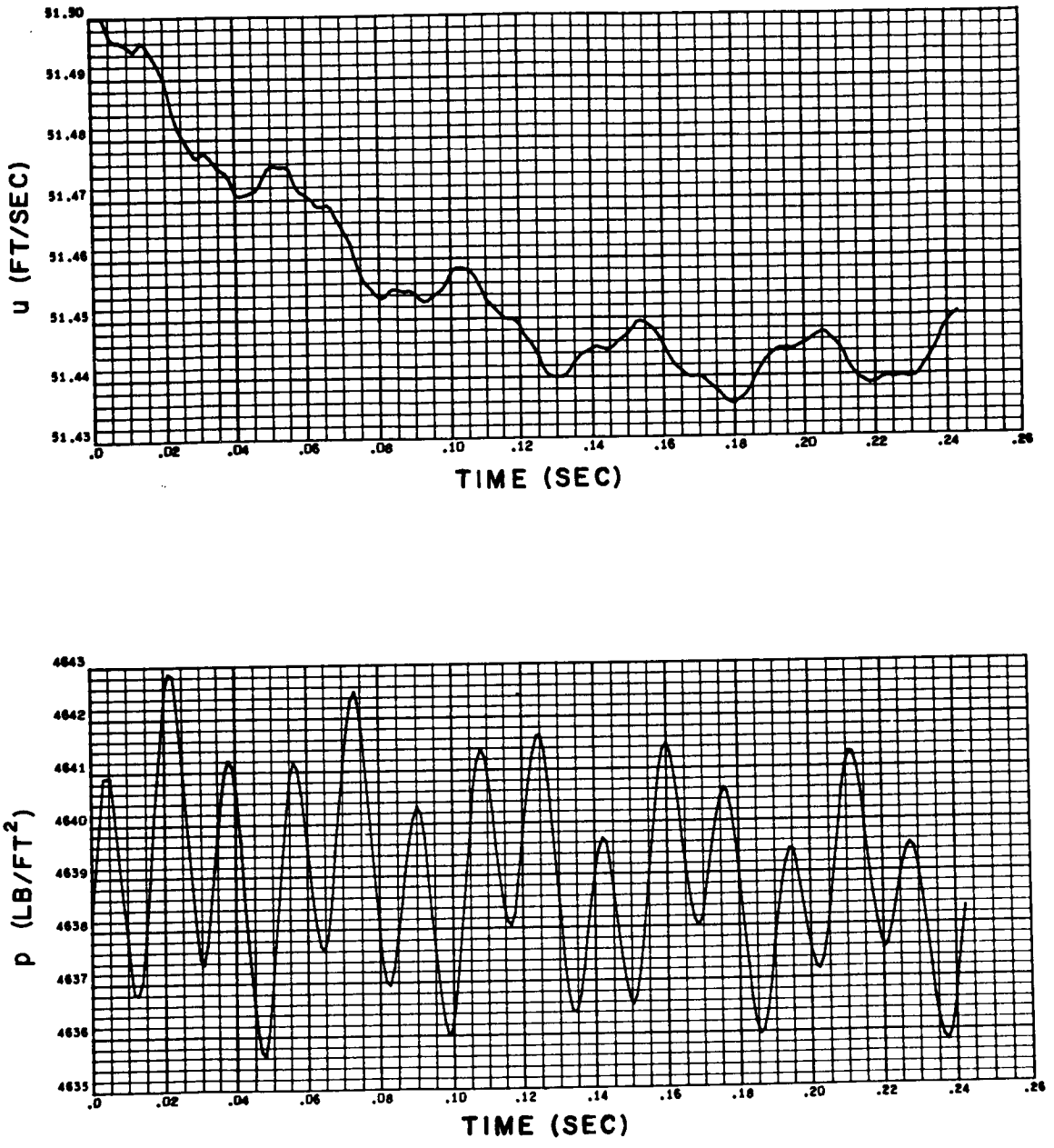

Figure B-48. Velocity and Pressure Time History at Midpoint of Feed Line With Air Chamber Under Sinusoidal Disturbance, Amplitude 5 Percent of Steady-State Velocity, Frequency 21.11 cps